ISSN 0038-531X

Russian Original Vol. 48, No. 1, January, 1980

July, 1980

SATEAZ 48(1) 1-70 (1980)

SOVIET ATOMIC ENERGY

АТОМНАЯ ЭНЕРГИЯ
(ATOMNAYA ÉNERGIYA)

TRANSLATED FROM RUSSIAN

CONSULTANTS BUREAU, NEW YORK

SOVIET ATOMIC ENERGY

Soviet Atomic Energy is a translation of *Atomnaya Énergiya*, a publication of the Academy of Sciences of the USSR.

An agreement with the Copyright Agency of the USSR (VAAP) makes available both advance copies of the Russian journal and original glossy photographs and artwork. This serves to decrease the necessary time lag between publication of the original and publication of the translation and helps to improve the quality of the latter. The translation began with the first issue of the Russian journal.

Consultants Bureau journals appear about six months after the publication of the original Russian issue. For bibliographic accuracy, the English issue published by Consultants Bureau carries the same number and date as the original Russian from which it was translated. For example, a Russian issue published in December will appear in a Consultants Bureau English translation about the following June, but the translation issue will carry the December date. When ordering any volume or particular issue of a Consultants Bureau journal, please specify the date and, where applicable, the volume and issue numbers of the original Russian. The material you will receive will be a translation of that Russian volume or issue.

Subscription (2 volumes per year)

Vols. 46 & 47: $147.50 per volume (6 Issues)
Vols. 48 & 49: $167.50 per volume (6 Issues)

Single Issue: $50
Single Article: $7.50

Prices somewhat higher outside the United States.

CONSULTANTS BUREAU, NEW YORK AND LONDON

227 West 17th Street
New York, New York 10011

Published monthly. Second-class postage paid at Jamaica, New York 11431.

Soviet Atomic Energy is abstracted or indexed in *Chemical Abstracts, Chemical Titles, Pollution Abstracts, Science Research Abstracts, Parts A and B, Safety Science Abstracts Journal, Current Contents, Energy Research Abstracts,* and *Engineering Index.*

SOVIET ATOMIC ENERGY

A translation of *Atomnaya Énergiya*

July, 1980

Volume 48, Number 1 January, 1980

CONTENTS

	Engl.	Russ.
ARTICLES		
Chemical Systems for Obtaining Tritium in Thermonuclear Power Generation — V. G. Vasil'ev.	1	3
Direct-Flow Scheme of Reactor with Smooth Tubular Fuel Elements for Maneuverable Atomic Power Plant — V. N. Smolin, V. I. Esikov, Yu. I. Mityaev, and S. A. Vasil'ev.	8	9
Regulating Reaction Neutron Field Using Inverse Models — I. Ya. Emel'yanov, E. V. Filipchuk, P. T. Potapenko, and V. G. Dunaev.	12	12
Statistical Estimation of Fast-Reactor Fuel-Element Lifetime — A. A. Proshkin, Yu. I. Likhachev, A. N. Tuzov, and L. M. Zabud'ko . .	17	16
Effect of Cold Working on the Radiation Swelling of Metals — N. A. Demin and Yu. V. Konobeev	22	20
Determination of the Adiabatic Compressibility, Isentropy Index, and Other Properties of Two-Phase Media — V. S. Aleshin	28	24
Neutron Resonances of Osmium Isotopes in the 1-550 eV Range — T. S. Belanova, S. I. Babich, A. G. Kolesov, and V. A. Poruchikov . .	33	28
LETTERS TO THE EDITOR		
Coice of Some Characteristics of Fast Breeder Reactor at Various Stages of Nuclear Power Development — M. F. Troyanov, V. G. Ilyonin, V. M. Murogov, V. Ya. Rudneva, and A. N. Shmelev.	39	33
Calculation of Reactor Water Flow Rate for Purification of Coolant in Boiling-Water Single-Loop Atomic Power Plants — V. V. Gerasimov, O. I. Martynova, O. T. Konovalova, and T. I. Kosheleva.	41	34
Reactivity Coefficients of Materials in Fertile Media with $K_\infty \approx 1$ — V. A. Dulin, Yu. A. Kazanskii, and V. F. Mamontov	43	35
Comparison of Cross Sections for the Production of ^{115}Cd and ^{140}Ba in the Photofission of ^{235}U, ^{238}U, ^{237}Np, and ^{239}Pu — P. P. Ganich, V. I. Lomonosov, and D. I. Sikora	45	36
Behavior of Boiling Reactor during Withdrawal of Shim Rods — R. E. Fedyakin and E. V. Kozin	48	38
Gamma Dose Buildup Factors in Air — I. N. Butueva and I. N. Trofimov	49	39
Precision Method of Measuring Heat Release in Critical Assemblies — A. T. Bakov, V. A. Volkov, and R. A. Musaev	50	39
Effect of Hydrogen on the Error in Measuring the Content of Fissionable Nuclides by Neutron Methods — V. I. Bulanenko and V. V. Charychanskii .	53	41
Dependence of the Intensity of X-Ray Radiation Excited by Protons (Ions) on the Ion Energy and the Target Thickenss — V. F. Volkov, A. N. Eritenko, and Yu. A. Malykhin	55	43
Experimental Determination of Tritium Conversion Ratios — D. I. Efgrafova, Z. V. Ershova, V. K. Kapyshev, and V. I. Sakharov	59	44
Possible Use of ^{145}Sm Source for Isotope-Excited X-Ray Fluorescence Assaying of Tin Ores — V. V. Smirnov, A. P. Ochkur, N. G. Bolotova, A. D. Gedeonov, E. P. Leman, V. N. Mitov, and B. N. Shuvalov.	62	46

CONTENTS

(continued)

Engl./Russ.

Gamma Rays and Neutrons from ^{239}Pu Fluorides — V. V. Ovechkin. 65 48
Effect of Additive Simulating Fission Products on the Elasticity Characteristics of UC — S. A. Balankin, V. S. Belevantsev, A. S. Bubnov, V. A. Zelyanin, R. B. Kotel'nikov, and D. M. Skorov 68 49

The Russian press date (podpisano k pechati) of this issue was 12/25/1979. Publication therefore did not occur prior to this date, but must be assumed to have taken place reasonably soon thereafter.

ARTICLES

CHEMICAL SYSTEMS FOR OBTAINING TRITIUM IN THERMONUCLEAR POWER GENERATION

V. G. Vasil'ev

UDC 539.17:541.121.124

In order to obtain tritium — the main component of the deuterium—tritium fuel in a thermonuclear reactor (TNR) — lithium material can be used by two methods, the optimization of which is the subject of considerable study nowadays [1-3]. In the first method the TNR serves as the source of neutrons which are used for the reproduction of tritium, and in the lithium zone of the blanket (the shield of the reactor the conditions necessary for the production and separation of tritium are created. In the second method the TNR is used for obtaining energy and nuclear fuel in a hybrid variant; this method uses tritium produced in fission reactors. This production can be carried out by the use of a symbiotic system [3] using molten salts, or by irradiating solid lithium materials [4-6].

There are two variants of the utilization of lithium materials: prolonged radiation for the accumulation of tritium, and short-term radiation for the production of tritium in the reactor itself [7]. Consequently, in order to obtain tritium from lithium materials, two chemical systems can be considered — a closed system and an open system.

In the closed system there is no mass exchange with other systems, but the system receives and gives off energy. The lithium material is situated in a hermetically sealed vessel and receives energy which is removed by heat transfer. The thermodynamic potential tends to a minimum value, and ΔG is negative.

In the open system there is both matter and energy exchange with other systems, i.e., both the mass and the energy can change. The system does not reach equilibrium; the process continues until the system changes its mass or energy (or both). In the open system, products of the nuclear reaction and radiolysis are taken out of the system.

We consider the connection between the amount of tritium accumulated in 1 cm^3 of lithium material and the irradiation time for the neutron flux density of 10^{13} neutrons/cm^2·sec and an effectiveness coefficient of 0.1 (Table 1). The first days of operation of a thermonuclear reactor are characterized by a tritium concentration of $\sim 10^{-2}$–10^{-4} mg/cm^3 in the lithium materials. The optimum amount of tritium in lithium materials irradiated in fission reactors can be accumulated in a few months [3].

When the tritium content of the lithium material is $\sim 10^{-2}$–10^{-1} mg/cm^3, for the closed system we can speak of the existance of an independent lithium tritide phase (when metallic lithium or its alloys with other metals are irradiated) or solutions of tritium water in the original oxygen compounds of lithium. Consequently, the closed system must be analyzed from

TABLE 1. Lithium Irradiation Time for Obtaining the Necessary Concentration of Tritium

Amount of tritium in 1 cm^3		Amount of lithium burned up for a density of 0.5 g/cm^3, mass %	Irradiation time, days
mg	atom		
10^{-4}	$2 \cdot 10^{16}$	$4 \cdot 10^{-5}$	0,23
10^{-3}	$2 \cdot 10^{17}$	$4 \cdot 10^{-4}$	2,3
10^{-2}	$2 \cdot 10^{18}$	$4 \cdot 10^{-3}$	23
10^{-1}	$2 \cdot 10^{19}$	$4 \cdot 10^{-2}$	230
1	$2 \cdot 10^{20}$	$4 \cdot 10^{-1}$	2300
10	$2 \cdot 10^{21}$	4	—

Translated from Atomnaya Énergiya, Vol. 48, No. 1, pp. 3-8, January, 1980. Original article submitted December 25, 1978.

0038-531X/80/4801-0001$07.50

TABLE 2. Products of Thermal Dissociation and Radiochemical Processes in Lithium Compounds

Chemical compound	Thermal dissociation		Radiolysis products	Source
LiH	$LiH \rightarrow Li + 0{,}5\ H_2$	500 °C	Colloidal lithium, hydrogen	[9—11]*, [12,13]†
$LiAlH_4$	$LiAlH_4 \rightarrow LiAlH_2 + H_2$	180–210 °C		
	$LiAlH_2 \rightarrow LiH + Al + 0{,}5\ H_2$	230–280 °C	Colloidal lithium, hydrogen	[14—17]*, [18]†
	$LiH \rightarrow Li + 0{,}5\ H_2$	370—480 °C		
$LiNO_3$	$LiNO_3 \rightarrow LiNO_2 + 0{,}5\ O_2$		Oxide of Li_2, $LiNO_2$, N_2, O_2	[19—21]*, [22—24]†
$LiNO_2$	$LiNO_2 \rightarrow 0{,}5\ Li_2O + 0{,}5\ NO + 0{,}5\ NO_2$			
Li_2C_2	$Li_2C_2 \rightarrow 2Li + 2C$	600 °C	Lithium, graphite	[25]*
LiF	LiF Vaporization	800 °C	Colloidal lithium, fluorine	[26,27]*, [28,29]†
	$LiF \rightarrow Li + 0{,}5F_2$	1300 °C		
Li_2O	Li_2O Vaporization	1000 °C	Li, O_2‡	[30—33]*
	$Li_2O \rightarrow LiO$, Li, O_2	1400 °C		
$LiAlO_2$	$LiAlO_2 \rightarrow Li + 0{,}5\ Al_2O_3 + 0{,}25\ O_2$	1400 °C	Li, O_2‡	[34—36]*
Li_2SO_4	$Li_2SO_4 \rightarrow$ Vaporization	600 °C	SO_3, SO_2, O_2	[37—39]*, [40—43]†
	$Li_2SO_4 \rightarrow Li_2O + SO_2 + 0{,}5\ O_2$			
Li_2SiO_3	$Li_2SiO_3 \rightarrow$ Vaporization			
Li_4SiO_4	$Li_2SiO_3 \rightarrow Li_2O + SiO_2$		Li, Si, O_2‡	

*By thermal dissociation.
†By radiolysis.
‡Hypothesis.

the viewpoint of the equilibrium state with respect to phases containing lithium in one or another chemical form.

For an equilibrium chemical system we use the well-known phase rule $C = K - \Phi + n$ (C is the number of thermodynamic degrees of freedom of the system, which defines the largest number of factors that can vary independently of one another, i.e., the number of independent parameters which completely define the state of the system in equilibrium; K is the number of independent components of the system that take part in the formation of the chemical compound; Φ is the number of phases; n is the number of external factors affecting the state of equilibrium in the given system. The component parts of the system are determined by K, which can be taken equal to the number of chemical elements making up the compound, plus the tritium formed in the system. The number of phases can be predicted if we determine the value of n. The systems under consideration are acted upon by pressure, temperature, and radiation (γ radiation, neutrons, and "hot" particles — helium and tritium).

The temperature regime of the irradiation of lithium materials, taking account of the construction of the ampule, the distribution of neutrons through the material as a function of the ^6Li concentration in it, and the thermophysical properties and composition of the gaseous phase, is the subject of an independent investigation. If we compare the results of the action of various types of radiation and high temperatures on the chemical compounds of lithium, we note that the products formed are identical (Table 2). The mechanism of formation of the products of dissociation of chemical compounds under heating and under the influence of hot particles is probably the same, since a high temperature is observed in the tracks of heavy particles of helium and tritium [8]. For metallic systems the action of radiation does not lead to the formation of chemical products of radiolysis except for the products of the nuclear reaction of helium and tritium. Consequently, the number n can be taken equal to 2, and for closed systems with lithium materials acted upon by neutron irradiation, the phase rule is written in the form $C = K - \Phi + 2$. The equilibrium in the system is affected by only two external factors — temperature and pressure.

The results of calculations of the number of phases and the composition of lithium systems for two-component, three-component, and multicomponent systems for different values of C are shown in Table 3. Metallic lithium and systems based on it are characterized by the formation of lithium tritide, which is considered in a lithium—lithium-tritide system in [44-46]; for lithium alloys with aluminum the formation of a three-phase system is most probable [47].

In three-component systems formed upon the irradiation of LiF, Li_2O, and Li_2C_2, the formation of systems with three or four phases is probable. For LiF the most probably result is the formation of a system with colloidal lithium; thus, the compound LiF·HF dissociates at a temperature of ∿200°C [48].

TABLE 3. Number and Composition of Phases for Closed Systems with Lithium and Lithium Compounds

System	No. of components, K	No. of deg. of freedom, C	No. of phases, Φ	Composition of phases (assumed)
Li—T	2	0	4	Gaseous phase Solid phase; lithium, lithium tritide Liquid phase
		1	3	Gaseous phase Solid phase; lithium, lithium
		2	2	Gaseous phase Solid phase: solid solution of lithium tritide in lithium
Li-Al (alloy with 3% lithium by mass)-T	3	0	5	Gaseous phase Solid phase: LiAl in alpha phase, LiAl in beta phase lithium tritide Liquid phase
		1	4	Gaseous phase Solid phase: LiAl in alpha phase, LiAl in beta phase lithium tritide
		2	3	Gaseous phase Solid phase: LiAl in alpha phase, lithium tritide
Li_2O—T	3	0	5	Gaseous phase Solid phase: Li_2O, LiOT, LiO Liquid phase
		1	4	Gaseous phase Li-Al (alloy with 3% lithium by mass)-T
		2	3	Gaseous phase Solid phase: Li_2O, LiOT,
Li_2SO_4—T	4	0	6	Gaseous phase Solid phase: Li_2SO_4 solid solution of T_2O in Li_2SO_4, solid solution of SO_3 in Li_2SO_4 Liquid phase
		1	5	Gaseous phase Solid phase: Solid solution of T_2O in Li_2SO_4, solid solution of SO_3 in Li_2SO_4, Li_2SO_4 solid solution of T_2O and SO_3 in Li_2SO_4
		2	4	Gaseous phase Solid phase: Li_2SO_4 solid solution of T_2O in Li_2SO_4 solid solution of SO_3 in Li_2SO_4

For systems with more than three components (irradiation of Li_2SO_4, $LiAlO_2$, etc.) the most probable number of degrees of freedom is two, since here it is possible that solid solutions of water with the original substance will be formed. For Li_2SO_4 the number of phases is equal to four, which is confirmed by the results of investigations of the systems Li_2SO_4 — SO_3 and Li_2SO_4 — H_2O — SO_3 [49-51].

Increasing the number of components in the system is reflected in the redistribution of tritium among the phases formed, whose number also increases. For hydrogen compounds of lithium containing Li_2O, Al_2O_3, SiO_2 and other oxides, tritium oxide will be distributed among these components.

The above reasoning gives us some idea of the formation of new phases and of the chemical state of tritium in closed systems acted upon by radiation. The quantitative relations can be found by means of thermodynamics, taking account of specific systems and the conditions of their irradiation, which vary with time.

The displacement of equilibrium (the removal of some of the products of the system) is carried out by vacuuming, using a carrier gas, and as a result of chemical reactions with the walls of the ampule or various types of absorbers. Under these conditions the system is regarded as open. We can regard as open systems the lithium materials irradiated during the first hours and days of operation of a thermonuclear reactor and a fission reactor. Published experimental data [52] on the properties of irradiated inorganic compounds of lithium (the kinetics of the generation of tritium and helium, the chemical forms of tritium in irradiated lithium compounds, radiolysis products) relate to the initial stages of irradiation. These data, in combination with data on the thermal properties of compounds, are necessary for a description of open systems.

The chemical forms of tritium formed in the lithium material as a result of the nuclear reaction can be predicted on the basis of the nuclear chemistry of hot particles. The slowing-down of hot atoms in the energy region in which they do not react is subject to laws

TABLE 4. Variation of log $P_{sat} = f(T)$ and Average Values of Heat of Vaporization

Compound and composition, mole	Temperature, °K	Method of measurement	$\lg P_{sat} = f(T)$, Hg	Heat of vaporization, kcal/mole	
				expt.	published data
LiF	833—1133	Langmuir	$\lg P = -\frac{11,85 \cdot 10^3}{T} + 8,34$	54,3±4,0	58,27 [26]
		Knudsen	$\lg P = -\frac{13,41 \cdot 10^3}{T} + 10,65$	61,0±4,0	67,6 [26]
BeF_2	833—1033	Langmuir	$\lg P = -\frac{9,60 \cdot 10^3}{T} + 7,62$	44±3,0	47—55 [64—65]
		Knudsen	$\lg P = -\frac{8,8 \cdot 10^3}{T} + 8,17$	40,5±3,0	
LiF—NaK—KF	833—1133	Langmuir	$\lg P = -\frac{9,25 \cdot 10^3}{T} + 6,65$	42,4±4,0	
46,5—11,5—42		Knudsen	$\lg P = -\frac{10,6 \cdot 10^3}{T} + 9,25$	48,6±4,0	
LiF—BeF_2	833—1033	Knudsen	$\lg P = -\frac{9,62 \cdot 10^3}{T} + 7,96$	44,0±3,0	
50—50		Langmuir	$\lg P = -\frac{8,70 \cdot 10^3}{T} + 6,40$	40±4,0	
LiF—BeF_2	833—1033	Knudsen	$\lg P = -\frac{9,6 \cdot 10^3}{T} + 8,37$	44,0±3,0	
66,7—33,3		Langmuir	$\lg P = -\frac{8,2 \cdot 10^3}{T} + 5,14$	37,5±2,0	

which follow from the assumptions on the collision of elastic particles. In this case, the slowing-down spectrum is calculated on the basis of equations which describe the process of thermalization of the neutrons [53]. The reactions of tritium recoil atoms take place through the direct single-stage interaction of the recoil atom with individual atoms, or more precisely, with chemical bonds. To calculate the yield of an individual tagged compound from a two-component system, the following expression has been proposed [54, 55]:

$$R_{ij} = (f/\xi)\, I - (f^2/\xi^2)\, K,$$

where f is the geometric probability of collision; ξ is the average logarithmic decrement of energy. The results of calculations performed for lithium halides, using experimental data on the tritium yield R from these compounds [18], are shown in Fig. 1. It can be seen

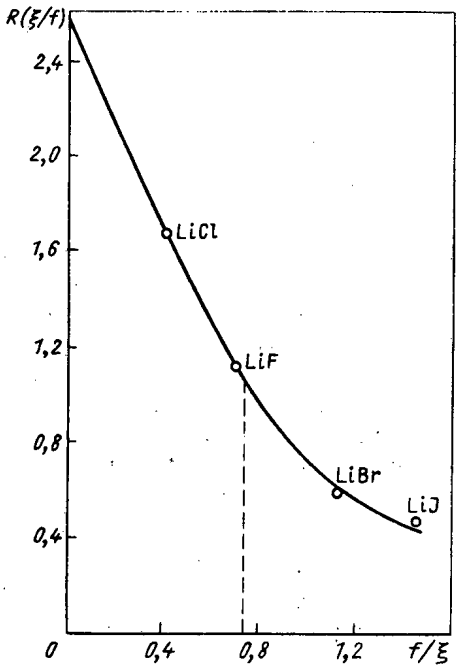

Fig. 1. Variation of R as a function of f/ξ for various compounds: ---) Li_2BeF_4; o) experiment.

TABLE 5. Phase Composition after Vaporization of Fluoride Systems in a Vacuum

System and composition mole %	Specimen	Vaporization temp, °C	Loss of mass, %	Composition, mass, %		
$LiF-BeF_2$ 50 50	Original composition			Li 9,6	Be 12,32	
	Solid residue	560	5,72	11,0	12,4	
$LiF-BeF_2$ 66,6 33,4	Original composition			14,15	9,09	
	Solid residue	660	6,35	14,64	9,15	
	Same	660	7,28	15,94	9,09	
	» »	760	20,2	12,2	7,54	
	» »	760	27,9	18,82	6,67	
$LiF-NaF-KF$ 46,5 11,5 42				Li	Na	K
	Original composition			7,91	6,41	39,7
	Solid residue	660	11,3	8,4	7,5	40,7
	Same	660	25,0	9,3	8,1	33,6
	Condensate	660		3,16	1,6	53,5

that we do not have a rigorous linear dependence of $R(\xi/f)$ on f/ξ. However, for Li_2BeF_4 we can determine R by calculating f and ξ. Calculations show that 70-80% of the tritium will be produced in the form of T_2, and the rest in the form of TF.

The thermal stability of lithium materials can be considered by using the example of nitric acid, sulfuric acid, and fluorine compounds, some of which form the basis of melts proposed for use in reactors. Here we should emphasize the connection between thermal and radiochemical stability. At a certain temperature, the rate of thermal dissociation will be greater than the rate of radiolysis, since the recombination processes for radiolysis products play an important role in the result of the annealing of defects. The rate of generation of dissociation products by the thermal method will be greater than the rate of their radiation generation, i.e., $G_0 I < (N/M) K_0 \exp(-E/RT)$. Using the example of $LiNO_3$, we can show that for $E = 15.8$ kcal/mole, $K_0 = 1.25 \cdot 10^{-1}$, $G_0 = 5.5$ ion/100 eV, and power $I = 10^{18}$ eV/(g·sec) at which the material is not heated above (100°C, $T < E/(2.3R \log K_0 N/MIG_0)$. At ~500°C, the chemical effect of the radiation in the decomposition of $LiNO_3$ is much less than the thermal effect.

For sulfate systems with lithium which contain $BeSO_4$, analogous laws should be noted. In the system Li_2SO_4 — $BeSO_4$ there is a eutectic 38 mol.% $BeSO_4$) with a melting point of 480 ± 5°C [56, 57]. Investigations of the equilibrium pressure of gaseous products of dissociation, the kinetics of thermal dissociation, eutectics, and $BeSO_4$ [58-60] have shown that a melt of a eutectic is thermally stable in a vacuum up to 600°C. The annealing of the products of γ radiolysis in these compounds takes place up to 500°C [43].

Melts of eutectic compositions in the systems LiK/SO_4, $LiNa/SO_4$, and $LiNaK/SO_4$ have a high thermal stability, since the salts in these systems are thermally stable up to 1000°C [39]. Analysis of the sublimates and the residue of a melt after vaporization of 7 and 20% by mass of the eutectic $LiNaK/SO_4$ (900°C) showed that the ratio of the alkali metals does not change and that there is no sulfate-ion depletion of the melt. The results obtained indicate that in these systems it is possible to have a transfer of mass of a substance through vaporization, and the action of radiation under the conditions of an open system leads to dissociation and removal of the gaseous products (O_2, SO_2, SO_3) [42, 43].

Mass transfer in the fluoride systems LiNaK/F, LiBe/F becomes significant, since they have highly volatile components [61-65].

For fluoride systems, there have been investigations of the rate of vaporization from an open surface (a platinum crucible) and from a diffusion chamber (nickel, copper; Clausing coefficient 0.8). The results of the calculations of the saturated vapor pressure are shown in Table 4. Beryllium fluoride was obtained by the thermal decomposition of ammonium fluoroberyllate in a vacuum [62, 63]. There was a change in the composition of the melt, which is illustrated by the data of Table 5. The tabulated properties of fluoride systems may complicate the production of tritium from them, since it may happen that the rate of vaporization of the material is close to the rate of extraction of the tritium.

Most of the inorganic thermally stable compounds of lithium do not have the drawbacks described above and are preferable for use in open systems, because of such properties as

TABLE 6. Chemical Systems in the Process of Irradiation

Characteristics of system	No. of burned-up atoms of ^6Li in 1 cm^3	Amount of tritium formed	
		mg/cm^3	Ci/cm^3
Open system*	$2 \cdot 10^{15}$ $2 \cdot 10^{16}$ $2 \cdot 10^{17}$	10^{-5} 10^{-4} 10^{-3}	10^{-4} 10^{-3} 10^{-2}
Transition region†	$2 \cdot 10^{18}$ $2 \cdot 10^{19}$	10^{-2} 10^{-1}	10^{-1} 1
Closed system‡	$2 \cdot 10^{20}$ $2 \cdot 10^{21}$	1 10	10 100

*Far from the equilibrium state.
†Formation of phases, change of structure, influence of helium on the mechanical properties of the material, fracture of the material.
‡Transition to the equilibrium state, formation of gaseous and solid phases containing tritium.

low vapor pressures, radiation stability, and safe operation in a reactor [66]. However, there are some experimental data [67] which indicate that lithium oxide is volatile at temperatures above 1000°C, especially in the presence of water.

The proposed classification of chemical systems enables us to find the connection between them when they are considered in the process of irradiation over the entire range of available concentrations of tritium in lithium materials. Table 6 shows the connection between the systems and the conditions of their existence. For tritium concentration of less than 10^{-1} Ci/cm^3 in the material, the system may be regarded as an open system far from the equilibrium state, whereas for a tritium concentration of more than 1 Ci/cm^3, it may be considered a closed system approaching equilibrium. The boundaries of the transition region are indicated provisionally, since the transition of the system from open to closed depends on the properties of the lithium material, the irradiation conditions, and the free volume.

Open nonequilibrium systems can be used in the tritium reproduction zone of the blanket of a TNR when arrangements are made for the continuous method of tritium production, whose advantages for TNR are described in [7]. The description of open systems requires a study of the chemistry of tritium at low concentrations (10^{-1}-10^{-2} Ci/g) in lithium materials, the behavior of helium, and the radiolysis products and their properties.

LITERATURE CITED

1. E. P. Velikhov et al., in: Proceedings of the All-Union Conference on Engineering Problems of Thermonuclear Reactors [in Russian], Vol. 1, Izd. GKIAÉ, NIIÉFA, Leningrad (1977), p. 5.
2. W. Price, Trans. Am. Nucl. Soc., 27, 78 (1977).
3. V. L. Blinkin and V. M. Novikov, Preprint IAÉ-2819, Moscow (1977).
4. A Method for the Continuous Production of Tritium. Czechoslovakian Patent No. 103871, Publ. June 15, 1962.
5. United States Patent No. 3079317, Class 204-154.2, Publ. Feb. 26, 1963.
6. Japanese Patent No. 030998, Class C0 1B4/00G21G, Publ. Mar. 20, 1974.
7. V. G. Vasil'ev et al., At. Energ., 44, No. 5, 440 (1978).
8. J. Deans and G. Vineyard, Radiation Effects in Solids [Russian translation], IL, Moscow (1960), p. 47.
9. D. Hurd, Chemistry of the Hydrides [Russian translation], IL, Moscow (1955).
10. E. E. Shpil'rain and K. A. Yakimovich, in: Lithium Hydride [in Russian], Standartov, Moscow (1972).

11. H. Ihle and C. Wu, J. Inorg. Nucl. Chem., 36, 2167 (1974).
12. F. E. Pretzel et al., J. Phys. Chem. Solids, 19, No. 14, 325 (1962).
13. E. L. Andronikashvili et al., in: Nuclear-Chemical Phenomena in Solids [in Russian], Metsniereba, Tbilisi (1968), p. 68.
14. V. L. Mikheeva et al., Dokl. Akad. Nauk SSSR, 109, 439 (1956).
15. J. Block and A. Gray, J. Inorg. Nucl. Chem., 4, No. 3, 304 (1965).
16. S. Aronson and E. Salzano, ibid., 8, No. 7, 1541 (1969).
17. M. McCarthy et al., J. Phys. Chem., 72, No. 12, 4009 (1968).
18. T. Costea and C. Mantescu, J. Inorg. Nucl. Chem., 28, 2777 (1966).
19. C. Hardy and B. Field, J. Chem. Soc., 11, 5130 (1963).
20. A. Brichler and J. Stanfer, J. Phys. Chem., 70, 4092 (1966).
21. E. A. Bordyushkova et al., Zh. Prikl. Khim., 11, No. 7, 1438 (1963).
22. Yu. A. Zakharov and V. A. Nevostruev, Usp. Khim., 37, No. 1, 143 (1968).
23. C. Hochandel, Rad. Res., 16, 286 (1962).
24. T. Ward et al., ibid., 33, 447, 456 (1968).
25. Yu. I. Ostroushko et al., in: Lithium, Its Chemistry and Technology [in Russian], Atomizdat, Moscow (1960), p. 52.
26. D. L. Hildenbrand et al., J. Chem. Phys., 40, 2882 (1964).
27. J. Berkowitz et al., ibid., 36, 2170 (1962).
28. L. I. Dzhordzhishvili et al., in: Electronic Processes in Solids [in Russian], Vol. 2, Menisreba, Tbilisi (1965), p. 19.
29. K. K. Shvarts and Yu. A. Ekmanis, in: Radiation Physics [in Russian], Vol. 4, Zinatne, Riga (1966), p. 111.
30. A. N. Nesmeyanov and L. P. Belykh, Zh. Fiz. Khim., 34, 841 (1960).
31. J. Berkowitz et al., J. Phys. Chem., 63, 644 (1959).
32. L. Brewer and J. Margrave, ibid., 59, 421 (1955).
33. W. Klewn and H. Scharf, Z. Anorgan. Chem., 303, 236 (1960).
34. O. S. Popkov and G. A. Semenov, Zh. Fiz. Khim., 45, 476 (1971).
35. D. Hildenbrand et al., J. Chem. Phys., 39, 2463 (1963).
36. D. White et al., ibid., 39, 296 (1963).
37. D. Powell and P. Wyatt, J. Chem. Soc. A, 3614 (1971).
38. W. Halstead, Trans. Faraday Soc., 66, 1966 (1970).
39. V. G. Vasil'ev and E. V. Dmitrievskaya, Zh. Fiz. Khim., 47, 2715 (1973).
40. H. J. Heal, Trans. Faraday Soc., 54, 1535 (1958).
41. V. V. Gromov and L. G. Karaseva, Khim. Vys. Energ., 1, 51 (1967).
42. L. G. Karaseva et al., ibid., 2, 562 (1968).
43. V. G. Vasil'ev and A. A. Vashman, ibid., 8, 349 (1974).
44. E. Veleckis et al., J. Less-Common Met., 55, 85 (1977).
45. E. Veleckis, J. Phys. Chem., 81, 526 (1977).
46. F. J. Smith et al., in: Proc. Conf. "Radiation Effects and Tritium Technology for Fusion Reactors," Gatlinburg, October 1-3, 1973, Vol. III, p. 539.
47. J. H. Owen and D. Randall, ibid., p. 433.
48. Yu. I. Ostroushko et al., [25], p. 63.
49. V. I. Spitsyn and I. E. Mikhailenko, Zh. Neorg. Khim., 2, 246 (1957); 3, 526 (1958).
50. V. G. Vasil'ev et al., ibid., 20, 2875 (1975).
51. V. G. Vasil'ev, ibid., 49, 1851 (1975).
52. V. G. Vasil'ev and E. V. Dmitrievskaya, Tritium in Inorganic Compounds of Lithium [in Russian], VNIINM, Moscow (1976).
53. A. M. Weinberg and E. P. Wigner, Physical Theory of Neutron Chain Reactors, Univ. of Chicago Press (1958).
54. E. S. Filatov and A. N. Nesmeyanov, Vestn. Mosk. Gos. Univ., Ser. Khim., 4, 13 (1964).
55. E. S. Filatov et al., Radiokhimiya, 4, 595 (1964).
56. I. I. Bosik et al., Zh. Neorg. Khim., 6, 256 (1961).
57. V. G. Vasil'ev et al., ibid., 19, 1601 (1974).
58. V. G. Vasil'ev and Z. V. Ershova, ibid., 17, 631 (1972).
59. V. G. Vasil'ev and E. V. Dmitrievskaya, Zh. Fiz. Khim., 47, 2715 (1973).
60. V. G. Vasil'ev and Z. V. Ershova, ibid., 46, 2958 (1972).
61. W. D. Powers et al., Nucl. Sci. Eng., 17, No. 2, 200 (1963).
62. V. G. Vasil'ev and V. S. Markov, Zh. Neorg. Khim., 21, 3215 (1976).
63. V. G. Vasil'ev, Zh. Fiz. Khim., 45, 1850 (1975).
64. N. É. Khandramirova et al., Zh. Neorg. Khim., 4, 2192 (1959).

65. V. I. Belousov et al., Zh. Fiz. Khim., 41, 2969 (1967).
66. V. G. Vasil'ev, in: Proc. US—USSR Symp. on Fusion—Fission Reactors, Livermore, July 13-16, 1976.
67. Van Arkel et al., in: Lithium [Russian translation], IL, Moscow (1959), p. 56.

DIRECT-FLOW SCHEME OF REACTOR WITH SMOOTH TUBULAR FUEL ELEMENTS FOR MANEUVERABLE ATOMIC POWER PLANT

V. N. Smolin, V. I. Esikov,
Yu. I. Mityaev, and S. A. Vasil'ev

UDC 621.039.577

At the present time plans for the European part of the Soviet Union call for the preferential growth of power plant capacity through the construction of atomic power plants. When atomic power plants account for 25-30% of the generating capacity of the energy systems it becomes necessary for the plants to operate with regulated load conditions. Hence there is the problem of constructing such special-purpose atomic power plants.

In creating a reliable and commercially viable atomic power plant to operate peak-load and semi-peak-load modes it is necessary to solve a number of complex engineering problems. The many aspects of this problem and possible ways of solving it were considered by N. A. Dollezhal' in [1] where, in particular, he showed that one of the main goals is to design a fuel element capable of withstanding repeated cyclical variations in the stresses as the result of variation of the thermal conditions under which it works. A possible variant of the solution to the problem is that of using tubular fuel elements of the dispersion type with a high thermal conductivity of the fuel composition, ensuring reliable thermal contact with the fuel cans. In such fuel elements, when the power changes by 1% the change in the temperature gradient in the cross section is 0.5-1.0°C whereas in the most common rod-type fuel elements of sintered uranium dioxide this change may reach 15-20°C [1]. With a frequently or rapidly varying load, such large temperature variations in rod-type fuel elements will lead to a considerable change in the stressed state of the structure and to its premature failure.

At the present time tubular fuel elements are made with steel cans, which worsens the neutron-physical characteristics of the reactor and increases the fuel component in the electricity costs. For a maneuverable power plant unit this disadvantage is felt less than for

TABLE 1. Experimental Data for Onset of Heat-Transfer Crisis

Mass velocity PW, kg/m²·sec	Pressure, MPa								
	7,85			9,8			11,8		
	t_{in}, °C	N_{cr}, kW	x_{out}	t_{in}, °C	N_{cr}, kW	x_{out}	t_{in}, °C	N_{cr}, kW	x_{out}
250	106	231,3	1,09	107	222,7	1,04	103	208,4	0,95
	152	214,5	1,11	155	204,5	1,06	134	194,1	0,91
	195	196,9	1,09	197	186,9	1,05	180	180,5	0,98
	238	177,3	1,08	254	160,4	1,04	268	140,3	0,96
	280	156,7	1,07	299	137,8	1,02	309	123,9	0,99
500	183	328,0	0,81	143	328,2	0,68	131	314,0	0,59
	199	316,0	0,82	175	308,0	0,71	175	283,0	0,60
	211	308,0	0,83	229	263,0	0,72	229	237,5	0,61
	245	279,5	0,84	265	233,0	0,73	283	190,0	0,63
	283	242,3	0,84	299	200,0	0,75	314	157,5	0,62
1000	278	330,0	0,53	255	334,0	0,42	248	332,0	0,36
	289	309,5	0,53	269	311,5	0,43	256	316,0	0,37
				283	292,0	0,44	270	296,0	0,38
				301	264,5	0,46	283	273,5	0,39
							313	217,5	0,40

Translated from Atomnaya Énergiya, Vol. 48, No. 1, pp. 9-12, January, 1980. Original article submitted March 25, 1979.

0038-531X/80/4801-0008$07.50

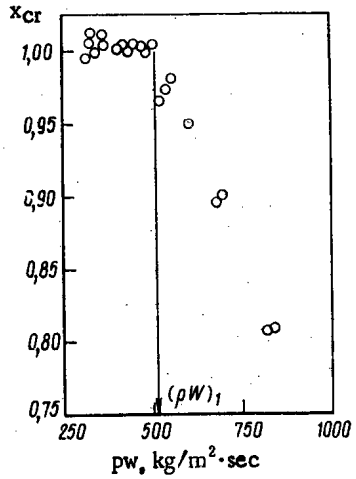

Fig. 1

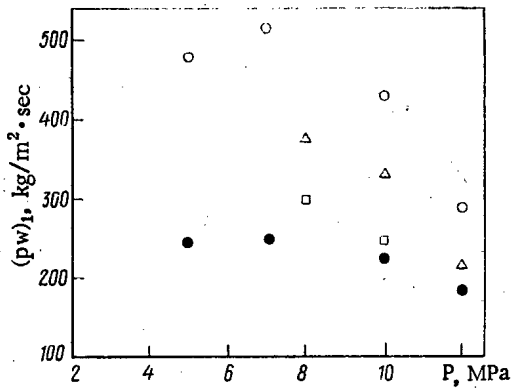

Fig. 2

Fig. 1. Example of determination of largest value of mass velocity $(\rho w)_1$ at which the critical steam content is equal to unity (P = 7.0 MP, d = 10.0 mm, L = 4960 mm [5]).

Fig. 2. Mass velocity $(\rho w)_1$ vs pressure: O) data of [5] (d = 10.0 mm, L = 4960 mm); ∇, □) data of present paper (d = 18 and 22 mm, respectively, L = 6000 mm); ●) data of [4] (d = 24.7 mm, L = 7100 mm).

atomic power plants operating under basic load conditions. However, the I. V. Kurchatov Beloyarsk Atomic Power Plant has achieved a substantial uranium burn-up (up to 30 kg/ton), which is high favorable for the economics of such atomic power plants. Moreover, tubular fuel elements with internal cooling have one more advantage over the rod type: preservation of the radiation cleanliness of the machine room should a fuel element break. This makes it possible to reduce the capital expenditures for the organization of radiation protection.

Since in the case of a maneuverable atomic power plant it is particularly important to ensure minimum unit capital expenditures, it is necessary in particular to employ the simplest flowsheet for the power unit. Furthermore, simplification of the flowsheet and elimination of some equipment increase the operating reliability of the atomic power plant. From this point of view, it is desirable to use a direct-flow arrangement with delivery of steam from the reactor directly to a turbine [2], thus making it possible to eliminate circulation pumps, steam separators, and the attendant fittings and piping, and thus significantly reduce the capital expenditures.

The principal obstacle to the construction of direct-flow reactors is the heat-transfer crisis during boiling, which is accompanied by a marked increase in the temperature of the fuel elements. This effect is initiated in some section of the fuel element when the coolant flow reaches a certain state. Thus, e.g., with present parameters for coolant in RBMK boiling reactors and the reactors of the Beloyarsk Atomic Power Plant (BAÉS) the heat-transfer crisis arises at a mass steam content x_{out} 0.3-0.4. It is possible to use various types of heat-exchange intensifiers in order to extend the range of crisis-free operation with respect to the outgoing steam content. However, this entails complication of the fuel elements and the introduction of additional structural materials into the reactor core. Moreover, the efficiency of the intensifiers depends on a change in the rate of coolant flow, which hinders the use of intensifiers with a variable load on the power plant.

There is another possibility of constructing a direct-flow system of coolant circulation with smooth tubular fuel elements with subcritical parameters. It is known that at a pressure below 10-12 MPa, as the mass velocity of the coolant decreases the heat-transfer crisis shifts to the region of higher values of steam content. As shown below by the results of experimental studies on the limiting power N_{cr} of imitators of tubular fuel elements, conducted in the Scientific Research and Design Institute of Power Engineering, for some ranges of operating parameters of coolant the heat-transfer crisis does not occur right up to total evaporation of the liquid in the channel. These results may serve as a real basis for the construction of a direct-flow reactor.

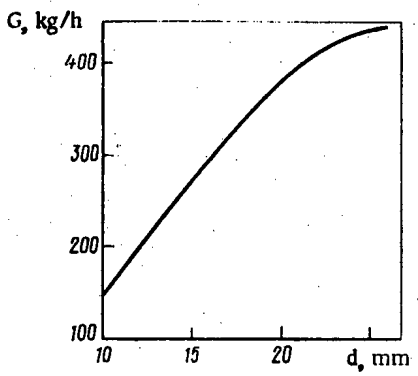

Fig. 3

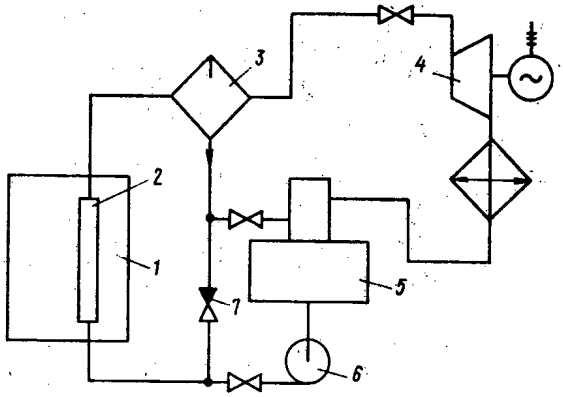

Fig. 4

Fig. 3. Coolant flow rates corresponding to values of $(\rho w)_1$ vs fuel-element diameter.

Fig. 4. Block diagram of atomic power plant with direct-flow reactor: 1) water—graphite reactor; 2) evaporator channels; 3) steam drier analogous to the centrifugal separator of once-through steam generators; 4) turbogenerator; 5) deaerator; 6) feed pump; 7) check valve.

The investigations were performed on a closed circulation facility. For the fuel-element imitators we used electrically-heated tubes of corrosion-resistant steel with a variable wall thickness over their length (this gave the necessary profile of heat liberation over the length of the tube, close to a cosinusoidal profile with the coefficient $q_{max}/q_{min} = 4$). The coolant motion was from the bottom to the top.

The heat-transfer crisis was recorded by thermocouples arranged over the length of the fuel-element imitator at intervals of 100 mm. This made it possible to monitor the section in which the heat-transfer crisis was initiated. With small mass velocities of the coolant the crisis always arose in the inlet section of the imitator so that the critical value of the steam content practically coincided with the outgoing steam content. Jumps in the temperature during the heat-transfer crisis did not exceed 100°C. The experimental set-up was described in detail in [3].

The experiments were conducted on imitators with an internal diameter of 14.6, 18, and 22 mm and a length of 6000 mm at a pressure P ranging from 7.85 to 15.7 MPa; mass velocity ρw ranging from 250 to 2000 kg/m^2·sec, and an incoming coolant temperature t_{in} of 80°C up to a temperature which is 10-15°C below the saturation temperature at the given pressure.

As shown by the experiments, at 7.85-9.8 MPa and coolant mass velocities of 250-350 kg/m^2·sec worsened heat-transfer conditions arise only when the balance mass steam content slightly exceeds unity. This is explained by the nonequilibrium steam and water flow when, with a balance steam content of unity is reached, in fact wet steam is flowing and the moisture contained in the flow is sufficient to wet the heat-liberating surface at moderate thermal fluxes ($q < 1 \cdot 10^6$ W/m^2).

Table 1 gives the experimental data characterizing the onset of worsened heat-transfer conditions for an imitator with an internal diameter of 22 mm. As seen from Table 1, at a pressure of 7.85 and 9.8 MPa and a mass velocity of 250 kg/m^2·sec the heat-transfer crisis does not occur over the entire range of steam contents right up to unity. With the growth of the pressure and the mass velocity, the critical value of the steam content decreases. Similar results were also obtained in [4, 5] in experiments with uniform heat liberation over the length.

Analyzing the results we obtained, we can determine a region of operating and geometrical parameters at which the limiting power is maximum for the case when the critical steam content is close to unity. Presenting the experimental data in the form of the plot of the critical steam content against the mass velocity (Fig. 1), we can find the largest value of mass velocity $(\rho w)_1$ at which the critical steam content is unity.

The maximum values of the mass velocity $(\rho w)_1$ found in this way for imitators of different diameters are given in Fig. 2. It is easily seen that in the pressure range 6-8 MPa the value of $(\rho w)_1$ is maximum. In the pressure range 3-12 MPa the value of $(\rho w)_1$ decreases as the imitator diameter is enlarged.

The values of the coolant flow rate corresponding to the maximum values of $(\rho w)_1$ for various imitator diameters are plotted in Fig. 3. It is seen from Fig. 3 that with an increase in the imitator diameter the coolant flow rate corresponding to the maximum value of the critical steam content increases, but does so nonlinearly, and its increase ceases as the imitator diameter approaches 22 mm. Since the limiting power of the fuel element is proportional to the coolant flow rate, it can be said that it reaches its greatest value at a fuel-element diameter $\sim$25 mm.

Analysis of the experimental data implies that the following coolant parameters are optimal (from the point of view of maximum power under crisis-free conditions for the fuel element): pressure 6-9 MPa, and mass velocity 250-300 kg/m^2·sec with an internal fuel-element diameter of 25-20 mm, respectively.

On the basis of the results it is appropriate to consider in greater detail the possibility of constructing a nuclear power plant of the direct-flow type with subcritical coolant parameters and smooth tubular fuel elements and to make an approximate assessment of its capabilities. The tentative design characteristics of the reactor are given below:

Thermal power of reactor, MW	1500
Electrical power of reactor, MW	500
Steam pressure at core outlet, MPa	7-8
Moisture content of steam at core outlet	0.15
Steam capacity (in terms of saturated steam), tons/h	3000
Feedwater flow rate, tons/h	3500
Feedwater temperature, °C	160
Maximum power of fuel channel, kW	1800
No. of fuel channels	1180
No. of fuel elements in channel	7
Internal diameter of fuel element, mm	22-25
Height of core, m	6
Diameter of core, m	8-9
Uranium charge in core, tons	70-80
Specific power of uranium, MW/ton	21.5-19
Uranium enrichment, %	2.0
Mean burn-up of unloaded uranium, MW·day/kg	20

The block diagram of the proposed atomic power plant is given in Fig. 4. Water from a deaerator is sent by a feed pump into parallel connected evaporator channels in which it is evaporated to a mass steam content of 0.85, which ensures the necessary reserve with respect to the heat-transfer crisis. From the channels the wet steam enters the steam drier where the liquid phase is separated from the steam. Then the steam is directed to the turbine and the liquid phase goes to the deaerator.

The pressure at the outlet from the evaporator channels can be recommended withing the limits 7-8 MPa and the internal diameter of the tubular fuel elements of the evaporator channels, 22-25 mm.

The proposed flowsheet does not rule out the possibility of nuclear superheating of the steam. The increase of somewhat more than 7-8 MPa that is necessary in pressure at the outlet of the evaporator channels does not lead to any appreciable reduction of the maximum power with the fuel-element diameter adopted (see Fig. 2).

Reliable cooling of the fuel elements in the evaporator channels is ensured by the following provisions. The coolant flow rate is assumed to be such that the critical steam content would be close to unity. The choice of a value of 0.85 for the operating mass steam content ensures a crisis-free operating conditions for the evaporator channels. The use of a feed pump for forced circulation makes it possible to get the necessary degree of orificing of the evaporator channels and their fuel elements in order to ensure the thermal-hydraulic stability of the flow rates in them. With the reactor at low power (at the level of the residual heat liberation) the fuel elements may cool down because of natural circulation through the line with the check valve.

Thus, the advantages of the proposed direct-flow reactor with subcritical parameters (reduction of capital costs, reduction of electricity consumption for internal needs, increase in reliability by elimination of pieces of equipment) hold out good promise for the construction of a maneuverable atomic power plant.

LITERATURE CITED

1. N. A. Dollezhal', At. Energ., 44, No. 3, 203 (1978).
2. P. I. Aleshchenkov, A. V. Bakanov, and G. A. Zvereva, in: Soviet Papers from Conf. on Twentieth Anniversary of Atomic Power [in Russian], Vol. II, Obninsk (1974), p. 99.
3. V. N. Smolin, V. I. Esikov, and S. V. Shpanskii, in: Problems of Atomic Science and Engineering. Series "Reactor Construction" [in Russian], No. 1, TsNIIatominform, Moscow (1972), p. 122.
4. K. Becker and C. H. Ling, KTH-NEL-13, Royal Inst. Technol., Stockholm (1970).
5. K. Becker et al., KTH-NEL-14, Royal Inst. Technol., Stockholm (1971).

REGULATING REACTOR NEUTRON FIELD USING INVERSE MODELS

I. Ya. Emel'yanov, E. V. Filipchuk, P. T. Potapenko, and V. G. Dunaev

UDC 621.039.562

A method of regulating the reactor neutron field by means of an reciprocal (inverse) model was proposed in [1]. The algorithm of [2] is a generalization of this method for an arbitrary distribution of sensors and control rods with a restriction on the control-rod displacements. In [3], a method of modal regulation developed for the stabilization of the reactor energy distribution at the Gently 1 atomic power station was described. Essentially, this algorithm too may be related to the algorithms with an inverse model. The aim of the present work is to extend the inverse-model method to the regulation of a large channel reactor for which neutron-field stabilization is a most urgent problem.

Harmonic-Regulation Algorithm

The neutron-field dynamics of the given reactor may be described with sufficient accuracy by a quarter adiabatic model [4]

$$\varphi(p) = \{A_0 W_0(p) + A_1 W_1(p) + A_*\}\,\mathbf{k}(p), \tag{1}$$

where $\varphi(p)$ is the deviation vector of the neutron field from the steady profile; $\mathbf{k}(p)$ is the perturbation or control vector.

In accordance with Eq. (1), the change in the neutron field due to perturbation of the reactivity may be described by the superposition of three independent motions:

1) the fundamental motion, with the transfer function of the fundamental harmonic $W_0(p)$ and the statistical transfer matrix A_0

$$\varphi_0(p) = A_0 W_0(p)\,\mathbf{k}(p); \tag{2}$$

2) azimuthal motion, with the transfer function of the first azimuthal harmonic $W_1(p)$ and the statistical transfer matrix A_1

$$\varphi_1(p) = A_1 W_1(p)\,\mathbf{k}(p); \tag{3}$$

3) noninertial redistribution over the high harmonics, associated with the matrix of stable form A_*

$$\varphi_* = A_*\mathbf{k}(p). \tag{4}$$

Translated from Atomnaya Energiya, Vol. 48, No. 1, pp. 12-16, January, 1980. Original article submitted July 17, 1978; revision submitted January 9, 1979.

0038-531X/80/4801-0012$07.50

It must be particularly emphasized that the dynamic characteristics of these motions are significantly different. The statistical matrices A_0, A_1, and $A*$ may be calculated by a semiempirical method [4].

The idea of an inverse model will now be used to construct an algorithm for the regulation of the neutron-field harmonics using a controlling computer. Note that, in the terminology adopted in [5], the realization of this algorithm corresponds to the lowest level of the hierarchy — direct control of the reactor using specialized autonomous mini- and microcomputers.

It is assumed that r fuel-element rods (up to tens) from the total number m of rods, and n neutron-flux detectors inside and outside the reactor are chosen for the stabilization of the fundamental and first azimuthal harmonics. According to the algorithm proposed, the controlling action compensating for the deviation of the neutron field from the base distribution consists of the sum of three components, which are realized by the regulation loops of the fundamental deviation harmonic, the azimuthal harmonic, and the higher harmonics

$$\mathbf{k}_0 = A_0^+ \varphi W_0^p;$$
$$\mathbf{k}_1 = A_1^+ \varphi_1^p;$$
$$\mathbf{k}_* = A_*^+ \varphi.$$

Here A_0^+, A_1^+, and A_*^+ are the pseudoinverse matrices of the matrices A_0, A_1, and $A*$, respectively. The regulator transfer functions W_0P and W_1P of the first two loops are chosen from the optimal-correction conditions for the functions of the fundamental and first azimuthal harmonics.

As a result of the large difference in the characteristic time constants of the unstable harmonics being regulated, the periodicity in the calculation of the controlling-action components also differs. For example, in the regulation loop for the fundamental harmonic or integral power, the action $\mathbf{k}_0$ is calculated with a period of 0.1-0.5 sec, whereas in the azimuthal-harmonic loop the period may reach several seconds. For the stable-higher-harmonic regulation loop, the calculation of the controlling action may have an even larger period. This separation allows the accuracy and reliability of regulation to be increased and — a very important feature — allows the requirement on the computational power of the controlling computer to be reduced. As a result of the instrumental separation of the harmonic-stabilization subsystems (using a microcomputer), the reliability and flexibility of the control system as a whole may be increased.

Consider how compensation of the deviation from the neutron-field base profile occurs in accordance with the given algorithm. The synchronous (unidirectional) r-rod displacement compensating an increment in the total power is achieved in accordance with an error signal, equal to the weighted sum of the deviations from the steady detector-signal level

$$\varepsilon_0 = \sum_{i=1}^{n} \alpha_i^0 \varphi_i, \tag{5}$$

where the weighting factors α_i^0, elements of the pseudoinverse matrix A_0^+, are identical for all the r rods when they lie in the equalized region, and are determined from the reading of each detector with respect to the base distribution. Calibration of the total reactor power from the signals of all n detectors inside and outside the reactor allows it to be maintained at a given level with high accuracy.

As follows from the mathematical model in Eq. (1), the deviation of the neutron field from the base distribution after compensation of the fundamental harmonic is mainly determined by the first azimuthal harmonic. The independent displacement of the j-th rod for its liquidation is determined by the error signal

$$\varepsilon_j^1 = \sum_{i=1}^{n} \alpha_{ij}^1 \varphi_i. \tag{6}$$

Here the weighting factors α_{ij}, the elements of the h-th row of the inverse-coupling matrix A_1^+, are determined from the values of the first azimuthal harmonic at the detector sites. Because all the n detectors are involved in calculating the amplitude of the azimuthal harmonic, the stabilization accuracy is increased.

In compensating the other increment due to superposition of the higher harmonics of the deviation from the base distribution, it is expedient to use all m control rods (of the

order of 100 in RBMK-type reactors), performing local regulation. Since the matrix A_0^+ is sharply attenuated (it lacks any elements of long-range coupling due to the fundamental and first azimuthal harmonics), the rod displacement is calculated practically from the signals of the nearest detectors only.

Compensation of the higher harmonics is basically a higher-level problem in the hierarchy of neutron-field regulation systems or even a problem of energy-distribution optimization, i.e., obtaining the base distribution [6]. Therefore, in the light of these consideration, it is assumed that the problem of compensating the higher harmonics is solved by an "operator adviser" program [5, 6].

Overall, the increase in harmonic-stabilization accuracy and reliability as a result of the maximal (in comparison with zonal regulation) use of reactor information may be regarded as an advantage of the given algorithm. It must be emphasized that this algorithm allows erroneous information to be easily discarded, since the calculation of the harmonic amplitudes proceeds with excess information.

As an illustration of the algorithm and the structure of the regulation system, consider this striking example. Suppose that four rods are positioned symmetrically with respect to the quadrants at the maximum in the radial function of the first radial—azimuthal harmonic. All the detectors and rods are positioned in the equalized region, with a neutron field of relative magnitude 1; the detector readings in each quadrant are added and averaged ("zonal" detector). For the matrix of the fundamental harmonic (power) A_0, all the terms of which are 1, the pseudoinverse matrix has identical elements, equal to 1/16. Thus, in the integral-power stabilization loop, the error signal for each rod is equal to the sum of the detector signals with a weighting of 1/4, i.e., each rod must compensate a quarter of the existing reactivity discrepancy.

In the stabilization loop of the first azimuthal harmonic, the appropriate form of the inverse-coupling matrix is

$$A_1^+ = \begin{bmatrix} 1/4 & 0 & -1/4 & 0 \\ 0 & 1/4 & 0 & -1/4 \\ -1/4 & 0 & 1/4 & 0 \\ 0 & -1/4 & 0 & 1/4 \end{bmatrix}.$$

Each detector is taken into account with a weighting of 1/4; the signals of detectors in different halves of the reactor take different signs with respect to each rod. Thus, each opposite pair of rods is moved in opposite directions, and compensates half of the available reactivity discrepancy associated with the sine and cosine components of the first azimuthal harmonic.

An important practicaly difference between the present algorithm and the algorithm of zonal or local regulation is that algorithms based on the inverse model use the amplitudes of the perturbed harmonics directly as error signals, rather than the value of the neutron field at the monitoring points, as in algorithms based on the local-regulation principle. However, combined systems are also possible.

Use of Local Regulators

Assume that on the basis of a few inertialess detectors a local-regulation algorithm is realized; analog realization is also possible. On a computer with a period considerably exceeding the time constant of β-emission detectors (a few minutes), the controlling action for the integral-power loop

$$\mathbf{k}_0 = A_0^+ \varphi$$

has been calculated by the given scheme, together with that for the azimuthal-harmonic stabilization loop

$$\mathbf{k}_1 = A_1^+ \varphi,$$

where φ is the vector of the field deviation from the base distribution, taking into account the work of local regulators.

Using obvious relations, the expected change in field distribution at the detector sites is found in accordance with the controlling actions obtained

$$\delta\Phi_0 = A_0 A_0^{\dagger}\varphi;$$
$$\delta\Phi_1 = A_1 A_1^{\dagger}\varphi. \qquad (7)$$

The results obtained are now used to correct or calibrate the local-regulator settings. At each of the r local regulators, a vector component $\delta\Phi_1$ is added to the corresponding setting, and to the setting of the integral-power regulator a vector component $\delta\Phi_0$. If the loops are combined (system without special power regulator) and the correction—calculation periods are the same for both loops, the i-th setting is calibrated by means of the value $(\Delta\Phi_0 + \delta\Phi_1)_i$.

It is important to note that the scheme with correction of the settings is particularly effective for the case when the matrix of the form A* relating the rod displacements to the signals of the corresponding detectors is not degenerate, which is certainly the case with local regulation. Then, specifying the optimal local-detector reading as the setting guarantees the optimal rod position. In particular, for a system of local regulation, the matrix A* may be taken to be diagonal.

In constructing a regulation system with detectors of different dynamic characteristics, an idea outlined in the review [7] may be used. The controlling-action calculation scheme corresponding to this may be elucidated for the example of the azimuthal-harmonic stabilization loop. The error signal for the rod displacement is formed of three components: the inertialess component

$$\varepsilon_1' = \sum_{k=1}^{l} \alpha_k^1 \varphi_k,$$

where l is the number of inertialess detectors; the weighted sum of the inertial component with the β-emission-detector function $W_g(p)$

$$\varepsilon_1'' = \sum_{i=1}^{n} \alpha_i^1 \varphi_i,$$

where n is the number of "slow" detectors of the inertial component; and the inertial component

$$\varepsilon_1''' = -\sum_{k=1}^{l} \alpha_k^1 \varphi_k W_g(p),$$

which compensates the first component in statics.

Thus, the dynamic behavior is mainly determined by the noncalibrated component ε_1' and the static by the calibrated component ε_1''. In comparison with the setting-calibration scheme, this scheme places a larger burden on the controlling computer, since the calculation of all the error-signal components must be carried out in the rhythm of change of the inertial-detector signal, and therefore analog realization of the filters W_g is more convenient. The structure based on local regulators is more effective for the stage of experimental verification and the initial period of introduction of the harmonic-stabilization system.

Regulation of High Harmonics

In regulating the radial energy distribution, considerable perturbation of the axial distribution is introduced. One of the methods of neutralizing the effect introduced by the regulation system for the radial energy distribution on the first (the most significant azimuthal subharmonic) high harmonic is to use a pair of upper and lower rods which are displaced in opposite directions, positioned in two nearby channels, as the regulating organ in each loop. This organ has an effect on the multiplication factor which is symmetric over the height, and as a result the first high harmonic is practically not excited.

A further development of the idea of independent harmonic regulation for the stabilization of the first high harmonic is an autonomous system which does not affect the integral power nor the azimuthal—radial distribution. On the basis of the inverse-model method, the difference in signals of the upper and lower detectors may be taken as the error signal of this system, while the regulating organ may be taken in the form of an abbreviated rod in the central part of the active region or a pair of upper and lower rods moving in the same direction, which may also be combined into a single rod divided by a nonabsorbing

section [6]. This regulating organ exerts the same controlling influence in the upper and lower halves of the active region.

Regulation of Higher Harmonics

Now consider the compensation loop for deviations from the steady distribution associated with higher harmonics. On the basis of the attenuation properties of the matrix A_*^+, taking into account the control constraints, a simplified algorithm may be proposed for the calculation of the rod position, realized in the "operator adviser" mode.

Solving the system of linearized neutron-field equations [1], and neglecting small terms associated with lagging neutrons and feedback, an algorithm for the construction of an inverse model may be obtained, in the following form

$$k_j(p) = \frac{1}{\Phi_j} \sum_{i=1}^{\nu} b_{\nu j} [\varphi_j(p) - \varphi_i(p)], \tag{8}$$

where ν is the number of differences between the signals of the j-th detector and the adjacent (i) detectors to be summed; $b_{\nu j}$ are the weighting factors of the differences, depending on the type of approximation adopted for the Laplace operator, and the number and respective positions of the detectors participating in the approximation. This algorithm is valid for reactors with both positive and negative reactivity power factors; regulation of the lower harmonics associated with the terms of the initial equation ignored in the algorithm of Eq. (8) is then taken care of by the regulation loops for azimuthal and fundamental harmonics.

Thus, in accordance with Eq. (8), the necessary rod displacements are calculated from the relative curvature of the neutron-field deviation curve close to the corresponding rod.

The constraints on controlling actions may be taken into account, by analogy with the algorithm proposed in [2], using a simple logical procedure: the rods emerging at the end controls are fixed in this position, and the steady positions of the other rods are refined after several interations by pseudorotation of the matrix A_*, truncated as a result of eliminating the rods emerging at the ends.

In accordance with the concept of independent regulation of the neutron-field harmonics, it is necessary to add to the optimization-problem constraints at the higher hierarchy level, by analogy and in conjunction with the constraints that the total power be constant and that reactivity balance be observed, a constraint taking account of the azimuthal reactivity balance, i.e., the condition that the azimuthal harmonic be unexcited. Mathematically, this may be expressed as the condition that, to a given accuracy (with respect to the reactivity), the controlling actions must be equal for two pairs of overlapping reactor positions or, equivalently, over the active-region quadrant.

Conclusions

Further development of the existing concept of automatic regulation for RBMK-type reactors involves the isolation and stabilization of the unstable first azimuthal harmonic of the neutron-field. The given regulation algorithm, based on the inverse model, assumed independent (autonomous) regulation of N unstable harmonics in the general case. This allows the requirement that calculations on energy-distribution optimization be operational to be considerably reduced, and permits equipment subsystem separation, which increases the reliability of the system as a whole.

The essence of the algorithm is that what is regulated is not the neutron-field deviation from a steady profile at the control points but the amplitude of the corresponding harmonic calculated using the inverse model. The controlling action for each rod is calculated from the signals from all the detectors, which also increases the reliability and accuracy of regulation.

The characteristic features of several practical structures of direct-regulation systems for the first neutron-field harmonics have been considered. Numerous computation experiments on models have shown that the proposed algorithms are effective. The present method is one of the possible means of neutron-field stabilization.

LITERATURE CITED

1. P. T. Potapenko, At. Energ., 27, No. 3, 189 (1969).
2. I. Ya. Emel'yanov et al., At. Energ., 42, No. 4, 263 (1977).
3. J. Kendall, in: Proceedings of Canadian Conference on Automatic Control, Fredericton (1973).
4. P. T. Potapenko, At. Energ., 41, No. 1, 25 (1976).
5. I. Ya. Emel'yanov et al., At. Energ., 44, No. 6, 483 (1978).
6. I. Ya. Emel'yanov et al., At. Energ., 44, No. 4, 310 (1978).
7. P. T. Potapenko et al., At. Tekh. Rub., No. 12, 3 (1977).
8. A. N. Kosilov et al., At. Tekh. Rub., No. 7, 17 (1975).

STATISTICAL ESTIMATION OF FAST-REACTOR FUEL-ELEMENT LIFETIME

A. A. Proshkin, Yu. I. Likhachev, A. N. Tuzov, and L. M. Zabud'ko

UDC 621.039.54

The accuracy of predicting fuel-element lifetimes in designing fast reactors is determined by several factors — the correctness of the model describing the stress—strain state, the applicability of the chosen fuel-element lifetime criteria, and the knowledge of the physicomechanical characteristics and behavior of the materials under conditions of irradiation.

On the basis of the available Soviet [1-3] and non-Soviet [4-6] experience in developing mathematical models for determining the fuel-element lifetime from an analysis of numerous experimental data, it may be concluded that the indeterminacy of the calculations associated with the models themselves (because of incompleteness in taking account of the factors that affect the fuel-element lifetime) is not the principal contribution to the indeterminacy of the calculation. The main contribution is evidently the inadequate knowledge of the physicochemical properties and behavior of the materials under conditions of irradiation.

At present, knowledge of material properties is limited, especially for neutron fluxes of more than 10^{23} neutron/cm^2 and $E > 0.1$ MeV, while the fuel elements of the projected reactors must operate at a neutron flux of $(2-3)\cdot10^{23}$ neutron/cm^2 and $E < 0.1$ MeV in conditions of high neutron-flux intensity and a high-energy spectrum. Therefore, the choice of fuel-element structure and permissible burnup depth is made, as a rule, on the basis of the most "pessimistic" estimates, i.e., for an unfavorable combination of parameters from the viewpoint of reliability of fuel-element operation. This approach is justified in the first stages of fast-reactor development because there is no experience of fuel-element operation in the conditions of a large fast reactor, and several properties of the materials have been little studied.

By performing a statistical analysis, it is possible to reflect more completely the general picture of the state of fuel-element operation, and to understand which characteristics or properties of the material introduce the most indeterminacy in the calculation of fuel-element lifetime and require urgent study. This analysis is also necessary for the statistical interpretation of experimental and theoretical data on fuel-element lifetime. The use of statistical methods also offers new approaches for the estimation of fuel-element lifetime. For example, whereas previously the limiting fuel burnup after which unsealing of the fuel elements could be expected was determined in the calculations, now the basic characteristic is the number of unsealed fuel elements at a given moment of reactor operation not exceeding the permitted value.

Translated from Atomnaya Énergiya, Vol. 48, No. 1, pp. 16-19, January, 1980. Original article submitted May 15, 1978.

0038-531X/80/4801-0017$07.50

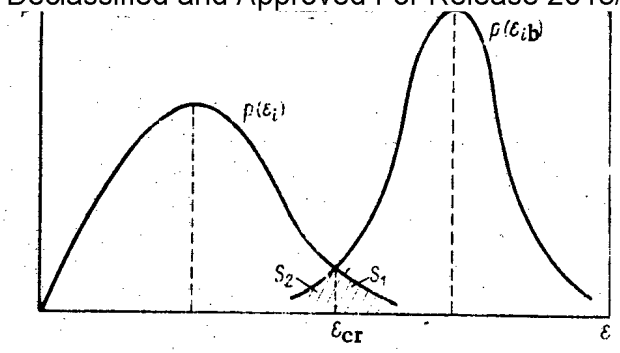

Fig. 1

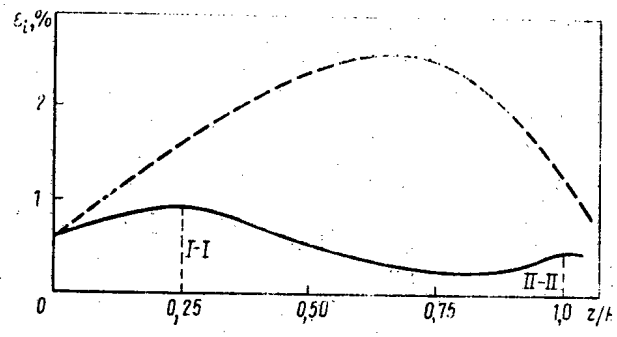

Fig. 2

Fig. 1. Probability-density distribution of calculated and breakdown strain values in the given cross section of the fuel-element shell.

Fig. 2. Distribution of total (---) and mechanical (———) strain over the height of the fuel element up to the end of reactor use.

Determining the Mathematical Expectations and Dispersions of Fuel-Element Lifetime Parameters

In calculating fuel-element lifetime from a particular model [1-3], the first step is to determine the kinetics of the fuel-element stress–strain state in the course of its operation in the reactor, and then the lifetime is estimated according to the chosen criterion. The calculation of the fuel-element stress–strain state depends on many parameters which are random quantities. Therefore, the state of the fuel-element determined is a function of random quantities. The problem is to find the numerical characteristics of this function (the mathematical expectation and dispersion) from the numerical characteristics of the arguments. The mathematical apparatus of probability theory allows the numerical characteristics of a function of random quantities to be found from the numerical characteristics of the arguments without taking their distribution laws into account. Such methods of directly determining the numerical characteristics are mainly applicable to linear functions. If the numerical characteristics of the arguments — the mathematical expectations ($m_{x_1}, m_{x_2}, \ldots, m_{x_n}$) and dispersion ($D_{x_1}, D_{x_2}, \ldots D_{x_n}$) — are given, the function $y = (x_1, x_2, \ldots, x_n)$ of the random quantities may be written in the form [7]

$$m_y = f(m_{x_1}, m_{x_2}, \ldots m_{x_n}); \tag{1}$$

$$D_y = \sigma_y^2 = \sum_{i=1}^{n} \left(\frac{\partial \varphi}{\partial x_i}\right) \sigma_{xi}^2 + 2 \sum_{i<j} \left(\frac{\partial \varphi}{\partial x_i}\right)\left(\frac{\partial \varphi}{\partial x_j}\right) r_{ij}\sigma_{x_i}\sigma_{x_j}, \tag{2}$$

where σ is the mean square deviation; r_{ij} is the correlation coefficient of x_i and x_j.

When $x_1, x_2, \ldots, x_n$ are not correlated, $r_{ij} = 0$ for $i \neq j$, and in this case

$$\sigma_y^2 = \sum_{i=1}^{n} \left(\frac{\partial \varphi}{\partial x_i}\right)^2 \sigma_{x_i}^2. \tag{3}$$

In some cases, there may be doubts as to the applicability of the linearization method; then the results must be improved by methods which retain in the expansion of the function not only linear terms but also those of higher order [7].

The criterion by which fuel-element lifetime in fast reactors is usually estimated is the degree of damage of the material ω or the intensity of inelastic mechanical strain ε_i [1]; hence, it is necessary to find the mathematical expectation and dispersion of these quantities at the given moment of time for the given fuel-element cross section.

In determining the dispersion of ω and ε_i in the framework of existing calculational programs [1], variation of the following parameters is performed: the yield point and creep rate of the fuel and shell materials (σ_{sh}, ξ_{sh}, $\bar{\sigma}_f$, $\bar{\xi}_f$); the swelling of the steel and the fuel (S_{st}, $\bar{\iota}_f$); the contact conductivity of the fuel–shell gap (α_c); the shell thickness and temperature (δ, T_{sh}); the pressure of the gaseous fission products (p_g); the fuel–shell gap (δ_G); the initial density of the fuel material ($\bar{\gamma}_f$); the volume heat liberation

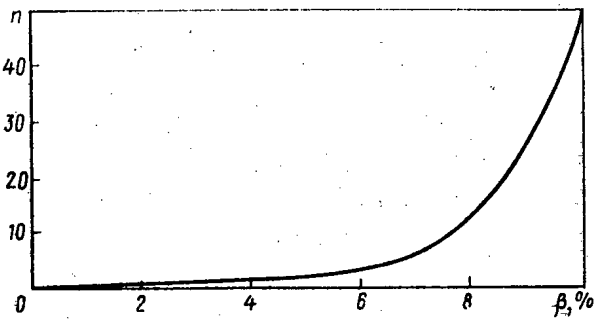

Fig. 3. Change in total number of unsealed fuel elements with increasing fuel burnup for an event reliability probability of 95%.

(q_V); the corrosion rate of the shell material at the heat-carrier side (ξ_{Na}) and the fuel side ($\xi_{C.f}$); the elastic modulus; linear-expansion coefficient and thermal conductivity of the shell and fuel materials (E, α, λ, $\bar{E}$, $\bar{\alpha}$, $\bar{\lambda}$). Correlational relations between the parameters are taken into account on the basis of the analytical dependences used in the calculational model.

In the present work, the mathematical expectations and dispersions of the parameters are calculated on the basis of Soviet and non-Soviet experimental data. For a sufficient number of experimental points (no less than 10) characterizing a given parameter, the mathematical expectation and dispersion are found from the well-known formulas of mathematical statistics. In the case of insufficient points, the dispersion is calculated assuming a normal distribution law of this parameter for given limiting values of its possible scatter.

Determining the Probability of Fuel-Element Unsealing

For a theoretical determination of the probability of fuel-element unsealing, it is necessary to know the distribution laws for ε_i and the breakdown values ε_{ib}.* At present, the distribution laws of these parameters are unknown, and therefore it may only be assumed that they are distributed according to some particular law. Since the values of ε_i cannot be negative, the choice adopted for this parameter was a normal logarithmic law [8], asymmetric to the right, which to a large degree reflects the physical aspects of the problem. A normal distribution law was chosen for the breakdown values ε_{ib}.

For any distribution laws of ε_i and ε_{ib}, the probability of fuel-element unsealing is written in the form

$$P_b = \int_a^b p(\varepsilon_{i_b})\, d\varepsilon_{i_b} \int_{\varepsilon_{ib}}^{b} p(\varepsilon_i)\, d\varepsilon_i, \tag{4}$$

where $p(\varepsilon_i)$ and $p(\varepsilon_{ib})$ are the probability densities of the calculated and breakdown strains; a and b are the limits of integration, depending on the form of the distributions $p(\varepsilon_i)$ and $p(\varepsilon_{ib})$.

For engineering applications, with the given choice of distribution laws, the probability of fuel-element unsealing may be determined according to [9] (Fig. 1)

$$P_b = P(\varepsilon_i > \varepsilon_{cr})\, P(\varepsilon_{ib} < \varepsilon_{cr}) = S_1 S_2, \tag{5}$$

where S_1 and S_2 are the shaded areas in Fig. 1.

Using the well-known dependence of [7, 8] for the normal logarithmic law and the normal distribution law of random quantities, Eq. (5) may be written in the following form

$$P_p = \left[\frac{1}{2} - \Phi\left(\frac{y - m_{\varepsilon_i}}{\sigma_{\varepsilon_i}}\right)\right]\left[\frac{1}{2} + \Phi\left(\frac{\varepsilon_k - m_{\varepsilon_{ip}}}{\sigma_{\varepsilon_{ip}}}\right)\right], \tag{6}$$

where m_{ε_i}, $m_{\varepsilon_{ib}}$, σ_{ε_i}, and $\sigma_{\varepsilon_{ib}}$ are the mathematical expectation and mean square deviation of the calculated mechanical strain and the breakdown strain for the fuel-element shell material; $y = \ln \varepsilon_{cr}$, while

*When the criterion ω is used, the approach is similar.

$$y = \ln \varepsilon_\kappa;\ \Phi(\xi) = \frac{1}{\sqrt{2\pi}} \int_0^{\xi} \exp\left(-\frac{1}{2}\xi^2\right) d\xi$$

is a Laplace function. Here

$$\xi = (x - m_i)/\sigma_i,\ x = \varepsilon_{br},\ y;\ i = \varepsilon_i,\ \varepsilon_{ib}.$$

The value ε_{cr} may be found from the relation

$$a_1\varepsilon_{cr}^2 - b_1\varepsilon_{cr} + l = d\ln^2\varepsilon_{cr} + c_1\ln\varepsilon_{cr}, \tag{7}$$

where

$$a_1 = \sigma_{\varepsilon_i}^2;\ b_1 = 2a_1 m_{\varepsilon_{ip}};\ c_1 = 2d(a_1 - m_{\varepsilon_i});\ d = \sigma_{\varepsilon_{ip}}^2;\ l = 2a_1 d\ln\frac{\sigma_{\varepsilon_{ip}}}{\sigma_{\varepsilon_i}} + a_1 m_{\varepsilon_{ip}}^2 - d m_{\varepsilon_i}^2.$$

After finding ε_{cr} from the solution of Eq. (7), the probability of fuel-element breakdown in the given cross section is determined from Eq. (6).

The conditions of fuel-element operation may differ significantly over the height (the level of radiational damage, shell temperature, etc.), which leads to the appearance of different physicomechanical properties of the shell material. In this case the probability of fuel-element unsealing may be determined, assuming that the conditions of operation in the individual sections are independent, from the relation

$$P_b = 1 - \prod_{i=1}^{n}(1 - P_{ib}), \tag{8}$$

where p_{ib} is the probability of fuel-element unsealing in the i-th zone.

After determining P_b, the lifetime of the fuel-element structure may be characterized by the reliability coefficient [8]

$$H = \lg(1/P_b).$$

Knowing the probability of unsealing of a single fuel element, and the number of fuel elements in the reactor active zone, the number of unsealed fuel elements at a definite moment of reactor operation may be found for a given reliable event probability [7].* Note that the probability of fuel-element unsealing P_b is an arbitrary quantity, and must be compared with the threshold of significance established on the basis of experience of fuel-element use.

At present, the permitted number of unsealed fast-reactor fuel elements is taken within the limits of 0.1-1% of the number of fuel elements in the active zone. This choice is determined by the conditions of overload and radiational shutdown of the reactor, the form of breakdown and the behavior of the defective fuel elements and their effect on the conditions of operation of the heat-liberating pile as a whole, the dismountability of the equipment, the conditions of fuel regeneration, etc. As experience of fast-reactor operation accumulates, this value will be further refined.

Results of the Calculations

According to the method outlined, a statistical analysis of the lifetime of fuel elements with oxide fuel (U, Pu)O_2 was conducted, for a steady power level of the fast reactor. In determining the fuel-element stress–strain state, the effect of irradiation on the physicomechanical properties and behavior of the shell and fuel material was taken into account.

Calculation of the total and mechanical strain over the height of the fuel element up to the end of reactor use for operation at constant power (fuel burnup $\beta = 10\%$ of heavy atoms) leads to Fig. 2. The probability of fuel-element unsealing up to the end of reactor use, as shown by calculations, is $P = 0.001$ (reliability coefficient $H = 3$). According to the calculation, fuel-element unsealing may occur predominantly in the region in the middle of the active region, while fuel-element unsealing in the upper cross sections is less probable.

*The calculations are made under the assumption that unsealed fuel elements have no effect on the lifetime of other fuel element.

Calculation of the relative contribution (%) of different factors to the total dispersion of the shell strain intensity for the calculational cross sections I—I and II—II (Fig. 2) leads to the following results

	I—I	II—II
ξ_{cst}	26	27
ξ_f	30	21
$l_{\tau f}$	16	11
S_{st}	15	3
δ	1	13
α_G	9	11
δ_{sh}	0	7
T_g	0,6	1,5
p_f	0,4	2
γ	2	3,5

*Taking account of shell-material corrosion.

The contribution of the other parameters is found to be practically negligible for the given conditions of reactor operation. As is evident, the greatest indeterminacy is introduced by parameters such as the steel creep rate (up to 30%); the swelling of the steel (up to 20%); the fuel creep rate (up to 30%); the swelling of the fuel (up to 20%); the shell-material corrosion (up to 15%); and the contact conductivity of the fuel—shell gap (up to 10%). The contribution of these parameters differs in each specific case depending on structure, operating conditions, and considered cross section of the fuel element. The contribution of the indeterminacy in the shell temperature to the total dispersion does not exceed a few percent. This is because, in steady conditions of reactor operation, the dispersion of the other parameters — primarily the physicomechanical properties of the materials — is large in comparison with the dispersion of the shell temperature or, in other words, the temperature conditions of fuel-element operation are known more accurately than certain properties of the materials.

With increased accuracy in the physicomechanical properties of the fuel-element materials, the role of the other parameters becomes larger. As calculations show, decrease in mean-square deviation of the physicomechanical properties of the materials by a half leads to an increase of almost an order of magnitude in the contribution of the temperature to the total dispersion ε_i. Note also that the indeterminacy associated with the breakdown values of prolonged plasticity, the damage coefficient of the material, and their dispersions introduces an error in determining the probability of fuel-element unsealing.

The change in the number of unsealed fuel elements as a function of fuel burnup for 40,000 fuel elements in the active zone of the reactor is shown in Fig. 3. As is evident from Fig. 3, the number of unsealed fuel elements begins to rise sharply after fuel burnup $\beta > 7\%$ of the heavy atoms.

Conclusions

On the basis of a statistical analysis, the main parameters having a significant influence on the theoretical determination of fuel-element lifetimes in the operation of power fast reactors in steady power conditions may be isolated. These include the creep and swelling of the fuel and shell materials, prolonged-plasticity lag, shell-material corrosion, gap contact conductivity, and the strain diagrams of the shell and fuel materials obtained for irradiated materials at the corresponding strain rates. By means of deeper investigation of these properties of the materials, it is possible to increase significantly the reliability of fuel-element lifetime predictions in designing fast reactors and to optimize the structure of fuel elements more correctly.

Another important result of the statistical analysis is information regarding the increase in the number of unsealed fuel elements with fuel burnup. It is shown that for the given conditions of reactor operation the number of unsealed fuel elements rises almost exponentially, beginning with a burnup $\beta > 7\%$ of heavy atoms. The results of such calculations must obviously be taken into account in the cost—benefit analysis of projected new reactors and in choosing the optimal fuel burnup.

LITERATURE CITED

1. Yu. I. Likhachev et al., in: Papers of the Second Symposium of COMECON Member-Countries [in Russian], Vol. 1, Obninsk (1973), p. 241.
2. Yu. I. Likhachev and V. Ya. Pupko, Strength of Nuclear-Reactor Heat-Liberating Elements [in Russian], Atomizdat, Moscow (1975).
3. Yu. I. Likhachev et al., At. Energ., 30, No. 2, 206 (1971).
4. J. Bump, Nucl. Appl. Tech., 9, No. 3, 37 (1970).
5. A. Boltax, Nucl. Technol., 16, No. 1, 42 (1972).
6. C. Cox and T. Homan, Nucl. Appl. Tech., 9, No. 3, 61 (1970).
7. E. S. Venttsel', Probability Theory [in Russian], Fizmatgiz, Moscow (1962).
8. G. J. Hahn and S. S. Shapiro, Statistical Models in Engineering, Wiley (1967).
9. I. A. Birger et al., Machine-Part Strength Calculations [in Russian], Mashinostroenie, Moscow (1966).

EFFECT OF COLD WORKING ON THE RADIATION SWELLING OF METALS

N. A. Demin and Yu. V. Konobeev

UDC 620.192.50

Cold working by 15-20% is now widely used for reducing the radiation swelling of austenitic stainless steels, which are now used as the chief construction material for parts of fast reactor cores and will probably be used for future first-generation thermonuclear reactors [1, 2]. Therefore, determination of the physical mechanisms through which the dislocations produced by cold working affect the swelling of the material is of practical and scientific interest. The assumptions [3-5] that the density of previously produced dislocations remains constant during irradiation are not supported by experimental data: The density of dislocations in a cold-worked material first decreases following exposure to a relatively small fluence and then reaches the value characteristic for the material irradiated in the annealed state as a result of the generation and growth of loops of interstitial atoms [6]. Simulation experiments have shown that the positive effect of cold working diminishes with an increase in the ion fluence [7]. According to reactor test data [8], cold working of austenitic stainless steel 304 shifts the swelling vs temperature curve toward higher temperatures and toward larger values of maximum swelling. Thus, the effect of cold working appears to be more complex than could be expected on the basis of simple considerations.

In connection with this, we analyzed the kinetics of metal swelling under irradiation with an allowance for radiation-stimulated annealing of the initial disclocations. The analysis is based on the assumption that the density of dislocations produced by cold working decreases at the start of irradiation due to the presence of fairly intensive sinks which do not have the capacity for preferred capture of any particular point defect (the so-called "neutral sinks"). Such sinks are considered to be screw dislocations, which are created during cold working in approximately the same numbers as edge dislocations. The analysis results indicate that such representation offers a better opportunity of explaining the observed trends in the swelling of metals irradiated in the cold-worked state.

Theoretical analysis of the metal swelling kinetics is performed on the basis of the function f(X, t) of vacancy pore distribution with respect to the number X of vacancies contained in them at the instant of time t. For the case where pores absorb and vaporize individual point defects, this equation assumes the following form:

$$\dot{f}(X, t) = J(X-1, t) - J(X, t), \quad (1)$$

where J(X, t) is the pore flux along the axis of X values.

For solving Eq. (1), we use an approach similar to that described [9], which is based on subdividing the axis of pore diameters d into groups. The number of pores Ni corresponding

Translated from Atomnaya Énergiya, Vol. 48, No. 1, pp. 20-24, January, 1980. Original article submitted July 24, 1978; revision submitted April 23, 1979.

 0038-531X/80/4801-0022$07.50

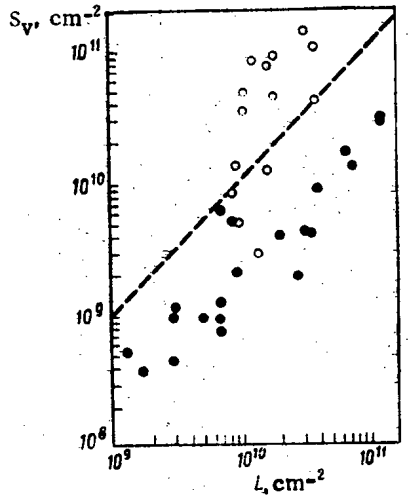

Fig. 1

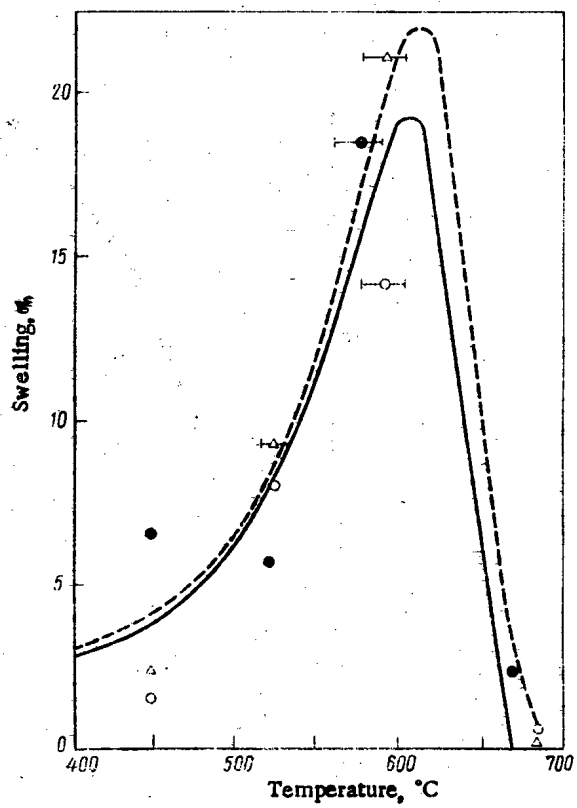

Fig. 2

Fig. 1. $S_V = 2\pi(d_V)N_V$ as a function of L, which is the total length of loops and dislocations in fast-neutron irradiated annealed austenitic stainless steels 316 (●) and 304 (○); ---) $S_V = L$.

Fig. 2. Temperature dependence of the swelling of austenitic stainless steel, irradiated in the annealed (———) and cold-worked (---) states. ●) Annealed stainless steel, dose of 72 displacements/atom; ○) cold-worked (20%) steel, dose of 81 displacements/atom; Δ) electron microscope data for cold-worked Steel 316, dose of 81 displacements/atom.

to the i-th group is described by an equation which is readily derived from Eq. (1) by integrating it with respect to all values of X in the given group.

From among the groups, we choose the group whose number is i = j, which includes the critical pore diameter

$$d_C = 4\gamma\Omega/KT \ln \frac{D_V C_V - D_i C_i}{D_V C_{V_0}}, \tag{2}$$

where D_V and D_i are the diffusion coefficients for vacancies and interstitial atoms, respectively, C_V and C_i are their concentrations established in the metal under irradiation, γ is the surface energy, $C_{V_0} = \exp(-E_V^f/KT)$ is the equilibrium concentration of vacancies, and E_V^f is the energy of vacancy formation.

For growing pores with the diameter $d_i > d_C$, in order to describe the transition from the i-th group to the (i+1)-th group, we assume that the flux J(X, t) is characterized by

$$J(X_i, t) = V_i(t) N_i, \tag{3}$$

where $V_i(t)$ is determined by the expression for the rate of change of the pore diameter (see Eq. (9)).

For dissolving pores ($d_i < d_C$), in describing the transition of pores from the i-th group, located to the left of the j-th group on the diameter axis, to the (i — 1)-th group, it is assumed that where

$$J(X_{i-1}, t) = W_{i-1}(t) N_i, \tag{4}$$

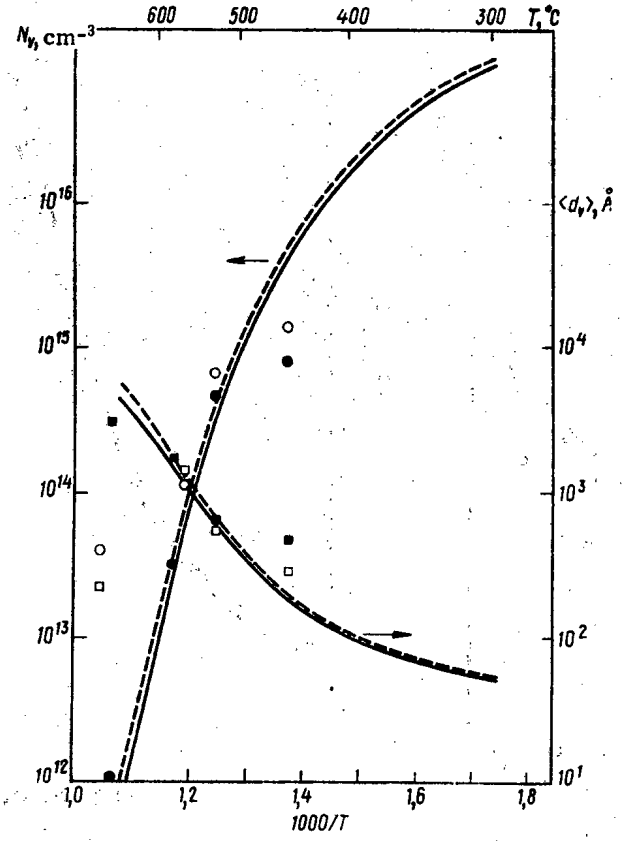

Fig. 3. Temperature dependences of the pore concentration and the mean diameter, calculated for stainless steel 316. ——) Annealed state, dose of 72 displacements/atom; ●) N_V; ■) $\langle d_V \rangle$; ---) cold-worked state, dose of 81 displacements/atom; ○) N_V; □) $\langle d_V \rangle$.

$$W_i(t) = \frac{d_i^3 - d_{i-1}^3}{d_{i+1}^3 - d_i^3} V_i(t). \tag{5}$$

A bivacancy is considered to be the smallest-diameter pore. Therefore, the left-hand boundary of the diameter axis corresponds to the dimension d_0, determined from $2 = \pi d_0^3/6\Omega$, where Ω is the atomic volume.

During the growth of sinks in the irradiated metal, the critical pore dimension can belong to different groups at different times. In order to describe more accurately the behavior of pores in the "critical group" j, the total number of pores N(j) in this group is subdivided into two parts: δ_1, pertaining to pores with the diameter $d_{j-1} \leq d \leq d_C$, whose size diminishes, and δ_2, which characterizes pores with the dimensions $d_C < d \leq d_j$, which pass to the neighboring group on the right ($\delta_1 + \delta_2 = 1$).

With the above approximations, the system of equations for N_i used here has the following form:

$$\begin{aligned}
\dot{N}_i &= W_{i-1}N_i - W_iN_{i+1} \quad \text{for} \quad 1 \leqslant i \leqslant j-2;\\
\dot{N}_{j-1} &= W_{j-2}N_{j-1} - W_{j-1}\delta_1 N_j;\\
\dot{N}_j &= W_{j-1}\delta_1 N_j - V_j\delta_2 N_j;\\
\dot{N}_{j+1} &= V_j\delta_2 N_j - V_{j+1}N_{j+1} + J_V(t);\\
\dot{N}_i &= V_{i-1}N_{i-1} - V_iN_i, \quad i \geqslant j+2,
\end{aligned} \tag{6}$$

where $J_V(t)$ is the pore generation rate.

The concentrations of vacancies and interstitial atoms are determined with respect to the well-known system of stationary balance equations:

$$K-\mu_R D_i C_i C_V - D_V C_V (D+D_0+L) + D_V C_{V0} (D_1+D_0+L_1) = 0;$$
$$K-\mu_R D_i C_i C_V - D_i C_i (D+D_0+\eta L) = 0, \quad (7)$$

where K is the rate of volume generation of point defects by bombarding particles, and μ_R is the coefficient of recombination of vacancies with interstitial atoms. The values of D and L characterize the intensities of pores and dislocations as point defect sinks, while D_1 and L_1 characterize their intensities as thermal vacancy sources. The parameter η reflects the enhanced ability of edge dislocations to absorb interstitial atoms, while D_0 accounts for the intensity of neutral sinks that are different from pores.

The rate of variation of the pore diameter d is determined under the assumption that the growth kinetics is surface-controlled, i.e.,

$$\dot{d} = \frac{2}{b_0}\left[D_V C_V - D_i C_i - D_V C_{V0} \exp\left(\frac{4\gamma\Omega}{dKT}\right)\right], \quad (8)$$

where b_0 is an adjusting parameter, which is independent of the temperature. Some of the calculations were performed for the diffusion-controlled growth of pores (see below). In this case, as is known, the 4/d factor figures instead of $2/b_0$ in the right-hand side of expression (8).

The choice of the expression for d determines the specific equations for D, D_1, and V_i. In particular, in using expression (8), the rate is

$$V_i(t) = \frac{6d_i^2}{b_0} \frac{D_V C_V - D_i C_i - D_V C_{V0} \exp(4\gamma\Omega/KTd_i)}{d_i^3 - d_{i-1}^3}. \quad (9)$$

The pore generation rate $J_V(t)$ is assumed to be

$$J_V(t) = AK/d_C^3, \quad (10)$$

where the constant A is the adjusting parameter. Although expression (10) does not have a theoretical basis, it provides a fairly good quantitative description of the pore concentration in stainless steel 316 after irradiation in a fast reactor in the temperature range 350-700°C. The expressions for $J_V(t)$ used in [3, 4, 9] do not have advantages over Eq. (10), since they contain a number of parameters that cannot be readily substantiated.

The value of L in Eqs. (7) is assumed to be equal to the total length of edge dislocations and loops per unit volume, while $L_1 = L$. Since a quantitative theory of the generation of dislocations under irradiation is presently lacking, the increase in L in the irradiated metal resulting from the generation and growth of loops is taken into account empirically, i.e., it is assumed that the total length L at any instant of time is directly proportional to the total pore diameter:

$$L = \rho_d^e + \beta 2\pi \langle d_V \rangle N_V, \quad (11)$$

where $\langle d_V \rangle$ and N_V are the mean diameter and the concentration of pores, respectively, ρ_d^e is the density of edge dislocations produced in the material during cold-working before irradiation (ρ_d^e varies in time as a result of the climb and annihilation of edge dislocations), and and β is the constant for the metal in question. Figure 1 indicates that the reactor test data for annealed stainless steel 316 support the existence of such a relationship [10, 11]. According to these data, $\beta = 5.5 \pm 2.0$ in the temperature range 370-700°C for an irradiation dose of up to 20-30 displacements/atom. The results given below were obtained for $\beta = 5.5$. It is also evident from Fig. 1 that, for a high fluence and a low temperature, this relationship also holds for reactor-irradiated stainless steel 304 [12] if we assume that the initial dislocation density is equal to $\rho_d = 10^{10}$ cm^{-2} and $\beta \approx 0.24$. The assumption concerning the existence of a linear relationship between L and $2\pi\langle d_V \rangle N_V$ must be introduced in order to explain the linear dependence of swelling on the dose, which is often observed in simulation experiments involving fast-particle irradiation of metals in accelerators.

The drop in the density of dislocations in the strained metal under annealing and irradiation conditions is caused by the climb and annihilation of screw and edge dislocations.

According to the latest concepts, edge dislocations in an irradiated metal climb due to the absorption of an excess flux of interstitial atoms. The uncompensated vacancy flux must run off to neutral sinks. In a cold-worked metal, the generation of pores at the initial stage of irradiation is suppressed. Therefore, edge dislocations will climb and be annihilated if screw dislocations, which, according to the isotropic elasticity theory do not interact at large distances with point defects (dilatation centers), play the role of intensive neutral sinks. It is known that a linear screw dislocation is unstable with regard to climb during the absorption of point defects and that it assumes the shape of a helicoid. The unwinding of the helicoids leads to the movement of screw dislocations, their mutual drawing together, and the subsequent annihilation if they are of opposite signs.

Assuming that the annihilation of climbing edge and screw dislocations that have been produced in the material by cold working occurs independently of the evolution of dislocation loops growing under irradiation, we can use the following equations to describe the variation in time of the densities of edge and screw dislocations ρ_d^e and ρ_d^s:

$$\dot{\rho}^e = -\alpha_e (\rho_d^e)^2 (\eta D_i C_i - D_v C_v + D_v C_{v0}),$$

$$\dot{\rho}_d^e = -\alpha_e (\rho_d^e)^2 (D_v C_v - D_i C_i - D_v C_{v0}), \qquad (12)$$

where α_e and α_s are constants, equal to the ratio of the fourfold annihilation radius to the Burgers vector. According to a rough estimate, $\alpha_e = 100$ if the maximum possible dislocation density in stainless steel amounts to $\sim 10^{12}$ cm^{-2} and the corresponding mean distance between dislocations, ~ 160 Å, coincides with the strong attraction radius, at which dislocations of opposite sign start to slide toward each other to be annihilated.

We used the following parameters in calculations: $E_V^f = 1.6$ eV; $D_V = 0.6 \exp(-1.3$ eV/kT) cm^2/sec; $\mu_R = 8 \cdot 10^{16}$ cm^{-2}; $\gamma = 10^3$ erg; $\Omega = 1.17 \cdot 10^{-23}$ cm^3 [$K = 10^{-6}$ displacements/(atom·sec)]. By solving simultaneously Eqs. (6)-(8) and (12), we calculated $\langle d_V \rangle$, N_V, the total dislocation density, and the swelling $S = (\Delta V/V)/(1 - \Delta V/V)$, where $\Delta V/V$ is the volume percentage occupied by pores. Numerous calculations were performed for the following initial states of the material and irradiation conditions.

A. Annealed stainless steel with an initial dislocation density of 10^9 cm^{-2}. The temperature range was 300-650°C. The radiation dose reached 72 displacements/atom (it was considered that the effect of a neutron fluence of 10^{22} neutrons/cm^2 at $E > 0.1$ MeV corresponded to a dose of 5.8 displacements/atom).

B. Cold-worked material with an initial dislocation density of $3 \cdot 10^{11}$ cm^{-2}, irradiated under the same conditions as material A.

Calculation Results and Discussion. The calculations of the pore characteristics for material A were performed in order to check the soundness of the model used and the chosen parameters. It is evident from Fig. 2 that the experimentally determined temperature dependence of swelling of stainless steel 316, irradiated in the annealed state 72 displacements/atom in an EBR-II reactor [13, 14], can be reproduced satisfactorily if the coefficient A in expression (10) is equal to $8 \cdot 10^{-8}$, while $b_0 = 2000$ Å (Eq. (8)) and $\eta = 1.033$. Attempts at describing the experimental data in the case of diffusion-controlled growth of pores were unsuccessful. Therefore, the calculations for annealed and cold-worked materials were performed under the assumption of the surface-controlled kinetics of pore growth.

As was to be expected, the observed drop in dislocation density in the cold-worked material after irradiation to 10 displacements/atom and the temperature dependence of swelling cannot be explained by assuming, as before, that the density of the dislocations produced remains constant during irradiation ($\rho_{d_0}^e = 3 \cdot 10^{11}$ cm^{-2}; $\rho_{d_0}^s = 0$). Calculations show that this conclusion also holds in the case where the intensity of screw dislocations as neutral sinks remains at a moderate ($\rho_{d_0}^s = 10^{10}$ cm^{-2}) and constant level, while the density of edge dislocations varies under irradiation in accordance with Eq. (12). The observed behavior of the dislocation density can be described if the values of ρ_d^e and ρ_d^s are initially equal and then vary according to Eqs. (12). In Fig. 2, the dashed curve illustrates the temperature dependence of swelling for material B, calculated for a dose of 81 displacements/atom and $\alpha_e = \alpha_s = 100$. It is evident that cold working shifts the temperature curve by approximately 15°C toward higher temperatures and toward higher values of maximum swelling. This phenomenon becomes more pronounced as α_e and α_s increase. The predicted behavior of swelling is in qualitative agreement with reactor test data for stainless steel 304 in

the cold-worked state [8] and for stainless steel 316 [13]. Calculations show that the temperature behavior as well as the maximum value of swelling can be varied considerably by changing the ratio of the densities of edge and screw dislocations in the initial microstructure of the metal.

The calculated relationship for the swelling of annealed and cold-worked materials in the dose range 0-50 displacements/atom is close to a power relationship, i.e., $S \sim (Kt)^n$, where $n \approx 1.4$ at 400°C, after which it increases, reaching 3.6 and ~5 at 650°C for annealed and cold-worked materials, respectively. Calculations show that cold-working leads to an increase in the "incubation period" of swelling: In the 0.1% swelling range, the "incubation" doses at 600°C amount to 8 and 20 displacements/atom for materials A and B, respectively. The steeper rise in the swelling of the cold-worked material indicates that the beneficial effect of cold working diminishes as the radiation dose increases.

Figure 3 shows the theoretical dependences (for $\alpha_e = \alpha_s = 100$) of the concentration and the mean diameter of pores on the irradiation temperature as well as the electron-microscope data [14] for stainless Steel 316, irradiated in the annealed and cold-worked (20%) states in an EBR-II reactor to neutron fluence values of $1.25 \cdot 10^{23}$ and $1.4 \cdot 10^{23}$ neutrons/cm^2 ($E > 0.1$ MeV), respectively. It is evident from Fig. 3 that, apart from the range of low temperatures, agreement with experimental data is fairly satisfactory for annealed stainless steel. For cold-worked stainless stell, such agreement is observed only in the 500-600°C range. At 650°C, with a dose of 72 displacements/atom, the calculated pore concentrations and mean diameter were larger in the case of material B ($N_V = 4.2 \cdot 10^{11}$ cm^{-3}; $\langle d_V \rangle = 5450$ Å), rather than in the case of material A ($N_V = 3.4 \cdot 10^{11}$ cm^{-3}, $\langle d_V \rangle = 4320$ Å). Analysis shows that this increase is connected with the stimulating effect of moderate values of the edge dislocation density on the rate of pore generation at the start of irradiation. However, the measured N_V values exceed considerably those found by calculation for the cold-worked material. Moreover, the observed pore concentrations in cold-worked stainless steel 316 proved to be higher than in annealed steel. The abnormally small mean diameter of pores in cold-worked stainless steel 316, irradiated at 650°C with a dose of 81 displacements/atom, apparently indicates that evolving helium affects the generation and growth of pores at high temperature, which has not been taken into account in the model discussed here.

LITERATURE CITED

1. J. Laidler, B. Mastel, and F. Garner, in: Properties of Reactor Structural Alloys after Neutron or Particle Irradiation, ASTM STP 570. American Society for Testing and Materials (1975), p. 415.
2. G. Kulcinski, in: Proc. of IAEA Workshop on Fusion Reactor Design Problems, Vienna, IAEA (1974), p. 479.
3. S. Harkness, J. Grappel, and S. McDonald, Nucl. Technol., 16, 25 (1972).
4. S. Harkness, J. Tesk, and Che-Yu-Li, Nucl. Appl. Technol., 9, 24 (1970).
5. R. Bullough and R. Perrin, in: Proc. Reading Conf. on Voids Formed by Irradiation of Reactor Materials, Harwell, BNES (1971), p. 79.
6. H. Brager and J. Straalsund, J. Nucl. Mater., 47, 105 (1973).
7. W. Johnston et al., J. Nucl. Mater., 48, 330 (1974).
8. T. Kenfield, W. Appleby, and H. Busboom, Am. Nucl. Soc. Trans., 24, 146 (1977).
9. S. Harkness and Che-Yu-Li, Met. Trans., 2, 1457 (1971).
10. H. Brager and J. Straalsund, J. Nucl. Mater., 46, 134 (1972).
11. P. Barton, B. Eyre, and D. Stow, in: Proc. European Conf. on Irradiation Behavior of Fuel Cladding and Core Component Materials, Karlsruhe, Dec. 3-5, 1974, p. 65.
12. D. Michel and H. Smith, in: Properties of Reactor Structural Alloys after Neutron or Particle Irradiation, ASTM STP 570. American Society for Testing and Materials (1975), p. 156.
13. T. Kenfield, W. Appleby, and H. Busboom, Am. Nucl. Soc. Trans., 26, 210 (1979).
14. T. Kenfield et al., J. Nucl. Mater., 75, 85 (1978).

DETERMINATION OF THE ADIABATIC COMPRESSIBILITY, ISENTROPY INDEX, AND OTHER PROPERTIES OF TWO-PHASE MEDIA

V. S. Aleshin

UDC 621.1.013

Investigation of the properties of two-phase media, and in particular steam—water mixtures, presents specific difficulties which are caused by the complexity of producing these mixtures with a sufficiently uniform finely dispersed structure over a wide range of variation in them of the relative mass content of the steam. In addition actual processes with two-phase media are usually nonequilibrium to a greater or lesser extent. The flow structure also differs significantly for different flow modes of two-phase media. Therefore in studying them it is advisable in the interests of obtaining these or the other dependences to dwell first on a discussion of some idealized two-phase medium and then to evaluate the degree of approximation of different actual processes to these conditions.

We will assume that the two-phase medium has a sufficiently finely dispersed structure, is uniform, and is in an equilibrium state (the pressure, temperature, and chemical potentials of the phases are equal to each other). The state of this medium is uniquely determined by two independent parameters — the pressure (or saturation temperature at a given pressure) and the mass content of steam in the mixture. We will discuss the possibilities of determining certain properties for a two-phase medium as x varies from zero to unity.

The speed of sound* a_m is, according to Laplace's equation, equal to

$$a_m = \sqrt{-v_m^2 (\partial p/\partial v)_s^m}, \tag{1}$$

where $(\partial p/\partial v)_s^m$ is a quantity which is the inverse of the adiabatic compressibility and v_m is the specific volume of the mixture, which is determined by the expression

$$v_m = v''x + v'(1-x). \tag{2}$$

One can write with Eq. (2) taken into account

$$(\partial v/\partial p)_s^m = (\partial v''/\partial p)_s x + (\partial v'/\partial p)_s (1-x) + (\partial x/\partial p)_s (v''-v') \tag{3}$$

for the adiabatic compressibility of a two-phase medium.

It has been shown in a number of papers [1, 2, and others] that the propagation of small disturbances (sound vibrations) in two-phase media is not accompanied by any kind of appreciable heat exchange between the liquid and vapor phases in the zone of rarefaction and compression of a sound wave. Thus assuming x = const, we have

$$(\partial v/\partial p)_s^m = (\partial v''/\partial p)_s x + (\partial v'/\partial p)_s (1-x). \tag{4}$$

It follows from Eq. (4) that the adiabatic compressibility of a two-phase medium in the case under discussion varies, similarly to the specific volume, according to a linear law from $(\partial v'/\partial p)_S$ at x = 0 to $\partial v''/\partial p$ at x = 1.

For steam—water media the determination of the adiabatic compressibility, and consequently the speed of sound, causes no difficulties, since there are tables of thermodynamic derivatives for water and water vapor [3] in which are given the values of the adiabatic compressibility $(dv''/dp)_S$ and $(\partial v'/\partial p)_S$ for the upper (x = 1) and lower (x = 0) boundary curves. The calculation of $(\partial v/\partial p)_S^m$ is difficult for other two-phase media; therefore an approximate dependence is proposed below which is convenient for calculation.

The isentropy index k_m is defined by the well-known expression:

*The dependence of the speed of sound on frequency is not taken into account.

Translated from Atomnaya Énergiya, Vol. 48, No. 1, pp. 24-28, January, 1980. Original article submitted January 15, 1979.

 0038-531X/80/4801-0028$07.50

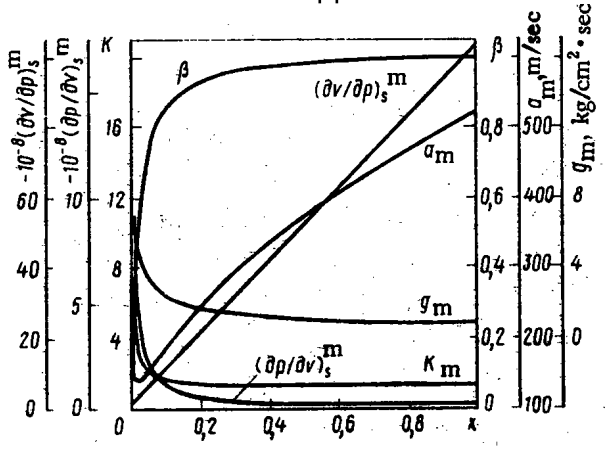

Fig. 1

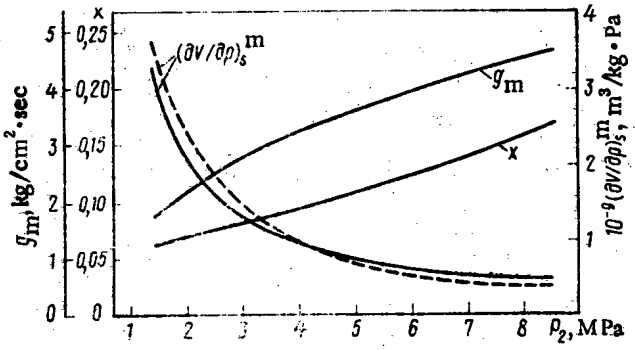

Fig. 2

Fig. 1. Dependences of β, $(\partial v/\partial p)_s^m$, $(\partial p/\partial v)_s^m$, a_m, k_m, and g_m on the mass concentration of steam x in the mixture.

Fig. 2. Dependence of g_m, x, and $(\partial v/\partial p)_s^m$ on the pressure p_2 in the exit cross section: ——) $(\partial v/\partial p)_s^m$ calculated from Eq. (16); ---) $(\partial v/\partial p)_s^m$ calculated from Eq. (4).

$$k_m = -v/p\,(\partial p/\partial v)_s, \tag{5}$$

as the ratio of the element of work expended in changing the kinetic energy of an element of the medium to the work of expanding this element. Eq. (5) is valid for gases, liquids, and two-phase media.

Substituting the values v_m and $(\partial v/\partial p)_s^m$ from Eqs. (2) and (4) into Eq. (5), we obtain

$$k_m = -\frac{v''x + v'(1-x)}{p\left[(\partial v''/\partial p)_s x + (\partial v'/\partial p)_s (1-x)\right]}. \tag{6}$$

For a saturated vapor (with x = 1)

$$(\partial v''/\partial p)_s = -(v''/k''p), \tag{7}$$

and for water (with x = 0)

$$(\partial v''/\partial p)_s = -(v'/k''p). \tag{8}$$

Therefore after substitution of Eqs. (7) and (8) into Eq. (6) with account taken of the fact that the mass vapor content x in the mixture is related to its volume content β by the dependence

$$\beta = \left[\left(\frac{1}{x} - 1\right)\frac{v'}{v''} + 1\right]^{-1}, \tag{9}$$

we finally obtain

$$k_m = \frac{1}{\beta}\left[\frac{1}{k''} + \frac{1}{k'}\left(\frac{1}{\beta} - 1\right)\right]^{-1}. \tag{10}$$

The values of k" and k' are given in [3] for steam—water media. As the calculations show, one can neglect the term 1/k' (1/β — 1) (i.e., the liquid in the mixture is incompressible) as x varies from 1 to 0.01, and then we obtain with a sufficient degree of accuracy a simple expression for k_m:

$$k_m = k''/\beta. \tag{11}$$

In the case of a variation of the pressure for a steam—water mixture from 0.1 to 10 MPa the calculation based on the approximate Eq. (11) gives a maximum error ∿4% at x = 0.01 in comparison with the calculation based on Eq. (10), which decreases to zero at x = 1. Calculations of k_m from Eq. (11) were compared with calculations according to the procedure outlined in [4] with p_2 = 2 MPa and a variation of x from 1 to 0.1. The discrepancy did not exceed 2.4% (at x = 0.1).

Similarly, we determine the speed of sound:

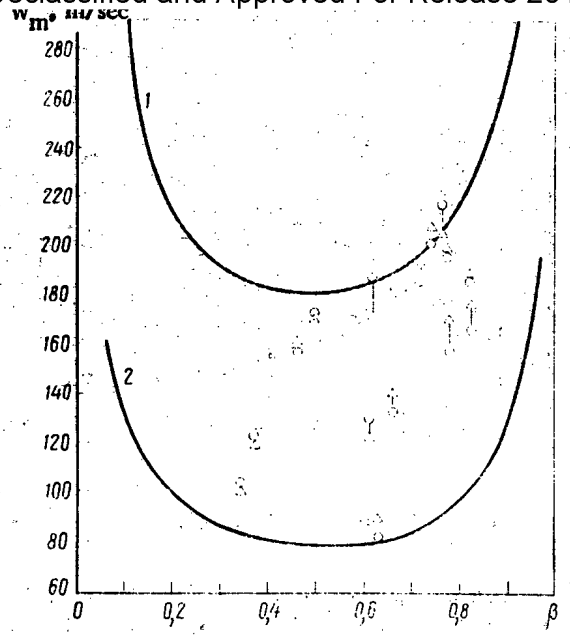

Fig. 3

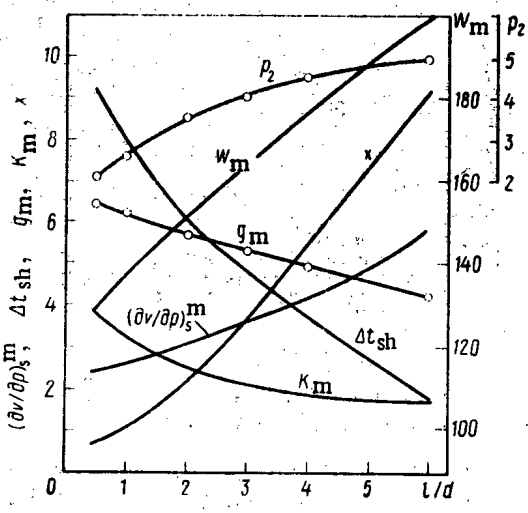

Fig. 4

Fig. 3. Dependence of the speed of sound in the critical cross section on β with (1) p = 5.5 and (2) p = 1.43 MPa: Δ — flow velocity calculated from the mass flow rate of the mixture; ○ — speed of sound calculated from p_2 and x in the exit cross section.

Fig. 4. Variation of p_2, MPa, W_m, m/sec, x, $(\partial v/\partial p)_s^m$, 10^{10} $m^3/kg \cdot Pa$, Δt_{sh}, °C, g_m, $kg/cm^2 \cdot sec$, and k_m as a function of the ratio l/d (○ — experimental points).

$$a_m = \sqrt{\frac{v''xp}{\beta^2}\left[\frac{1}{k''}+\frac{1}{k'}\left(\frac{1}{\beta}-1\right)\right]^{-1}}. \tag{12}$$

Neglecting the term 1/k' (1/β − 1) in Eq. (12), we obtain an approximate dependence for the speed of sound which is similar to the one given in [5]:

$$a_m = \sqrt{\frac{v''x}{\beta^2}k''p}. \tag{13}$$

After substitution of Eqs. (7) and (8) into Eq. (4) we obtain for the adiabatic compressibility

$$\left(\frac{\partial v}{\partial p}\right)_s^m = -\frac{v''x}{k''p} - \frac{v'(1-x)}{k'p}, \tag{14}$$

and the approximate dependence has the form

$$\left(\frac{\partial v}{\partial p}\right)_s^m = -\left(\frac{v''x}{k''p}\right). \tag{15}$$

The accuracy of the calculation based on Eqs. (13) and (15) in comparison with Eqs. (12) and (14) is the same as for k_m according to Eq. (11).

The calculated dependences of the variation of the specific volume v_m, the volume content β of steam in the mixture, $(\partial v/\partial p)_s^m$, $(\partial p/\partial v)_s^m$, a_m, and k_m on the mass content of steam in a steam—water mixture at p = 3 MPa are given in Fig. 1.

The variation of the speed of sound is determined by the nature of the variation of $(\partial p/\partial v)_s^m$ and v_m. Since $(\partial p/\partial v)_s^m$ remains practically constant and close to $(\partial p/\partial v'')_s$ upon a decrease of x from 1 to 0.3, the variation of a_m is determined by the decrease of the specific volume of the mixture. Upon a further decrease of x from 0.3 to 0 the variation of a_m depends mainly on $(\partial p/\partial v)_s^m$. A similar calculation of the speed of sound at p = 0.1 MPa shows that the minimum value is a_m = 24 m/sec at x = 0.001.

The limiting values of the specific mass flow rate of the mixture in the case of critical flow conditions, when the flow speed in the exit cross section is equal to the local speed of sound, are also given in Fig. 1, but p = 3 MPa and is constant for all values of x from 1 to 0. Thus one can determine the characteristics listed above for two-phase steam—water media from the derived dependences for any specified parameters (p and x), and it is possible to find k_m, $(\partial v/\partial p)_s^m$, and a_m for any two-phase media from the approximate Eqs. (11), (13), and (15).

In real processes a two-phase medium in the exit cross section of a sufficiently long cylindrical channel ($l/d > 6$–8) corresponds most completely under critical flow conditions to the idealized conditions under discussion. Thus according to the experimental data [6 and others] in the case of the outflow of saturated water through cylindrical channels with sharp entrance edges phase transformations are completed, the state of the flow is close to the equilibrium state, and the flow structure is finely dispersed and sufficiently uniform. The velocities of the liquid and vapor phases in the critical cross section are equal to each other, and the flow velocity is equal to the local speed of sound.

Assuming that the process is isentropic, one can determine $(\partial v/\partial p)_s^m$, the flow velocity W_m, and the isentropy index k_m for the exit critical cross section from experimental data of the mass flow rates of the mixture g_m and the pressure p_1 and p_2 and the temperature t_1 and t_2 in the entrance and exit cross sections, respectively, and one can compare the results obtained with calculations based on the dependences given above.

For the determination of the adiabatic compressibility from the mass flow rate measured in experiments we use the relation

$$(\partial v/\partial p)_s^m = -(1/g_m^2), \tag{16}$$

which can be obtained from Eq. (1) with account taken of the fact that the flow velocity in the critical cross section is equal to the local speed of sound:

$$W_m = a_m = g_m v_m \tag{17}$$

We will determine the specific volume from Eq. (2) and the mass steam content from the expression

$$x = \frac{S_1' - S_2'}{S_2'' - S_2'}, \tag{18}$$

where S_1' is the isentropy of the liquid at the entrance to the outflow channel and S_2' and S_2'' are the entropy of the liquid and the saturated vapor at the exit cross section.

The value of $(dv/\partial p)_s^m$ calculated from the known flow rate of the mixture, i.e., from Eq. (16), and calculated from Eq. (4) in the case of the outflow of saturated water ($\Delta t_{sat} = 0°C$) through a cylindrical channel ($l/d = 18.4$) and variation of the initial pressure from 2.45 to 14.7 MPa are given in Fig. 2, and the flow rate of the mixture and the mass steam content are also shown. Similar calculations were performed for the same pressure range in the case of underheating of the water to saturation temperature by $\Delta t_{sat} = 10$, 20, and 50°C. In all cases the discrepancy in the values of $(\partial v/\partial p)_s^m$ does not exceed ~15–17%.

The flow velocities calculated from the mass flow rates for some experimental points are given in Fig. 3, along with the local speeds of sound for these same points obtained by calculation from the adiabatic compressibility with p_2 and x in the exit cross section. The discrepancy does not exceed 10–12%. A similar error is obtained in connection with the determination of the isentropy index.

The completely satisfactory agreement of the values $(\partial v/\partial p)_s^m$, a_m, and k_m calculated from the experimental data and the computational dependences confirms that in the first place one can neglect phase transitions in connection with the propagation of small disturbances in two-phase media and assume Eq. (4) to be valid; secondly, the adiabatic velocity defined by Eqs. (12) or (13) is realized in the critical cross section; thirdly, one can use the derived dependences with an accuracy sufficient for practical purposes in solving different engineering problems, including for calculations of the flow rates of the mixture in the flows of the reactor loops of an atomic electric power plant with a VVR reactor.

The derived Eqs. (11), (13), and (15) can also be applied to the calculation of two-phase two-component mixtures. The effect of nitrogen dissolved in the coolant on the

properties under discussion was estimated. Thus at a pressure of 14.7 MPa in the first loop, t = 300°C, and a nitrogen content of ∿3000 nml/kg in the loop, the adiabatic compressibility increases by 30%, and the speed of sound and the isentropy index decrease by ≈20%, which cannot be neglected in a discussion of the hydrodynamics and heat exchange in the active zone of a nuclear reactor.

We note that the discrepancies obtained (up to 15-20%) are evidently the result of errors in the measurements (especially the pressure) at the exit edge and also evidently of some incompleteness of phase transitions and nonuniformity in the flow structure.

Upon outflow through short channels ($l/d < 4$-6) phase transitions do not have time to be completed, the liquid is in a superheated state, and the flow is significantly nonequilibrium. It is of interest to consider the variation of x, $(\partial v/\partial p)_s^m$, and other characteristics of the flow in the exit cross section as a function of the ratio l/d. The experimental determination of these quantities is very complicated, but they can be calculated from the measured mass flow rates g_m, the pressure p_1 and temperature t_1 in the entrance cross section, and the pressure p_2 in the exit cross section.

We find $(\partial v/\partial p)_s^m$ from Eq. (16). One should emphasize that the value of $(\partial v/\partial p)_s^m$ is found with the actual nonequilibrium nature of the process (incompleteness of steam formation, superheating of the liquid and so on) taken into account.

We then find $(\partial v'/\partial p)_s$ and $(\partial v''/\partial p)_s$ from the tables of [3] according to the value of p_2, and we calculate the mass steam content x from Eq. (4). Then we find v" and v' from the value of p_2 and calculate v_m. We determine the value of v_2'' proceeding from the assumption that the steam temperature is equal to the saturation temperature at the pressure p_2, and we find v_2' with the superheating Δt_{sh} of the liquid taken into account (by means of a number of approximations). We determine the flow velocity from Eq. (1), the superheating temperature from Eq. (18), the isentropy index k_m from Eq. (5), and the volume steam content from Eq. (9).

The dependence of a number of quantities on the ratio l/d at a pressure $p_1 = 9.8$ MPa and $\Delta t_{sat} = 0$°C is shown in Fig. 4. The parameters in question have a similar nature for other values of p_1 at the entrance to the outflow channel.

It follows from consideration of the results obtained that in the case of outflow through short channels of a metastable vapor—liquid flow the main characteristics are determined, just as in the case of outflow through long channels, by the pressure p_2 in the exit cross section, the mass vapor content x, and the specific volume of the mixture v_m calculated with the actual superheating of the liquid towards the exit cross section taken into account.

In conclusion we note that the pressure p_2 and x_m in the exit cross section will also uniquely determine $(\partial v/\partial p)_s^m$, a_m, and k_m in this cross section in the case of critical flow conditions through channels of great length, when it is impossible to neglect hydraulic drag in the channel and the process is not isotropic.

Moreover, if any two-phase flow in the out-flow channel is, or one can assume it to be, sufficiently uniform and finely dispersed, then one can determine the isentropy index from the known p and x for any arbitrary cross section taken, and this predetermines the possibility of the calculation of the pressure and temperature variation along the channel length for the adiabatic flow of two-phase media.

LITERATURE CITED

1. N. I. Semenov and S. I. Kosterin, Teploenergetika, No. 6, 46 (1964).
2. V. V. Sychev, ibid., No. 3, 67 (1961).
3. S. L. Rivkin, A. A. Aleksandrov, and E. A. Kremenevskaya, Thermodynamic Derivatives for Water and Water Vapor [in Russian], Énergiya, Moscow (1977).
4. M. E. Deich et al., Teploenergetika, No. 12, 51 (1965).
5. V. V. Dvornichenko, ibid., No. 6, 58 (1967).
6. V. S. Aleshin, Yu. A. Kalaida, and V. V. Fisenko, At. Energ., 38, No. 6, 375 (1975).

NEUTRON RESONANCES OF OSMIUM ISOTOPES IN THE 1-550 eV RANGE

T. S. Belanova, S. I. Babich,
A. G. Kolesov, and V. A. Poruchikov

UDC 621.039.556

The investigation of the neutron resonances of osmium isotopes is of obvious interest for obtaining values of the force functions (S_0) and the radiative widths (Γ_γ) of neutron resonances in the region of nuclei having masses of 186-192, which is the transition region from deformed nuclei to spherical ones, and such an investigation is also of interest for the study of nonstatic effects both in the alternation of the neutron levels of even isotopes and in the energy dependence of the reduced neutron width of the levels [1].

One should note that neutron resonance parameters of osmium isotopes have been studied little mainly due to the absence of single-isotope samples of optimal sizes. As a rule, multiple-isotope osmium samples distinguished by high enrichment of individual isotopes have been investigated (Table 1). However, identification of levels and obtaining resonance parameters from the transmission of such samples is a very laborious process which does not give reliable results in many cases. First the transmission of a sample made out of a natural mixture of osmium isotopes was measured with a selector at Argonne; resonance parameters have been calculated up to an energy of 29 eV only for ^{189}Os [2]. Using samples enriched in individual osmium isotopes, the selector group of the institute of Nuclear Research of the Academy of Sciences of the Ukrainian SSR [3, 4] has obtained more extensive data below an energy of 500 eV on the resonance parameters of six osmium isotopes. Appreciable information on the position of the levels of the odd isotopes ^{187}, ^{189}Os has been obtained in connection with the determination of the spins of neutron resonances [5-9]. Earlier we published preliminary data on the position of the levels and their distribution among the six osmium isotopes [10].

The investigations have been conducted using the mechanical selector of an SM-2 reactor [11]. The transmissions of six osmium samples enriched with the isotopes $^{186-190,192}$Os were measured in the 1-550 eV range of neutron energies. The best resolution of the spectrometer on a time-of-flight baseline of 91.7 m was 70 nsec/m. The samples were prepared from metal powder and had the shape of a rectangular parallele piped (see Table 1). The amount of ^{184}Os in all the samples did not exceed 0.05%. The statistical accuracy of the measurements was 0.5-1.5%, and background amounted to from 0.7 to 3% of the effect being studied.

In contrast to [10], the present measurements were made under more refined experimental conditions (the thickness of the investigated samples is increased by a factor of 2-3.5, the background conditions of the spectrometer are improved, the statistical accuracy of the measurements is increased, a more refined program for calculation of the resonance parameters with a BÉSM-6 computer is utilized, and so on), which increased the accuracy of identification of the levels of osmium isotopes and also permitted calculating the values of the resonance parameters. It should be noted that a portion of the levels of osmium isotopes were

TABLE 1.

Sample no.	Sample wt., mg	Isotope compound in sample											
		^{186}Os		^{187}Os		^{188}Os		^{189}Os		^{190}Os		^{192}Os	
		10^{-4} atoms/b	%	10^{-4} atoms/b	%	10^{-4} atoms/b	%	10^{-4} atoms/b	%	10^{-4} atoms/b	%	10^{-4} atoms/b	%
1	169,5	31,7	42,1	7,21	9,6	13,3	17,9	6,83	9,2	7,75	10,5	7,8	10,7
2	132,5	0,51	0,8	11,4	18,1	26,4	42,2	18,8	25,3	4,83	7,8	3,56	5,8
3	451	0,83	0,5	0,82	0,5	130,8	80,1	16,7	10,3	9,5	5,9	4,3	2,7
4	394,5	$<$ 0,08	$<$ 0,05	0,49	0,4	3,52	2,9	96,3	79,8	16,7	13,9	3,56	3,0
5	879	$<$ 0,14	$<$ 0,05	$<$ 0,14	$<$ 0,05	2,4	0,9	10,7	4,0	240	89,9	13,7	5,2
6	800	$<$ 0,14	$<$ 0,05	$<$ 0,14	$<$ 0,05	0,74	0,3	1,63	0,6	6,2	2,3	259	96,8

Translated from Atomnaya Énergiya, Vol. 48, No. 1, pp. 28-32, January, 1980. Original article submitted November 20, 1978.

0038-531X/80/4801-0033$07.50

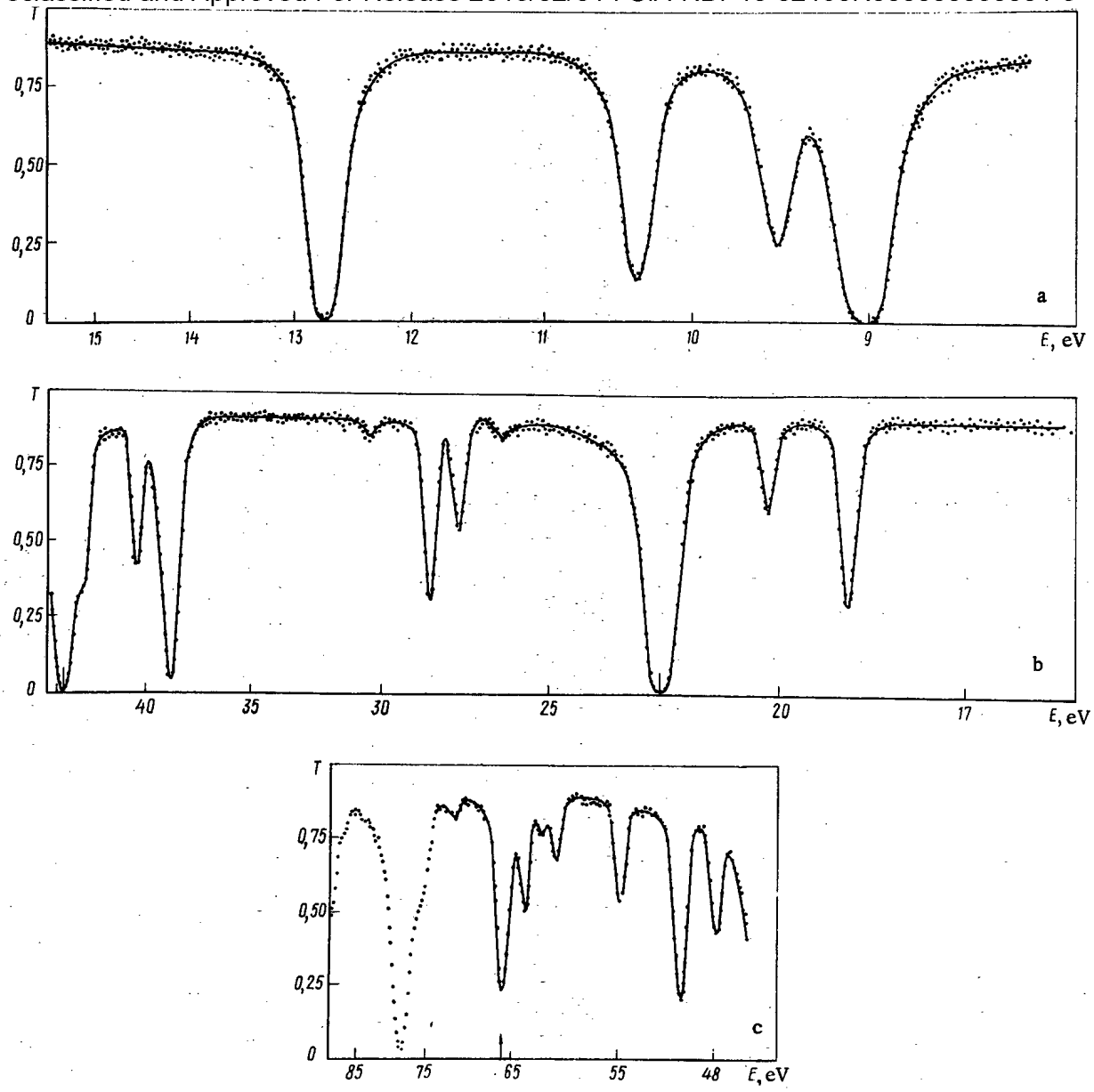

Fig. 1. Transmission of osmium sample at (a) 8-16, (b) 16-46, and (c) 46-90 eV: ●) experiment; ——) theoretical calculation by the shape method.

not correctly identified in [10]. The results of the present measurements have permitted redistributing these levels among the isotopes of osmium.

The transmission of one of the osmium samples (No. 1) in the 8-90 eV range of neutron energies is shown in Fig. 1 as an example. The parameters of the neutron resonances (position of the levels E_0, values of the neutron $2g\Gamma_n$ and total Γ widths) were calculated by the area and shape method from the single-level Breit–Wigner formula. The cross section of potential scattering of the neutrons σ_{sc} was simultaneously calculated for each isotope. The parameters obtained are given in Tables 2-4; they were used for calculation of the theoretical transmission curve (solid curve in Fig. 1). The resonance parameters from the publications [2-4] are given for comparison in these tables.

Odd isotopes of osmium. The parameters of the neutron resonances of ^{187}Os and ^{189}Os are calculated up to an energy of 72 eV from the transmission of samples 2 and 4 (see Table 1). It is evident that sample 2, the main one used for investigation of the isotope ^{187}Os, has weak enrichment (^{187}Os-18.1%) and a small amount of material (132 mg). This fact complicated the identification of levels and caused an increase in the error of the determination of the neutron resonance parameters. For example, it is necessary for calculation of the parameters of the ^{187}Os level with energy 28.43 eV to take correct account of the

TABLE 2. Parameters of Neutron Resonances of ^{187}Os

E_0, MeV	$2g\Gamma_n$, meV		Γ, meV		E_0, eV *
	this paper	[3, 4]	this paper	[3, 4]	
9,5	1,75±0,02	2,71±0,18	86±3	91±6	99,1±0,7
12,73	11,2±0,1	13,63±0,21	105±3	114±10	115,8±1,1
20,24	1,97±0,03	2,6±0,2	84±7	143±40	165±2
26,34	0,50±0,05		90±40	—	172±2
28,43	0,5±0,2			—	176±2
39,46	2,5±1,0			—	211±3
40,45	16,8±1,0	28±4			246±4
43,33	15,3±2,0	—			279±4
47,65	21,8±1,5	22,7±2,1			
49,54	3,5±1,0	57,3±19,8			
50,15	65±10				
61,9	9±1				
63,5	36±5	79,6			
65,5	1,5±0,8				
71,5	1,9±0,5				

*Only levels obtained above 71.5 eV as a result of the reidentification of the data of [10].

†Level is omitted.

‡Doublet.

contribution of an ^{189}Os resonance with energy 28.46 eV to the transmission of the sample. A similar situation was encountered for the ^{187}Os levels with energy 39.46, 43.33, 49.54, 50.15, 63.5, 65.5, and 71.5 eV. It did not prove possible to obtain from the transmission of sample 2 the parameters of the 49.54 and 50.15 eV levels of ^{187}Os due to the large contribution to the transmission of the ^{189}Os levels with energy 50.28 and 51.21 eV. The parameters of these levels are obtained from the transmission of sample 1. The values of Γ are determined only for the first four relatively isolated levels of ^{187}Os. The average value found for the radiative width ($\bar{\Gamma}_\gamma$ = 88 meV) was adopted in the calculation of the parameters

TABLE 3. Parameters of Neutron Resonances of ^{189}Os

E_0, eV	$2g\Gamma_n$, MeV			Γ, MeV			E_0, eV*
	this paper	[3, 4]	[2]	this paper	[3, 4]	[2]	
6,75	2,83±0,05	3,02±0,10	3,21±1,04	98±2	96±5	84±3	97,4±0,7
9,02	8,4±0,2	8,4±0,6	10,41±0,96	108±3	97±3	110±10	163±2
10,35	3,35±0,05	3,84±0,31	4,1±0,4	99±3	98±2	102±10	183±2
13,95	0,020±0,001	†	—	—	—		202±3
18,82	4,97±0,10	5,19±0,43	10,42±1,74	100±14	105±30		224±4
21,95	7,6±0,5	8,46±1,41	8,63±1,41	112±7	—		294±5
22,96	0,21±0,05	—	†	97±20	—		
27,56	4,2±0,1	5,25±1,05	7,11±0,75	106±8	—		
28,46	9,5±0,5	20,17±5,31	14,9±1,06	103±7	150±20		
30,45	0,74±0,02	1,05±0,11	—	123±10			
39,04	4,1±0,8	2,91±0,50	†	—			
41,66	0,79±0,03	0,64±0,52	†	99±20			
43,24	2,23±0,07	1,58±0,33	—	104±14			
50,28	19,6±1,0	31,8±2,8	—				
51,21	1,3±0,2	†	†				
54,76	19,2±1,0	28,0±4,4	†				
60,5	13,7±0,8	6,83±1,09					
63,7	11,5±1,0	80‡					
65,0	13±6						
65,7	6±3	†					
71,9	3,2±0,3	†					
75,0	—	—					
76,1		†					
77,6		†					
78,9		†					
87,4							

*Only levels obtained above 90 eV as a result of the reidentification of the data of [10].

†Level is omitted.

‡Doublet.

TABLE 4. Parameters of Neutron Resonances of Even Isotopes of Osmium

E_0, eV	Γ_n, MeV		Γ, MeV		E_0, eV	Γ_n, MeV		Γ, MeV	
	this paper	[3, 4]	this paper	[3, 4]		this paper	[3, 4]	this paper	[3, 4]
		^{186}Os			190,5				
22,38	10,0±0,5	11,35±1,42	82±6	131±10	251		*		
44,61	67,5±2,5	81,9±6,7	178±15	252±50	314				
66,04	20,5±2,0	84±30			384				
89,3					473				
137					523				
273							^{190}Os		
337		*			91,3±0,5		24,7		
		^{188}Os			145±1		90		
38,67†	32,7±1,5	42,8±3,7	138±5	153±20	226±2		*		
46,92†	0,08±0,01	*			341±3		*		
78,3	320±40	460±40			528±5		*		
149		*					^{192}Os		
					20,45±0,10	0,028±0,001	0,008±0,002		
					127±1	—	4,48±0,45		
					505±5		*		

*Level is omitted.
†Possibly a level of ^{184}Os.

of the remaining ^{187}Os resonances. The ^{187}Os levels discovered as a result of reidentification of the data of [10] are found above 72 eV in Table 2. The analogous levels of ^{189}Os above 90 eV are given in Table 3.

The effect of the strong ^{186}Os levels with energy 22.38 and 66.04 eV and the ^{188}Os level with energy 38.67 eV on the transmission of sample 4 worsened the accuracy of the determination of the parameters of the ^{189}Os resonances with energy 21.95, 22.96, 39.04, 65.0, and 65.7 eV. The values of Γ found for the 11 levels of ^{189}Os permitted determining the value $\Gamma_\gamma = 101$ MeV, which was then used in calculating the remaining levels. The values of E_0 obtained for the ^{187}Os and ^{189}Os resonance are in good agreement with the values published in [8, 9]; however, there are discrepancies with the data of [10]. In particular, the existence of levels with energy 18.2, 21.0, and 69.1 eV is not confirmed for ^{187}Os. The first two levels are assigned to ^{189}Os, and the position of the third one is refined to 71.5 eV.

In comparison with our results seven resonances each are omitted in [3, 4] for ^{187}Os up to 72 eV and for ^{189}Os up to 90 eV (they are also observed in [8, 9]). Doublets at 50.0 eV for ^{187}Os and 64.2 eV for ^{189}Os are not resolved (a possible cause of the overestimation of $2g\Gamma_n$ for most of the ^{189}Os levels in [2-4] are in agreement with our data within the limits of the indicated errors. A systematic overestimation of $2g\Gamma_n$ by 20-40% is observed for ^{187}Os. The deviations noted are caused most likely by the contribution, which is difficult to take into account, to the transmission of the sample of the resonances of other osmium isotopes whose energies are close to the energy of the levels under investigation.

Even Isotopes of Osmium. The parameters of the neutron resonances of ^{186,188,190,192}Os are obtained from the transmission of samples 1, 3, 5, and 6 (see Table 4). Seven levels have been discovered for ^{186}Os up to an energy of 350 eV; the resonance parameters are calculated for the first three levels. It was assumed in the calculation of Γ_n of the 66.04 eV level that $\Gamma_\gamma = 90$ eV. A resonance with energy 337 eV has not been observed earlier. The

TABLE 5. Characteristics of Osmium Isotopes

Isotope	This paper				Data of [4, 12]			
	σ_{sc}/b	$\bar{\Gamma}_\gamma$, MeV	$\bar{D}$, eV	$s_0 \cdot 10^4$	σ_{sc}, b	$\bar{\Gamma}_\gamma$, mEV	$\bar{D}$,eV	$s_0 \cdot 10^4$
^{186}Os	21±5	90±7	22±4	2,2±1,6	18±5	145±45	22±6	$5,6^{+7,8}_{-2,3}$
^{187}Os	8±4	88±5	4,4±0,4	2,3±0,9	7,5±6	110±30	8±1,6	$2,0^{+2,0}_{-0,85}$
^{188}Os	9±2	100±10	38±6	3,7±2,1	6,5±1	110±20	47±10	$5,0^{+9}_{-2,5}$
^{189}Os	11±2	101±3	3,4±0,2	1,78±0,58	14±10	100±20	3,8±0,7	$2,0^{+1,0}_{-0,6}$
^{190}Os	21±2	—	—	—	18±2	—	52±14	—
^{192}Os	28±2	—	—	—	17±1	—	140±35	$0,6^{+0,9}_{-0,2}$

existence of levels with energy 19.45, 24.71, 25.31, 99.1, 163, and 202 eV [10] is not confirmed. The present measurements have shown that the levels 19.45, 25.31 (after refinement of the energy), and 99.1 eV should be assigned to ^{187}Os, and the 162 and 202 eV levels should be assigned to ^{189}Os. The 24.71 eV resonance was not uniquely identified (it is possibly a level of ^{184}Os).

Ten resonances were found for ^{188}Os, five of which (46.9, 149, 251, 473, and 523 eV) are obtained for the first time. The parameters are calculated for the first three levels. It was assumed in the calculation of Γ_n of the 46.92 and 78.3 eV levels that $\Gamma_\gamma = 100$ meV. The 46.92 eV resonance has not been uniquely identified; possibly it belongs to ^{184}Os. The existence of the 25.7, 33.45, 57.3, 165, 176, and 279 eV levels [10] has not been confirmed. As analysis of the transmissions has shown, one should attribute the 25.7, 165, 176, and 279 eV levels to ^{187}Os and the 57.3 eV level to ^{189}Os after refinement of its energy. Having a sample approximately ten times thicker, we did not confirm the rather strong resonance of ^{188}Os with energy 44.3 eV [3, 4], although levels with a smaller neutron width were recorded for ^{188}Os. Evidently this sample also proved to be too thin for detection of the ^{188}Os levels with energy 149, 251, and 523 ev [3, 4].

The position of the resonances has been determined for ^{190}Os and ^{192}Os, and their identification has been accomplished. A comparison of the results of previous [10] and the present measurements has shown that the 28.40 eV level of ^{190}Os should, just as the 115.8 eV level of ^{192}Os, be attributed to ^{187}Os, and the resonances of ^{192}Os with energy 23.03, 43.9, and 95.7 eV should be attributed to ^{189}Os. After refinement of the energy the 36.17 eV level of ^{192}Os was assigned to ^{188}Os (also see [3, 4]).

The values of Γ_n and Γ for the levels of ^{186,188}Os have been overestimated by 20-30% and three resonances of ^{190}Os have been omitted in [3, 4] in comparison with the results of this paper. The existence of the 165 eV level of ^{190}Os and the 241 eV level of ^{192}Os has not been confirmed; most probably these are resonances of ^{187}Os, and also the ^{190}Os level with energy 11.14 eV has not been confirmed, although the amount of this isotope in our sample is approximately seven times greater. A certain portion of the resonances of osmium isotopes in these papers requires reidentification.

The discrepancies noted with the data of [3, 4] are evidently produced by the following causes. The amount of $^{186-190,192}$Os in the samples of the indicated papers is approximately 2.4, 1.2, 9.5, 3, 7.2, and 1.8 times lower, respectively. With practically an identical energy resolution of both spectrometers, the spectrometer of the present paper (a high-transmission selector with a reactor having a high neutron flux) has a lower background — effect ratio. Without getting into the details, we note that the resonance parameters in the present paper have been calculated on a BÉSM-6 computer using a more refined program. One can state that a higher measurement accuracy is characteristic of the data obtained.

The average characteristics of the osmium isotopes are given in Table 5. The values of the average distance between levels $\bar{D}$ for ^{187,189}Os are calculated up to an energy of 72 eV, and S_0 was determined from the slope of the straight line from the plot of the dependence of the sum of the reduced neutron widths ($\Sigma 2g\Gamma_n^0$) on the neutron energy. The energy range above $\sim$200 eV was not considered to be sufficiently resolved; this situation did not permit calculating $\bar{D}$ for ^{190}Os. For comparison the analogous data from [4, 12], in which the values of $\bar{D}$ for odd osmium isotopes are calculated up to an energy of 64 eV, are given in Table 5. It follows from a comparison of our data with the analogous data of [12] (see Table 5) that within the limits of the indicated experimental errors the values of $\bar{\Gamma}_\gamma$ agree with each other.

The overestimation of $\bar{D}$ of ^{187}Os in [12] is explained by the omission of five levels up to an energy of 64 eV. Taking the contribution of these levels into account gives $\bar{D}$ = 4.5 eV. Taking account of the two ^{198}Os levels omitted up to an energy of 64 eV would permit obtaining a more accurate value $\bar{D}$ = 3.5 eV. One should say the same about $\bar{D}$ for ^{188}Os. With account taken of the omitted level up to an energy of 187 eV $\bar{D}$ = 37 eV would be obtained. The values of $\bar{D}$ for ^{190,192}Os in [12] do not appear to be reliable. The value of $\bar{D}$ for ^{190}Os is calculated in the 0-165 eV energy range from four resonances, of which the existence of the first one (11.14 eV) is doubtful, and the last one (165 eV) belongs to ^{187}Os. A similar situation exists for ^{192}Os.

The overestimation of S_0 of ^{186,188}Os by [12] is caused by an overestimation of the values of Γ_n for the greater part of the levels of these isotopes. The agreement of S_0

for ^{187}Os in spite of the discrepancy of $2g\bar{\Gamma}_n$ and $\bar{D}$ is accidental and evidently caused by an identical degree of overestimation of $2g\bar{\Gamma}_n^0$ and $\bar{D}$, which determine the value of S_0.

The values $\bar{\Gamma}_\gamma = 92 \pm 10$ meV and $S_0 = (2.0^{+2.2}_{-0.2}) \cdot 10^{-4}$ obtained in [2] for ^{189}Os are in agreement with the data of Table 5; the observed overestimation of $\bar{D} = 4.5$ eV is caused by the omission of four resonances in the 0-61 eV energy range.

The results of future measurements of the transmission of practically single-isotope samples of optimal thickness with high energy resolution can introduce clarity into the discussion of the questions touched on.

LITERATURE CITED

1. F. N. Belyaev et al., in: Transactions of Conference on Neutron Physics [in Russian], Part 2, Izd. FÉI, Obninsk (1974), p. 221; A. B. Popov, Kh. Faikov, and Kvan Cher Gu, JINR Preprint No. R3-10377, Dubna (1977).
2. H. Jackson et al., Phys. Rev., 124, 1142 (1961).
3. V. P. Vertebnyi et al., in: Transactions of Conference on Neutron Physics [in Russian], Part 1, Naukova Dumka, Kiev (1972), p. 181; Nuclear Physics Research in the USSR [in Russian], No. 12, p. 70.
4. V. A. Pshenichnyi, Author's Abstract of Candidate's Dissertation, Kiev (1975).
5. K. Wetzel et al., Phys. Rev., C-1, 1501 (1970).
6. É. N. Karzhavina, Kim Sek Su, and A. B. Popov, JINR Preprint No. R3-6092, Dubna (1971).
7. N. N. Balabanov et al., JINR Preprint No. R3-7376, Dubna (1973).
8. A. Namenson et al., Nucl. Phys., A-237, 45 (1975).
9. A. Stolovy et al., Phys. Rev., 14, 965 (1976).
10. T. S. Belanova et al., At. Energ., 37, No. 5, 437 (1974).
11. T. S. Belanova et al., Preprint P-6 (272), Dimitrovgrad (1976).
12. V. P. Vertebnyi et al., Yad. Fiz., 22, No. 4, 674 (1975).

LETTERS TO THE EDITOR

CHOICE OF SOME CHARACTERISTICS OF FAST BREEDER REACTOR AT VARIOUS STAGES OF NUCLEAR POWER DEVELOPMENT

M. F. Troyanov, V. G. Ilyunin,
V. M. Murogov, V. Ya. Rudneva,
and A. N. Shmelev

UDC 621.039.5

The study of various models of nuclear power (NP) in the development stage includes a search for reactor parameters which would satisfy the optimality criteria for NP. A question arises in this case: how distinguishable will the optimal parameters of reactors be, depending on the various stages in the development of the system, i.e., in fact, on the ratio of the number of fast breeder reactors and thermal reactors in the NP system?

In the first stage of NP development the fast reactors are still few in number, breeder reactors operate on plutonium obtained in thermal reactors, and up to a certain time the internal production of plutonium does not have any serious effect on the system. This is the stage of mastering breeder reactors and beginning to introduce them into the nuclear power industry. The most important thing here is to ensure reliable and safe operation of fast reactors, to create a base for further development of breeders, and also to prepare conditions for the improvement of the latter.

With further development the fraction of breeder reactors will grow and when it becomes equal to the fraction of thermal reactors the specific charge of plutonium in the reactors and the rate of accumulation of excess plutonium in them will be extremely important for the system.

The uranium deficit with a further development of NP may result in breeder reactors producing fuel for thermal reactors as well, although one cannot rule out supplemental supplies of nuclear fuel to the system as the result of production of fuel, e.g., in hybrid thermonuclear reactors.

If, in a nuclear power system comprising thermal reactors as well as breeders ensuring the development of NP because of the build-up of excess nuclear fuel, dynamic equilibrium is established with the ratio between fast and thermal reactors, N_f/N_t, then the development rate ω and the doubling time T_2^{NP} of such a system can be found by using the expressions from [1]:

$$T_2^{NP}=\frac{\ln 2}{\omega}=\ln 2\,\frac{(N_f/N_t)\,g_f+g_t}{(N_f/N_t)\,r_f-q_t}, \tag{1}$$

where r_f and g_f are the specific excess conversion ratio and charging of the breeder reactor (i.e., per unit power) and q_t and g_t are the specific rates of fuel make-up and charging of the thermal reactor.

Solving the relation for N_f/N_t, we get an expression which allows us to calculate the necessary ratio of breeders and thermal reactors as a function of the given rate of development of the system of reactors and their parameters:

$$\frac{N_f}{A_t}=\frac{q_t+\omega g_t}{r_f-\omega g_f}. \tag{2}$$

The initial characteristics of the breeders affect the doubling time and the structure (N_f/N_t) of the two-component system. Let us fix the parameters of the thermal reactor, having the VVÉR-1000 water-moderated—water-cooled power reactor in mind [2]. As an example let us consider a BN fast reactor with a thermal rating of 3000 MW operating on oxide fuel with a thermal stress Q of 300 to 800 kW/liter in the core (Fig. 1a). Such a reactor,

Translated from Atomnaya Énergiya, Vol. 48, No. 1, pp. 33-34, January, 1980. Original article submitted July 3, 1979.

0038-531X/80/4801-0039$07.50

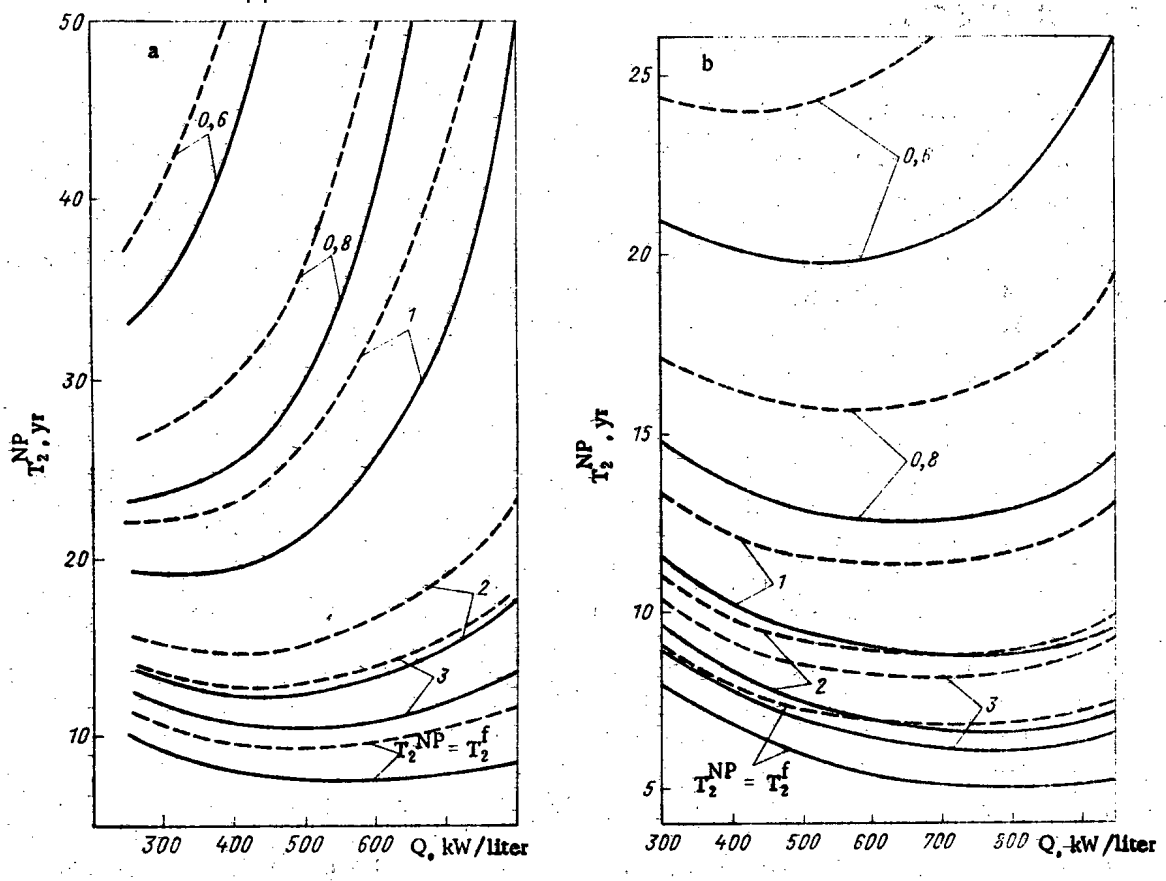

Fig. 1. Doubling time of power of NP vs thermal stress of core of fast reactor with oxide (a) and metallic (b) fuel for various values of structure of NP model considered (numbers next to curves) with external fuel-cycle times of 0.5 yr (——) and 1 yr (---).

which is optimal in respect of intrinsic doubling time T_2^f, is characterized by a mean thermal stress of 450-550 kW/liter. With a decrease in Q there is an increase in the specific rate r_f of excess conversion and specific charging g_f. The growth of r_f is not compensated by the growth of r_f and this results in an increase in T_2^f. If the NP system consists of fast and thermal reactors, then the optimum in respect to T_2^{NP} shifts to the region of lower thermal stresses in thermal reactors. The more thermal reactors there are in the system, the smaller the thermal stresses which correspond to the minimum values of T_2^{NP}. Similar results for a breeder reactor with metallic fuel are presented in Fig. 1b.

The results obtained illustrate the fact that in a two-component NP system in a state of dynamic equilibrium the optimal breeder should have different core design parameters than does a reactor optimized according to T_2f in a system consisting of only breeder reactors of one type. The shift of the optimum T_2^{NP} towards lower Q means that for the system it is preferable to have fast reactors with a high conversion factor, although the specific charge in this case is greater. The increase in the charge, however, should not be inordinate, i.e., it is important that in Eq. (2) the difference $r_f - \omega g_f$ should grow when r_f and g_f increase simultaneously. It can be pointed out that optimization of a breeder reactor according to the fuel component of the design costs also to a less stressed core than required by optimality according to T_2^f [3].

These examples indicate that when designing a fast reactor whose service life should be no less than 30 years, one should make allowance for its being adapted to the stages in the development of the system of reactors. A flexible core design, which at a given power would permit the thermal stress and, possibly, the form of the fuel to be changed will allow the breeder with highest efficiency to operate in a system with varying requirements. For example, as seen from Fig. 1, if in a fast reactor the oxide fuel is replaced by metallic fuel while the previous thermal stress Q of the core is maintained, then such a breeder proves to be close to the optimum in respect of rate of development of a two-component NP system.

The authors express their gratitude to V. S. Kagramanyan for his useful discussions of the topics raised.

LITERATURE CITED

1. V. V. Orlov, V. N. Sharapov, and A. N. Galanin, in: Atomic Power Plant Operating Experience and Ways of Further Developing Nuclear Power [in Russian], Vol. I, Izd. Fiz.-Energ. Inst., Obninsk (1974), p. 251.
2. V. A. Sidorenko, At. Energ., 43, No. 5, 325 (1977).
3. V. B. Lytkin, M. F. Troyanov, and A. I. Novozhilov, At. Energ., 21, No. 5, 320 (1966).

CALCULATION OF REACTOR WATER FLOW RATE FOR PURIFICATION OF COOLANT IN BOILING-WATER SINGLE-LOOP ATOMIC POWER PLANTS

V. V. Gerasimov, O. I. Martynova, O. T. Konovalova, and T. I. Kosheleva

UDC 621.039.524.44

In working out the water regime of an atomic power plant with boiling-water reactors one must determine the flow rate of reactor water for purification (purging) of the coolant. Such calculations are made according to the content of both soluble impurities and corrosion products (CP) of iron, which as a rule determine the efficiency of purification of the reactor water.

Because of its ramified surface, the condensate-feedwater loop is the principal source of iron CP introduced into the circulation loop of the reactor. Concurrently with removal there is the reverse process, i.e., deposition of suspended CP particles on the surface of the circulation loop, primarily in stagnant zones. These processes upset the balance between the arrival of iron CP in the reactor circulation loop and their content in the water in that loop. Thus, the balance equation for soluble impurities is not applicable in the calculation of the flow rate of water for removing iron CP from the coolant. Generalization of the operating experience with boiling steam generating plants working on nuclear and organic fuel made it possible to quantitatively estimate the process of CP deposition in the loop. As a result, the right member of the materials balance equation was supplemented with one term, upon which the equation took on the form

$$G_{fw} + G_{cl} = pC_{rw}\mu_1 + C_{\pi}D_{\pi}\mu_2 + C_{rw}V_{cl}\gamma\omega, \quad (1)$$

where G_{fw} is the quantity of iron CP introduced from the feedwater (for plants under design this is calculated from the removal of CP and from the dimensions of the surfaces of the condensate-feedwater and steam loops of the turbines with allowance for the effeciency of purification in filters) (g/h), G_{cl} is the arrival of iron CP from the surface of the circulation loop (g/h), p is the flow rate of reactor water for purification (purging) (tons/h), D_s is the steam capacity of the reactor (tons/h), C_{rw} and C_s are the determined concentrations (or normalized contents) of iron CP in the reactor water and the saturated steam, respectively (g/ton), μ_1 and μ_2 are the efficiencies of the removal of iron CP by filters of in-loop purification and condensate purification, respectively, V_{cl} is the volume of the reactor circulation loop (m^3), γ is the water density under normal conditions (tons/m^3), and ω is the constant of deposition of iron CP on the surface of the reactor circulation loop (h^{-1}).

The constant ω in the equation given above determines the kinetics of deposition and depends on the thermophysical and hydraulic processes in the coolant. To determine ω in steady-state and transient regimes we used the operational and experimental data obtained for existing domestic commercial and semi-commercial power plants and atomic power plants with boiling-water reactor. It turned out that if the volume-to-surface ratio in the

Translated from Atomnaya Énergiya, Vol. 48, No. 1, pp. 34-35, January, 1980. Original article submitted November 4, 1977; revision submitted June 18, 1979.

0038-531X/80/4801-0041$07.50

circulation loop of a boiling reactor is 0.014-0.054 m, then in all cases the value of ω is identical and is equal to $(53 \pm 8) \cdot 10^{-2}$ h^{-1}. The deposition constant found in this way makes allowance for the effect of many processes and factors, as a result of which it can be used in the designing of single-loop installations of the RBMK type, while contributing an error of no more than ±15%.

In steady-state regimes of plant operation the flow rate of reactor water for purification can be estimated from the equation given above if ω is known. In transient regimes this water flow rate is found from the condition

$$p/V\gamma \geqslant \omega, \tag{2}$$

whence p $V\omega\gamma$. The identical values of ω for the steady-state and transient regimes of operation of a given plant allow Eq. (1) to be analyzed further. The left member of the equation for a given regime remains constant. The term $C_S D_S \mu_2$ in the right member of the equation depends on the operating parameters and, to some degree, on the separation devices. The term $C_{rw} V_{cl} \gamma \omega$ is not affected by the operating regime of the plant since the value of ω remains constant. Consequently, it is not possible to act on this term. What remains is the term $pC_{rw}\mu_1$ which determines the amount of iron CP in the volume of the loop. The flow rate of reactor water to establish loop purification can be increased, which will entail higher capital and operating costs, or the concentration of iron CP in the water used for purification can be increased. The latter can be accomplished by changing the inlet and outlet for the water. In steady-state operating regimes these places are stagnant zones with a comparatively low rate of circulation and it is possible to make systematic "rounds" of these places.

There is a very substantial (up to 50-fold) increase in the concentration of iron CP during transient periods of operation, which should be exploited to the maximum to eliminate these products from the loop. In the given case, evidently, it is necessary to also increase the flow rate of water for coolant purification since the increase CP concentration in the loop is not maintained for a long time ($\sim$2-2.5 h). Moreover, during these periods it is desirable to artificially stir up the CP, e.g., by changing the circulation rate by switching pumps.

The proposed recommendations have already been taken into accountin the RBMK-1500 reactor project. During the transient periods, a larger volume of water used for purification should pass only through mechanical filters whereas the volume of water entering the ion-exchange filters can remain the same as in the steady-state regime. It must be emphasized that the considerable quantity of suspended iron CP in the stagnant zones of the loop is explained by their arrival with the feedwater since condensate purification takes place directly after the turbine. One remedial measure is to purify the feedwater in rinsable ion-exchange filters which are distinguished by a high efficiency and are capable of functioning at elevated temperatures.

REACTIVITY COEFFICIENTS OF MATERIALS IN FERTILE MEDIA WITH $K_\infty \approx 1$

V. A. Dulin, Yu. A. Kazanskii, and V. F. Mamontov

UDC 621.039.51

The use of integral characteristics, measured in critical assemblies, to verify and correct nuclear data is meaningful only if the conditions of the experiment are adequately described by a computational model.

Integral experiments on BFS critical assemblies showed [1] that calculation using the BNAB-70 system of constants [2, 3] unsatisfactorily describes the reactivity coefficients (RC) of typical absorbing, scattering, and fissionable elements. It was of interest to study RC in assemblies for which calculations can be made with minimal errors due to idealization of the three-dimensional calculations. Such conditions were met by the BFS-31-4, 33-2, and 35-1 assemblies whose central parts had compositions ensuring $K_\infty \approx 1$ [4], quite large dimensions and a structure that displays little heterogeneity. The observed divergences between experiment and calculation in this case are due to the constant component of the computational error.

The BFS-35-1 assembly consisted of metallic uranium with 5.61% enrichment and was a copy of the SNEAK-8 assembly [5]. The BFS-33-2 consisted of uranium oxide with 8.35% enrichment while in the BFS-31-4 the oxide of ^{235}U was replaced by metallic ^{239}Pu. The RC measurements were made in the center of the assemblies with specimens of various sizes. The results of the measurements are averaged over the heterogeneous structure of the assemblies within the limits of the central cell (4-6 cm). Figure 1 gives the measured CR for specimens of ^{239}Pu, ^{10}B, and ^{12}C of various sizes; the RC are given as ratios to the CR of ^{235}U of zero size. Analysis of the RC ratios permit the errors of the three-dimensional calculations to be eliminated and to emphasise the constant component of the errors of calculation. The size of the specimens in Fig. 1 are characterized by the value $\sigma_0 = 1/nl$, where n is the nuclear density of the specimen, $l = 4\ V/S$ is its mean geometric size, V is the volume, and S is the surface of the specimen.

The calculations were performed according to the M-26 program [6] in the P_1 approximation using the BNAB-70 system of constants and its modification, OSKAR-76 [7]. Allowance was made for the effect of the heterogeneous structure of the assemblies on the RC ratio [8, 9]. The finite size of the specimens was taken into account by methods described in [1, 10]. Figure 1 gives the results of these calculations for the real structure of an assembly (BFS-31-4) and its homogeneous model. For other assemblies the computational difference between the homogeneous and heterogeneous models is an order of magnitude smaller. For ^{12}C the dependence of the RC on the size of the specimens is due primarily to the unblocking the surrounding medium, which was taken into account in [11]. As seen from Fig. 1,

TABLE 1. Comparison of the Results of Measurements and Calculations of RC Ratio

BFS assembly	RC ratio	Expt.	Calc.	
			BNAB-70	OSKAR-76
31-4	$^{239}Pu/^{235}U$	1,192±0,015	1,133	1,197
	$^{10}B/^{235}U$	−0,74±0,02	−0,590	−0,725
	$^{12}C/^{235}U$	−0,0114±0,0005	−0,0134	−0,0112
32-2	$^{239}Pu/U^{235}$	1,260±0,015	1,220	1,257
	$^{10}B/^{235}U$	−0,895±0,015	−0,733	−0,890
	$^{12}C/^{235}U$	−0,0042±0,0003	−0,0082	−0,0045
35-1	$^{239}Pu/^{235}U$	1,49±0,02	1,413	1,475
	$^{10}B/^{235}U$	0,52±0,03	−0,409	−0,452
	$^{12}C/^{235}U$	−0,0226±0,0010	−0,0218	−0,0238

Translated from Atomnaya Énergiya, Vol. 48, No. 1, pp. 35-36, January, 1980. Original article submitted January 30, 1978.

0038-531X/80/4801-0043$07.50

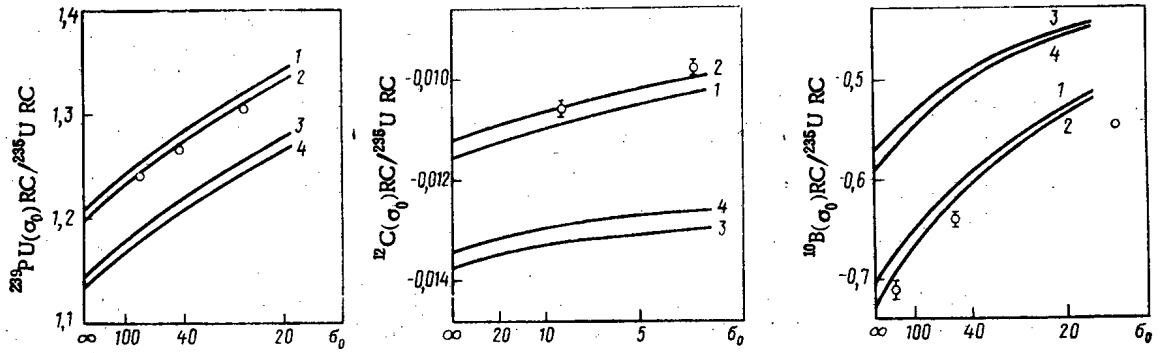

Fig. 1. Ratio of reactivity coefficients of ^{239}Pu, ^{12}C, and ^{10}B to reactivity coefficient of ^{235}U in BFS-31-4 assembly: 1, 2) calculation according to OSKAR-76 for homogeneous and heterogeneous models; 3, 4) calculation according to BNAB-70 for homogeneous and heterogeneous models; O) experiment.

the dependent of the RC ratio on the specimen size is described well by calculations, as noted earlier in [1].

Table 1 gives the results of calculations of the RC ratio, obtained by first-order perturbation theory (in Fig. 1 this value of the RC ratio at $\sigma_0 = \infty$). Corrections for the heterogeneous structure of the assemblies were introduced into the calculations. Calculations with OSKAR-76 are in much better agreement with the results of experiment. This is not surprising since the results of experiments with BFS-31 and BFS-33 assemblies were used in constructing this version [7]. Thus, the divergences between the calculated and measured RC ratios for typical fissionable, absorbing, and scattering elements are explained by the existence of the constant component of the errors of calculation.

LITERATURE CITED

1. V. A. Dulin et al., At. Energ., 40, No. 5, 377 (1976).
2. L. P. Abagyan et al., Group Constants for the Calculation of Nuclear Reactors [in Russian], Atomizdat, Moscow (1964).
3. L. P. Abagyan et al., Preprint FÉI-325, Obninsk (1974).
4. E. N. Kuzin et al., Preprint FÉI-698, Obninsk (1976).
5. M. Darrouzet, J. Chandat, and E. Fisher, in: Proc. Int. Symp. on Physics of Fast Reactors, Tokyo, Oct. 16-19 (1973), Vol. 1, p. 537.
6. Sh. S. Nikoalaishvili et al., in: Proc. Trilateral Soviet—Belgian—Dutch Symp. on Some Problems of Physics of Fast Reactors [in Russian], TsNIIatominform, Moscow (1970), Vol. 1, p. 192.
7. L. N. Usachev et al., in: Proc. Conf. "Neutron Physics" [in Russian], TsNIIatominform, Moscow (1977), Part IV, p. 27.
8. V. A. Dulin et al., in: Nuclear Constants [in Russian], Atomizdat, Moscow (1976), No. 21, p. 126.
9. V. A. Dulin, At. Energ., 45, No. 2, 107 (1978).
10. V. A. Dulin and V. F. Mamontov, Preprint FÉI-392, Obninsk (1973).
11. N. E. Gorbatov et al., in: Proc. Conf. "Neutron Physics" [in Russian], TsNIIatominform, Moscow (1977), Vol. 2, Paper D36.

COMPARISON OF CROSS SECTIONS FOR THE PRODUCTION OF ^{115}Cd AND ^{140}Ba IN THE PHOTOFISSION OF ^{235}U, ^{238}U, ^{237}Np, AND ^{239}Pu

P. P. Ganich, V. I. Lomonosov, and D. I. Sikora

UDC 539.172.3

In the investigation of photofission processes in transuranium elements it is of interest to know the yields and the cross sections for the photoproduction of fragments in symmetric and asymmetric fission as a function of the γ energy. Data have recently been published [1-4] on the yields of photofission products in the maximum and minimum of the mass distribution of fragments (or their ratio) as a function of the maximum photon energy for ^{235}U, ^{238}U, ^{237}Np, and ^{239}Pu nuclei. The photofission cross sections for these nuclides in the giant resonance region are given in [1].

The existence of such data permits the calculation of the total fission-fragment yield, the yields of the ^{140}Ba and ^{115}Cd fragments (normalized to one electron incident on the bremsstrahlung target) as functions of the maximum photon energy E_0, and from the ^{140}Ba and ^{115}Cd yield curves the integral and differential cross sections as functions of the photon energy. The calculation was performed in the following way. The total fragment yield per electron $Y_f(E_0)$ as a function of the maximum photon energy E_0 is

$$Y_f(E_0)=\int_{E_n}^{E_0}\sigma_{\gamma f}(E)\,P(E_0,\,E)\,dE.$$

The values of the photofission cross section $\sigma_{\gamma f}(E)$ were taken from [1], and the tabulated numbers of photons $P(E_0, E)\,dE$ in the bremsstrahlung spectrum from [5] (E_n is the photofission energy threshold).

The yield of an individual photofission fragment $Y_0(E_0)$ is

$$Y_0(E_0)=\frac{Y(E_0),\ \%}{200}\,Y_f(E_0).$$

The values of the percentage yield of fragments were first smoothed out by the least-squares method.

The cross section for the photoproduction of a fragment $\sigma_{\gamma 0}(E)$ was found from successive solutions of the equation

$$Y_0(E_0)=\int_{E_n}^{E_0}\sigma_{\gamma 0}(E)\,P(E_0,\,E)\,dE$$

for various values of E_0.

Figures 1-3 show the results of the calculations of $Y_f(E_0)$ (curve 1) and the values of $Y_0(E_0)$, $\sigma_{\gamma 0 \text{int}}(E)$, $\sigma_{\gamma 0}(E)$ (curves 2 and 3) multiplied by the factors in parentheses. It

TABLE 1. Cross Sections for the Production of ^{140}Ba and ^{115}Cd for E = 10.5 MeV

Reaction	$\sigma_{\gamma 0}(E)^{140}$Ba, mB	$\sigma_{\gamma 0}(E)^{115}$Cd, μb	$\frac{10^{-3}\sigma_{\gamma 0}(E)}{\sigma_{\gamma f}(E)}{}^{115}$Cd
^{235}U (γ, f)	2,55±0,8	102±30	1,6
^{238}U (γ, f)	1,43±0,4	23±6	0,5
^{237}Np (γ, f)	3±0,1	120±40	1,06
^{239}Pu (γ, f)	5,7±1,8	180±60	0,95

Translated from Atomnaya Énergiya, Vol. 48, No. 1, pp. 36-38, January, 1980. Original article submitted November 27, 1978; revision submitted May 3, 1979.

0038-531X/80/4801-0045$07.50

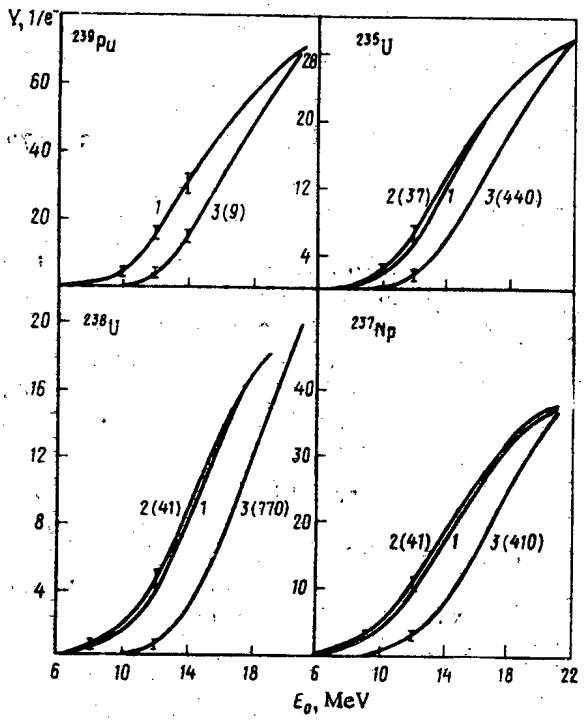

Fig. 1

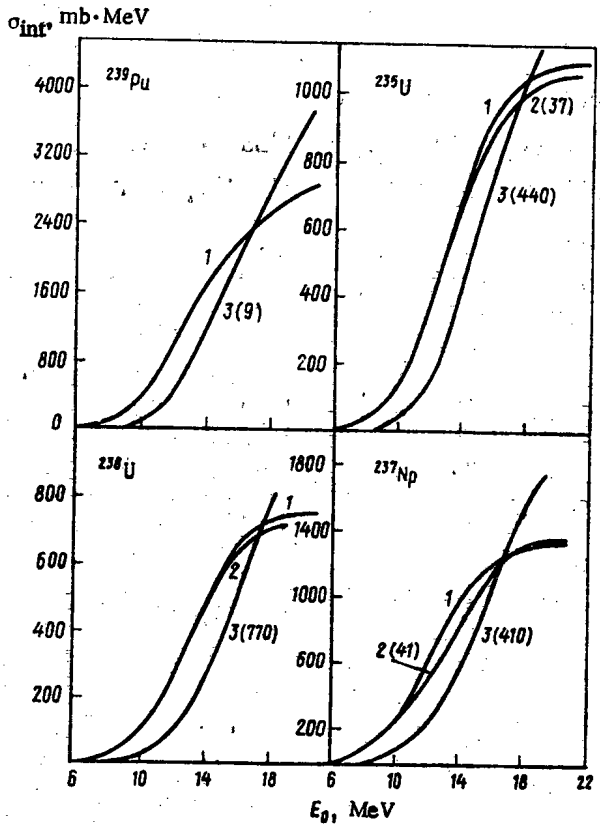

Fig. 2

Fig. 1. 1) Photofission yield; 2) photoproduction of ^{140}Ba; 3) photoproduction of ^{115}Cd. The value of the ordinate must be multiplied by $3.9 \cdot 10^{-25}$ to obtain the absolute value of the photofission yield.

Fig. 2. Integral cross sections for 1) photofission; 2) photoproduction of ^{140}Ba; 3) photoproduction of ^{115}Cd.

is clear from the figures that, within the limits of error, curves 2 for the photoproduction of ^{140}Ba coincide with the corresponding curves for the photofission of ^{235}U, ^{238}U, and ^{237}Np.

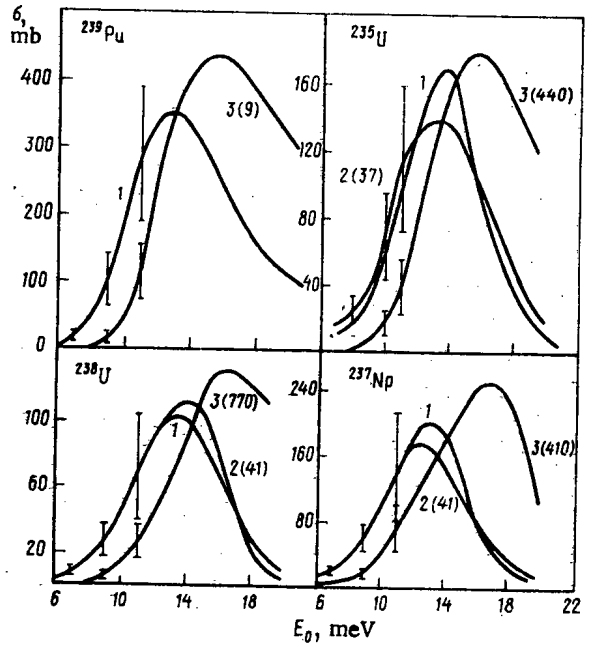

Fig. 3. Differential cross sections for 1) photofission [1]; 2) photoproduction of ^{140}Ba; 3) photoproduction of ^{115}Cd. For ^{239}Pu curve 3 is in relative units.

The ratio of the yields

$$K(E_0) = Y_0(E_0)_{^{115}Cd} / Y_0(E_0)_{^{140}Ba}$$

for ^{239}Pu is given in [4] as a function of the maximum photon energy. Under the assumption that the shapes of the curves for ^{239}Pu characterizing the dependence of the integral and differential cross sections for the photoproduction of ^{140}Ba are the same as those for photofission, it is possible to compare the relative yields $Y_0'(E_0)$ and the relative cross sections $\sigma'_{\gamma 0}(E)$ for the photoproduction of ^{115}Cd with the corresponding functions for the photofission of ^{239}Pu (Figs. 1-3 for ^{239}Pu).

The relative yield of the photoproduction of ^{115}Cd was determined from the relation

$$Y_0'(E_0) = K(E_0) Y_f(E_0),$$

and the relative values of the functions $\sigma'_{\gamma 0}(E)$ and $\sigma'_{\gamma 0 int}(E)$ were determined in the same way as $\sigma_{\gamma 0}(E)$ and $\sigma_{\gamma 0 int}(E)$.

The relative error in determining the fragment yield $\Delta Y_0(E_0)/Y_0(E_0)$ was assumed equal to the relative error in measuring the percentage yield of fragments [1], and did not exceed 10%. The maximum errors shown in Table 1 and Fig. 3 were determined by the reciprocal matrix method [5].

A comparison of the data obtained shows:

1) The curves for $Y_0(E_0)$, $\sigma_{\gamma 0 int}(E)$, $\sigma_{\gamma 0}(E)$, $Y_0'(E_0)$, $\sigma_{\gamma 0 int}(E)$, and $\sigma'_{\gamma 0}(E)$ for the photoproduction of ^{115}Cd are shifted with respect to the analogous curves for the photoproduction of ^{140}Ba or the photofission of ^{235}U, ^{238}U, ^{237}Np, and ^{239}Pu by 2-3 MeV toward higher photon energies. Such a shift is observed for photon energies up to 12 MeV, and cannot be accounted for by computational errors.

2. In the fission of ^{235}U, ^{238}U, ^{237}Np, and ^{239}Pu by 10.5-MeV photons the cross section for the production of ^{140}Ba is larger than the cross section for the production of ^{115}Cd. Table 1 shows that the cross section for the production of ^{115}Cd is of the same order of magnitude as the cross section for the production of isomers in (γ, n) reactions in plutonium and americium nuclides [6].

This behavior of the yield curves and the cross sections for symmetric and asymmetric photofission may be related to the fact that in the interaction of γ rays with a nucleus there is an octupole deformation as shown in [6, 7] in which the height of the second fission barrier is lowered by 2-3 MeV, and the probability of asymmetric fission is greater than that for symmetric fission.

In conclusion, the authors thank V. M. Strutinsky and B. D. Kuz'minov for helpful advice and assistance with the work.

LITERATURE CITED

1. V. M. Gorbachev, Yu. S. Zamyatnin, and A. A. Lbov, Interaction of Radiation with Nuclei of Heavy Elements, and Nuclear Fission (Handbook) [in Russian], Atomizdat, Moscow (1976).
2. M. Ya. Kondrat'ko, V. N. Korinets, and K. A. Petrzhak, At. Energ., 34, 52 (1973).
3. M. Ya. Kondrat'ko, V. N. Korinets, and K. A. Petrzhak, At. Energ., 35, 214 (1973).
4. M. Ya. Kondrat'ko, V. N. Korinets, and K. A. Petrzhak, At. Energ., 40, 72 (1976).
5. O. V. Bogdankevich and F. A. Nikolaev, Work with a Bremsstrahlung Beam [in Russian], Atomizdat, Moscow (1964).
6. S. M. Polikanov, Isomerism of Atomic Nuclei [in Russian], Atomizdat, Moscow (1977).
7. V. Strutinsky, Nucl. Phys., A95, 420 (1967); Rev. Mod. Phys., 44, 320 (1972).

BEHAVIOR OF BOILING REACTOR DURING WITHDRAWAL OF SHIM RODS

R. E. Fedyakin and E. V. Kozin

UDC 621.039.58

An important aspect in the study of problems of reactor safety is that of reactor behavior in various emergency situations. One dangerous situation can arise in the event of an unforeseen withdrawal of shim rods, as a result of which excess reactivity is released, causing a sharp rise in the neutron density and heat liberation and, in the final account, this leads to the destruction of the fuel elements. To prevent such an emergency, control and safety systems have provisions for limiting the rate of withdrawal of the absorber rods and, as a rule, they are moved in steps.

In the VK-50 boiling reactor in the critical state without boiling in the core as well as in VVÉR (water-moderated—water-cooled power reactors) [1] the withdrawal of any group of shim rods by 20-25 mm results in a rapid increase in the neutron density (with a period <20 sec). However, once conditions of developed boiling have been reached the reaction of the core to the withdrawal of the shim rods is weakened substantially.

Experiments with the withdrawal of shim rods were carried out at low pressure (P = 1.5 MPa) and high pressure (P = 7 MPa) in the reactor. The reactor power was 16 and 110-130 MW, respectively, and the mean steam content by volume in the core was 25 and 34%.

Groups of rods (three in each) were withdrawn continuously at the rate of 2.5 mm/sec, at first on the periphery and then in the center of the core. The initial position of the shim rods corresponded to the region of their maximum efficiency. The rods were withdrawn 300 mm, the average rate of increase in reactivity being $1.7 \cdot 10^{-4}$ sec^{-1}. As a result, an excess reactivity of ~2% was introduced in 2 min. Notwithstanding this, during the withdrawal of the rods the reactor power increased with a period of 4-5 min, by a total of 25% at low pressure and 15% at high pressure.

At a pressure of 7 MPa and a power reactor of 130 MW the central shim rod was withdrawn to a distance of 400 mm at the rate of 35 mm/sec. The mean rate of reactivity increase in this case was $2 \cdot 10^{-3}$ sec^{-1}. But in this case, as before, the period of reactor power build-up was 4 min. Once the withdrawal of the rods was stopped, the increase in reactor power also ceased.

The experiments carried out showed that when excess reactivity in introduced during the withdrawal of rods it is rapidly compensated because of the additional generation of steam. Consequently, in the operation of the VK-50 vessel-type boiling reactor in the developed boiling regimen there is no dangerous increase in the rate of power increase, even in cases of damage to the control system or erroneous actions by the operator, resulting in a continuous withdrawal of the absorption rods.

Translated from Atomnaya Énergiya, Vol. 48, No. 1, pp. 38-39, January, 1980. Original article submitted January 24, 1979.

0038-531X/80/4801-0048$07.50

GAMMA DOSE BUILDUP FACTORS IN AIR

I. N. Butueva and I. N. Trofimov

UDC 539.121.72:539.122

It has recently become necessary to calculate the penetration in air of γ rays with energies up to 10 MeV and higher.

We have calculated dose buildup factors in air for energies from 0.5 to 15 MeV using a modification of the Monte Carlo method permitting calculations for deep penetrations [1]. The essence of the modification consists in specifying a uniform distribution of first collision sources over the thickness of the shield, which ensures the wandering of particles to any depth, and the use of splitting. The splitting surfaces were spaced uniformly with a separation of 0.8 mfp at the source energy. When this modified method was checked by test calculations of buildup factors in water and iron [1], the results agreed with those of Goldstein and Wilkins [2] to within 5-10% on the average, with a maximum difference of no more than 15%.

The dose buildup factors in air were calculated for plane monodirectional and plane isotropic sources, using constants from [3]. The value for a point isotropic source was calculated from the results for a plane isotropic source by using the formula given in [1]. The lower limit of the differential energy spectrum was chosen as 20 keV. The results of the calculations are shown in Table 1.

The statistical error of the results varied from 5 to 20% for shield thicknesses from 1 to 20 mfp.

LITERATURE CITED

1. I. N. Butueva et al., At. Energ., 45, 125 (1978).

TABLE 1. Gamma Dose Buildup Factors in Air

μx	E, MeV									
	0,5	1	2	3	4	5	6	8	10	15
Plane monodirectional source										
1	2,6	2,2	1,85	1,74	1,69	1,62	1,53	1,45	1,41	1,30
2	4,2	3,2	2,60	2,35	2,21	2,06	1,93	1,78	1,70	1,58
4	8,1	5,8	4,5	3,7	3,3	3,0	2,7	2,45	2,2	1,95
7	16,5	10,5	7,2	5,7	4,9	4,4	4,0	3,5	3,0	2,5
10	29	17	10,3	7,8	6,5	5,8	5,1	4,4	3,7	3,1
15	59	32	16,2	11,5	9,1	7,9	6,9	5,6	4,7	4,0
20	115	59	24,5	16,4	12,9	10,7	9,3	7,8	6,4	5,3
Plane isotropic source										
1	3,45	2,85	2,3	2,1	2,0	1,93	1,82	1,76	1,65	1,46
2	6,4	4,8	3,4	2,9	2,65	2,55	2,35	2,12	2,0	1,75
4	16	9,5	5,7	4,8	4,05	3,7	3,2	2,85	2,6	2,3
7	40	18,2	9,8	7,4	5,9	4,9	4,3	3,8	3,5	2,9
10	70	30	14,2	10,3	7,8	6,3	5,6	4,8	4,3	3,4
15	146	54	23	15	11,2	9,1	7,8	6,6	5,8	4,3
20	280	91	37	20,5	15,1	12,4	10,5	8,7	7,7	5,6
Point isotropic source										
1	2,25	1,83	1,7	1,62	1,6	1,55	1,5	1,49	1,42	1,3
2	3,9	3,24	2,6	2,25	2,16	2,15	2,02	1,85	1,76	1,56
4	11,4	7,45	4,65	4,1	3,5	3,3	2,88	2,58	2,35	2,12
7	31,8	15,3	8,6	6,6	5,3	4,5	3,95	3,5	3,25	2,75
10	59	26	12,8	9,5	7,2	5,8	5,2	4,5	4,0	3,25
15	127	49	21	14,1	10,5	8,5	7,35	6,25	5,5	4,15
20	250	82	34	19,5	14,3	11,7	10	8,3	7,35	5,3

Translated from Atomnaya Énergiya, Vol. 48, No. 1, p. 39, January, 1980. Original article submitted January 8, 1979.

0038-531X/80/4801-0049$07.50

2. H. Goldstein and J. Wilkins, Fundamental Aspects of Reactor Shielding, Johnson Repr. (1959).
3. E. Storm and H. Israel, "Photon cross sections from 1 keV to 100 MeV for elements Z = 1 to Z = 100," Nucl. Data, 7A, 565 (1970).

PRECISION METHOD OF MEASURING HEAT RELEASE IN CRITICAL ASSEMBLIES

A. T. Bakov, V. A. Volkov, and R. A. Musaev

UDC 539.1.073/074

The compact arrangement of the primary loop equipment of fast reactors, such as the BN-600, complicates the design of the thermal shield which is placed between the core and the heat exchangers and is one of the principal elements of the integral arrangement. The heating of the shield is important in the thermal behavior of the assembly. The study of gradients of the volumetric heat-release rate at boundaries between regions with different material compositions is of particular interest from the technological point of view. The methods available for calculating such composites are not accurate enough, and it is necessary to study the distribution of the volumetric heat-release rate in mock-ups.

At the present time the most widely used methods of studying the total volumetric heat-release rate in critical assemblies are the calorimetric method [1, 2] and a method using thermoluminiscent dosimeters [3]. These methods either are not direct, or the detectors are large and complex and perturb the temperature and neutron distributions in the reactor. We propose a method based on the measurement of the dynamics of temperature distributions in various parts of the critical assembly as a function of the reactor power.

The heat-release rate at the center of the volume under study is measured with a temperature sensing device which makes reliable thermal contact with the structural elements. the rate of change of temperature is measured at zero power, the reactor is brought up to power, and the time rate of change of temperature is measured at constant reactor power. In this case the volumetric heat-release rate Q is

$$Q = \frac{\sum_i c_M^i n_i}{N_0}\left[\frac{dT}{dt} + f(t)\right], \quad (1)$$

where dT/dt is the rate of change of temperature at constant reactor power, deg/sec; c_m^i, is molar specific heat of the i-th element in the reactor zone being measured, cal/mole deg; n_i, number density of nuclei of the i-th element in the reactor zone being measured, nuclei/cm^3; N, Avogadro's number; f(t), rate of change of temperature at zero power, deg/sec.

The function f(t) characterizes the kinetics of the redistribution of temperature when there is a gradient of the volumetric heat-release rate in the region being measured as a result of the previous increase in reactor power. A temperature drift of the zone was noted in the experiment even after a long reactor shutdown because of the temperature instability of the external medium. The nature of the temperature drift of the zone was measured before and after each increase in reactor power. In this case

$$f(t) = \frac{1}{2}\left(\frac{dT_B}{dt} + \frac{dT_A}{dt}\right), \quad (2)$$

where dT_B/dt and dT_A/dt are, respectively, the rates of temperature drift before and after an increase in reactor power.

In critical assemblies the volumetric heat-release rate in the core is very small, and very small temperature changes must be recorded in measuring the dynamics of the temperature distribution. Thus, inside the core the temperature varies at a rate of $\sim 10^{-2}$ °C/min, and in the shield at $\sim 10^{-4}$ °C/min. To record such slow temperature changes the temperature-sensitive element must have a high sensitivity. Quartz thermometers have large metrological

Translated from Atomnaya Énergiya, Vol. 48, No. 1, pp. 39-41, January, 1980. Original article submitted January 24, 1979.

 0038-531X/80/4801-0050$07.50

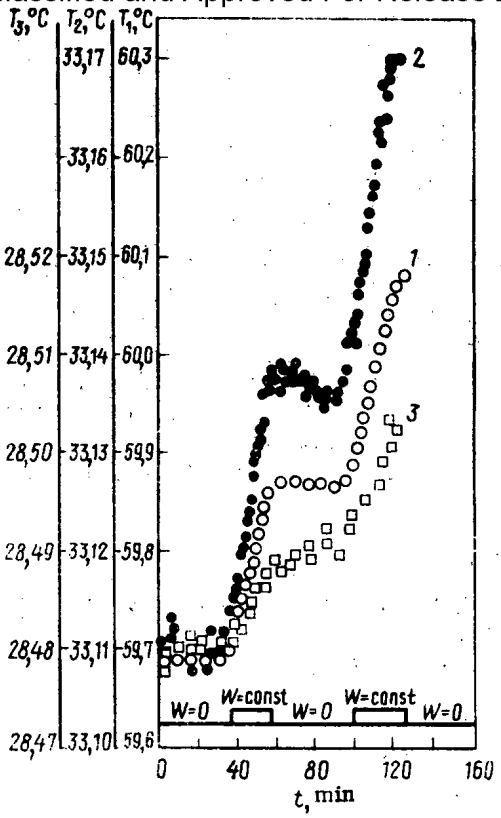

Fig. 1

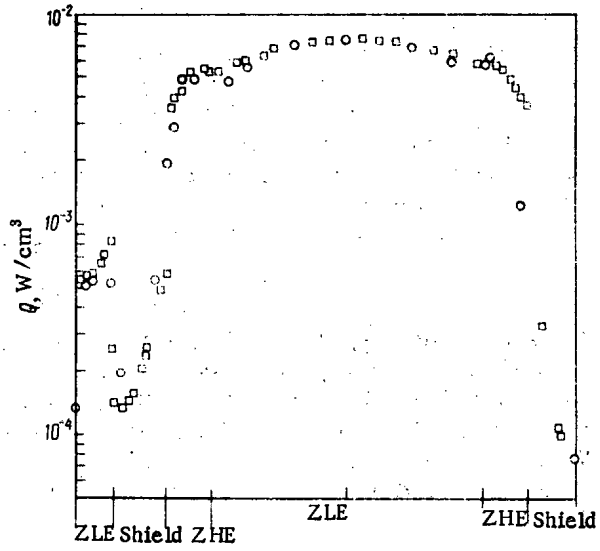

Fig. 2

Fig. 1. Time variation of temperature 1) at core center; 2) at the core-thermal shield boundary; 3) at the thermal shield-biological shield boundary, measured with quartz thermometers, for various power levels.

Fig. 2. Distribution of total volumetric heat-release rate (○) measured with a quartz thermometer, and heat-release rate resulting from fission reactions (□), measured with a fission chamber.

parameters [4]. These devices make use of the change of natural frequency of a quartz resonator with temperature. The circuit for measuring the temperature contains a temperature sensor with a frequency output, and a digital frequency meter. The parameters of the resonator crystal vary with temperature. In the oscillator circuit of the temperature sensor, serving as a frequency transformer, these parameters are transformed into a frequency. The quartz resonator combines in the temperature sensor the functions of an element synchronizing the frequency, and a temperature—sensitive element. High sensitivity is achieved by using quartz resonators with a high resonant frequency f_0 and a large temperature coefficient K. The nonlinearity of the temperature coefficient of a quartz resonator in the 0-100°C range is 0.074°C.

The frequency output of the temperature sensing element permits locating the digital temperature measuring device at a large distance from the object being measured without introducing additional errors. Quartz resonators with $f_0 \approx 5$ MHz and $K \approx 170$ Hz/°C were used in the experiments. Information from the digital temperature measuring device was fed into a computer through standard modules. The temperature-sensitive elements were also connected through standard modules.

It should be noted that relative measurements of the volumetric heat-release rate can be made while the reactor is in transition from one power level to another (Figs. 1 and 2). Figure 1 shows how the temperature varies in various zones of a critical assembly for various powers. Figure 2 shows the radial distribution of the volumetric heat-release rate in a critical assembly, measured in a central plane. The measurements were performed by the contact kinetic method and small-scale fission chambers [5].

The counting rate obtained with a fission chamber is transformed to the volumetric heat-release rate by the expression

$$Q = \sum_i AN_i E_f^i n_i (\langle \sigma_f^i \rangle / \langle \sigma_f^{235} \rangle), \quad (3)$$

where N_i is the relative fission chamber counting rate of the i-th fissionable element; E_f^i, part of the energy liberated per fission of the i-th fissionable element which is turned into heat; n_i, number of nuclei of element i per cm³ of the assembly; $\langle \sigma_f^i \rangle / \langle \sigma_f^{235} \rangle$, ratio of the fission cross sections of corresponding elements averaged over the neutron spectrum.

The ratio of the average reaction cross sections of fissionable elements was determined experimentally. The coefficient A was determined with an absolute fission chamber at the core center. In calculating the total volumetric heat-release rate by Eq. (1), the values of the molar specific heats were taken from [6]. It turned out that in zones of low enrichment (ZLE) and zones of high enrichment (ZHE) the results obtained by the two methods agree within the limits of error. The difference in the shield is in complete agreement with the calculated value of the contribution of secondary gamma radiation to the total volumetric heat-release rate. The statistical error of the measured distributions was no more than 1% in the core, and 3-5% in the shield.

LITERATURE CITED

1. O. A. Gerashchenko, V. B. Klimentov, and A. V. Nikonov, At. Energ., 32, 232 (1972).
2. A. S. Zhilkin et al., At. Energ., 42, 502 (1977).
3. G. Simons and T. J. Yule, Nucl. Sci. Eng., 53, 162 (1974).
4. V. V. Malov, Piezoelectric Resonant Transducers [in Russian], Énergiya, Moscow (1978).
5. V. V. Bondarenko et al., At. Energ., 24, 82 (1968).
6. I. K. Kikoin (editor), Handbook of Physical Quantities [in Russian], Atomizdat, Moscow (1976).

EFFECT OF HYDROGEN ON THE ERROR IN MEASURING THE CONTENT OF FISSIONABLE NUCLIDES BY NEUTRON METHODS

V. I. Bulanenko and V. V. Charychanskii

UDC 621.039.548

The requirements of safety and material accountability in the production of fuel for nuclear power reactors necessitates reliable methods and means of measuring the content of fissionable nuclides in various media. These measurements can be made by active and passive neutron methods. In using fast neutrons (active methods) and neutron self-radiation of the medium (passive methods) for inducing fissions in water-free media, the presence of an uncontrollable amount of hydrogen in the material being analyzed can introduce further errors into the measured result [1]. In this case the error causes a change in the fission reaction rate, a change in the multiplication, and a softening of the energy spectrum of the leakage neutrons as a result of their slowing down in interactions with hydrogen nuclei in the medium being monitored. A change in these parameters can lead to a change in the response of the detecting system which is not related to a change in the content of fissionable nuclides.

As an example of the effect of hydrogen on the error in measuring the content of fissionable nuclides in water-free media we consider the monitoring of ^{235}U enrichment in uranium hexafluoride UF_6. The uranium enrichment in UF_6 in shipping containers is monitored by using the neutron self-radiation arising from the ^{19}F (α, n) ^{22}Na reaction [2]. Although ^{234}U is the dominant alpha emitter among the uranium isotopes, in view of the practically constant isotopic ratio $^{235}U/^{234}U$ for low (up to 5%) ^{235}U enrichment, the neutron yield from the (α, n) reaction can be considered a measure of the ^{235}U content [3].

In general the response of the detecting system used to determine enrichment is a function of the enrichment J and the hydrogen content C_H:

$$N \approx f(J, C_H). \tag{1}$$

An approximate expression for the response function can be obtained by calculating the neutron distributions in a system containing UF_6 with various uranium enrichments and various hydrogen contents. The method of calculation is based on the solution of multigroup equations describing the interaction of neutrons with matter in the P_1 approximation. Calculations were performed for a cylinder with a ratio of height to diameter of the order of unity, filled with UF_6 with a density of 5 g/cm^3 for a range of uranium enrichments from natural to 5%, and containing from 0 to 0.05 wt.% of hydrogen uniformly distributed through the UF_6. The detector was a neutron counter with a ^3He radiator with and without a cadmium cover, and also with a boron carbide (B_4C) shield.

The neutron detector counting rate was determined from the calculated group fluxes and the known group efficiency. The results of the calculations are shown in Fig. 1. These results permit the following conclusions which simplify subsequent calculations:

1. The change in neutron multiplication in the system can be neglected over the range of hydrogen content in UF_6 considered. The relative change in k_{eff} does not exceed 5%; for a 5% enrichment and no hydrogen $k_{eff} = 0.297$.

2. A variation of uranium enrichment in UF_6 from natural to 5% leaves the energy spectrum of the leakage neutrons practically unaffected.

3. In the range investigated the dependence of the neutron counting rate on enrichment can be represented by a straight line of the form

$$N_0 = A + BJ, \tag{2}$$

Translated from Atomnaya Énergiya, Vol. 48, No. 1, pp. 41-42, January, 1980. Original article submitted January 24, 1979.

0038-531X/80/4801-0053$07.50

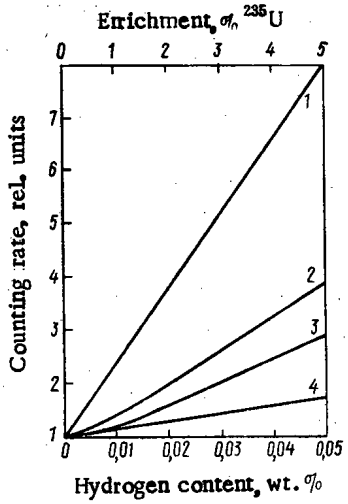

Fig. 1

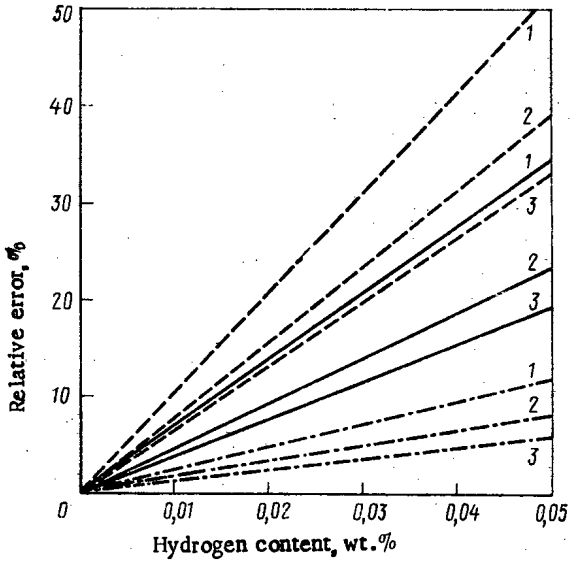

Fig. 2

Fig. 1. Dependence of neutron counting rate on enrichment (1) and hydrogen content (2, 3, 4) measured with a thermal detector (2) and detectors with Cd (3) and B_4C (4) shields.

Fig. 2. Relative error in measurement of uranium enrichment in UF_6 as a function of hydrogen content: ---) thermal detector; ——) epithermal detector; -.-·) detector shielded with B_4C; 1-3) enrichment 0.7, 1.8, 3.6%, respectively.

where A is the constant contribution of ^{238}U to the counting rate, and B is the constant change in neutron counting rate per 1% change in enrichment.

4. The dependence of the neutron counting rate on hydrogen content is approximated by a linear function of the form

$$N = N_0(1+\gamma C_H). \tag{3}$$

Here γ is the constant change in the neutron counting rate per 0.1% change in hydrogen content. The values of γ are different for a thermal detector and detectors with Cd and B_4C shields. Consequently, an approximate expression for the explicit dependence of the counting rate on enrichment and hydrogen content can be written as follows:

$$N = (A+BJ)(1+\gamma C_H). \tag{4}$$

From Eq. (4) we obtain an analytic relation for determining the enrichment from the measured neutron counting rate for an arbitrary hydrogen content

$$J = \frac{1}{B}\left(\frac{N}{1+\gamma C_H} - A\right). \tag{5}$$

We now assume that the component errors in measuring enrichment which are not related to the presence of hydrogen have been reduced to a minimum and are known exactly. Then the error introduced by the uncertainty in the hydrogen content can be estimated as:

$$\Delta J_{(\Delta C_H)} = (\partial J/\partial C_H)\,\Delta C_H. \tag{6}$$

From Eqs. (4)-(6) it is easy to obtain an expression for the relative error in determining the uranium enrichment in UF_6 introduced by the uncertainty in the hydrogen content:

$$\delta_J = \frac{\gamma}{B}\,\frac{A+BJ}{1+\gamma C_H}\,\frac{\Delta C_H}{J}. \tag{7}$$

Figure 2 shows the values of δ_J calculated by using A = 1, B = 1.5 (1/1% ^{235}U); γ = 1.4, 3.5, 5.8 (1/0.1% H) respectively for detectors shielded with B_4C, Cd, and bare. The values of the constants A, B, and γ were found by using Eq. (4) and the calculated results shown in Fig. 1.

Thus, the presence of an uncontrollable amount of hydrogen in the medium being analyzed leads to an appreciable error in the measurement of the enrichment (~6-10% per 0.01% of hydrogen, depending on the enrichment, when a thermal detector is used). In view of this, in measuring the content of fissionable materials in water-free media by neutron methods it is necessary to monitor the hydrogen content or to eliminate its effect on the measurements. This can be done to some extent by using a combination of threshold and 1/v neutron absorbing filters or a detecting system whose efficiency is independent of energy.

The authors thank V. V. Frolov for posing the problem and for a discussion of the results.

LITERATURE CITED

1. D. Close, R. Bearse, and H. Menlove, Nucl. Instrum. Methods, 136, 131 (1976).
2. R. Walton et al., Nucl. Technol., 21, 133 (1974).
3. T. Sampson, Nucl. Sci. Eng., 54, 430 (1974).

DEPENDENCE OF THE INTENSITY OF X-RAY RADIATION EXCITED BY PROTONS (IONS) ON THE ION ENERGY AND THE TARGET THICKNESS

V. F. Volkov, A. N. Eritenko, and Yu. A. Malykhin

UDC 535.33/34:539.183:539.184

Investigators have been showing increasing interest lately in the x-ray radiation arising in the passage of accelerated protons (ions) through matter. By recording this radiation, it is possible to determine small amounts of impurities of various elements in the material, their distribution along the thickness of the specimen, etc. [1]. The low intensity of bremsstrahlung in comparison with electron bombardment and scattered radiation in photon excitation makes this method more sensitive in comparison with x-ray fluorescent analysis and the electron-probe method [2].

Our purpose is to derive an analytical expression for the intensity of the characteristic radiation excited by protons (ions) as a function of the proton (ion) energy and the target thickness. In the model of linear proton (ion) trajectories, the intensity of the spectral line i due to a semi-infinite target consisting of atoms of one type is given by

$$I_i = k\omega_q p_{jq} \frac{N_A \rho}{A} \int_{E_q}^{E_0} \tilde{\sigma}(E_x)\,(-dx/dE)\exp(-\mu_i x(E_x)/\sin\Psi)\,dE_x, \quad (1)$$

where k is a coefficient accounting for the recording efficiency and the experimental geometry, p_{jq} is the probability of radiative transition between levels j and q, $\tilde{\sigma}(E_X)$ is the ionization cross section of atoms located at the depth x, where the proton energy is equal to E_X, E_0 is the initial proton energy, Ψ is the angle of radiation emergence from the target, measured from its surface, $(-dE/dx)$ is the proton energy loss, μ_i is the linear coefficient of radiation attenuation of the i-th line in the target, N_A is the Avogadro number, ρ is the density, A is the atomic mass, and ω_q is the fluorescence yield.

TABLE 1. Dependence of β on ξ_0

ξ_0	$\beta \cdot 10^{-3}$	ξ_0	$\beta \cdot 10^{-3}$
0,08	5,5	0,32	52
0,12	13	0,4	77
0,2	22		

Translated from Atomnaya Énergiya, Vol. 48, No. 1, pp. 43-44, January, 1980. Original article submitted February 5, 1979.

0038-531X/80/4801-0055$07.50

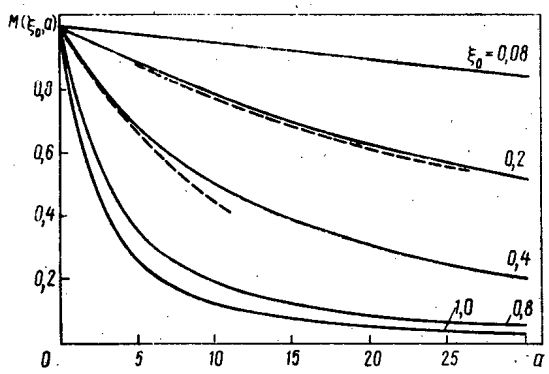

Fig. 1

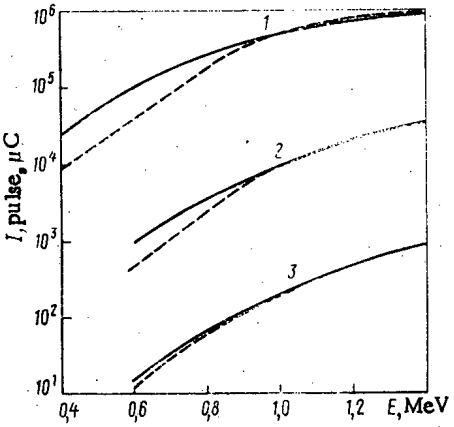

Fig. 2

Fig. 1. $M(\xi_0, a)$ as a function of a. ---) Calculation by means of expression (5); ——) calculation by means of the exact equation (4).

Fig. 2. X-ray radiation intensity as a function of the proton energy for Al (1), Ni (2), and Nb (3). ---) Calculation based on Eq. (4); ——) experiment [8] (the curves are joined at the energy of 1.4 MeV).

Using the Lindhard—Scharf equation for the ion energy loss [3], we can readily derive an expression which approximates the loss with an error of ∿10% in the energy range from 0.1 to 3 MeV:

$$-dE/dr = BN(Z/E)^{1/2}, \tag{2}$$

where $B = 5.44\ \pi Z_1^2 e^4 m_p^{1/2}/m_e v_0$; $Z_1 e$ is the ion charge, m_p and m_e are the ion mass and the electron mass, respectively, $v_0 = 2.2 \cdot 10^8$ cm/sec, N is the number of atoms per unit volume, and Z is the atomic number of target atoms. By integrating Eq. (2), we obtain the linear ion range:

$$R_0 = E_0^{3/2}/BNZ^{1/2}. \tag{3}$$

Comparison of the ranges for aluminum, copper, and gold calculated by means of (3) with data from [4] shows that this expression can be used with an accuracy sufficient for analytical purposes in the approximate proton energy range from 0.1 to 5 MeV.

By introducing the dimensionless ionization cross section σ/σ_{max} and proton energy $\xi = E/E_{max}$ and using expression (2), we write the equation (1) for the radiation intensity in the following form:

$$I_i = k\omega_q l' j_q \frac{N_A \rho Z_1^2 a \sigma_{max} \sin\Psi}{A E_q^2 \mu_i} Q(\xi_0, a), \tag{4}$$

where σ_{max} is the maximum value of the ionization cross section of the element whose radiation is recorded, $a = \mu_1 R_{max}/\sin\Psi$, R_{max} is the range of protons (ions) with the energy E_{max} for which the maximum ionization cross section is reached, $\xi_0 = E_0/E_{max}$, $\xi_q = E_q/E_{max} = \text{const}$ (E_0, Z), and

$$Q(\xi_0, a) = \int_{\xi_q}^{\xi_0} \eta(\xi)\, \xi^{1/2} \exp\left[-a\left(\xi_0^{3/2} - \xi^{3/2}\right)\right] d\xi;$$

$$\eta(\xi) = \sigma(\xi)/\sigma_{max}$$

It is evident that the function $Q(\xi_0, a)$ is a universal function for all elements, which depends on the initial energy and the parameter a that characterizes the absorbing and stopping power of the target material. The function $Q(\xi_0, a)$ has been tabulated for practical application for ξ_0 values from 0.01 to 1 and the values of the a parameter from 1 to 50. In calculating the $Q(\xi_0, a)$ function, the ionization cross section was computed by means of the expression

$$\lg\sigma = \sum_{n=0}^{7} A_n \lg^n (E m_e/m_p E_q); \quad \sigma = E_q^2 \tilde{\sigma}(E)/Z_1^2,$$

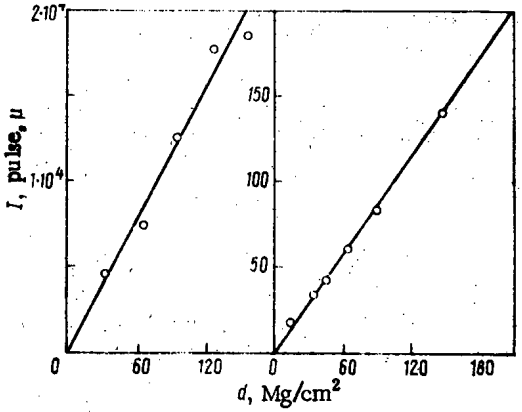

Fig. 3. X-ray radiation intensity as a function of the target thickness for the proton energy $E_0 = 1.4$ MeV for Ag (a) and Cu (b). ——) Calculation based on expression (6); O) experiment [8].

given in [5], which approximates with an error of ∿1% the Garcia table of cross sections [6]. The values of the A_n coefficients are given in [5]. Figure 1 shows the dependence of the function $Q(\xi_0, a)/Q(\xi_0, 0) = M(\xi_0, a)$ on ξ_0; $M(\mu_0, a)$ determines the percentage of radiation emerging from the target. With an increase in the proton energy, the percentage of radiation emerging from the target decreases considerably due to the fact that the thickness of the layer where ionized atoms are formed increases considerably, so that the radiation emerging from deep-lying layers is heavily attenuated as a result of absorption by the above-lying layers of the material. Since the radiation attenuation factor μ is proportional to $Z^4\lambda^3$ [7], long-wave radiation is more attenuated than short-wave radiation, i.e., the target operates as a filter of radiation generated within the target. Since the proton (ion) range is proportional to $Z^{1/2}$, the parameter a is equal to $a \sim Z^{9/2}\lambda^3$, and, therefore, the percentage of radiation emerging from targets consisting of heavy elements is much smaller than in the case of light-element targets.

Numerical analysis shows that the function $Q(\xi_0, a)$ can be represented in the following form:

$$Q(\xi_0, a) \approx Q(\xi_0, 0)\exp(-\beta a). \tag{5}$$

The values of β as functions of ξ_0 are given in Table 1. The analytical expression (5) provides a good approximation of the function in the energy range from 0.01 to 0.2 E_{max} for all values of the parameter a and in the energy range from 0.2 to 0.4 E_{max} for $a \leq 5$.

Using the calculated and the tabulated function $Q(\xi_0, a)$, we plotted the intensity of K_α radiation as a function of the proton energy for aluminum, nickel, and niobium and provided comparison with experimental data from [8] (Fig. 2). The difference between the theoretical and experimental values of the intensity of K_α radiation for aluminum can probably be explained by the inaccuracy of the initial data on the ionization cross sections and experimental errors.

Figure 3 shows the calculated and the experimental dependences of the intensity on the target thickness. The dependence of the intensity on a target with the thickness d was calculated by means of the expression

$$I_i(d) = k\omega_q p_{jq}\frac{N_A \rho Z_1 a\sigma_{max}\sin\Psi}{AE_q^2\mu_i}\left[Q(\xi_0, a) - e^{-\mu_i d/\sin\Psi}Q(\xi_d, a)\right], \tag{6}$$

where $\xi_d = E_d/E_{max}$, and E_d is the proton (ion) energy upon emergence from a film with the thickness d. After calculating the function $Q(\xi_0, a)$, we found its values for ξ_0 and ξ_d. The universal function $Q(\xi_0, a)$ can be used for quick estimates of the radiation intensity as a function of the specimen's composition and thickness and the proton energy with an error not worse than 10%.

LITERATURE CITED

1. V. M. Kolyada, A. K. Zaichenko, and R. V. Dmitrenko, X-Ray Spectral Analysis with Ion Excitation [in Russian], Atomizdat, Moscow (1978).
2. M. A. Blokhin and S. M. Blokhin, Zavod. Lab., 43, No. 12, 1452 (1977).
3. Yu. V. Gott and Yu. N. Yavlinskii, Interaction of Slow Particles with Matter and Plasma Diagnostics [in Russian], Atomizdat, Moscow (1973).
4. L. Northcliffe and R. Shilling, Nucl. Data, A7, No. 3, 458 (1970).
5. W. Reuter et al., J. Appl. Phys., 46, No. 7, 3194 (1977).
6. J. Garcia, R. Fortner, and T. Kavanaugh, Rev. Mod. Phys., 45, No. 2, 111 (1973).
7. M. A. Blokhin, X-Ray Physics [in Russian], Gostekhteorizdat, Moscow (1953).
8. Maryse Poncet et al., Analysis, 3, No. 6, 283 (1975).

EXPERIMENTAL DETERMINATION OF TRITIUM CONVERSION RATIOS

D. I. Evgrafova, Z. V. Ershova,
V. K. Kapyshev, and V. I. Sakharov

UDC 546.11.02.3:621.039.6

One of the principal characteristics of the blanket of a thermonuclear reactor is the tritium conversion ratio K_T [1-8]. Numerous calculations have been made of K_T but experimental work in this area was begun only in recent years [6-10].

The principal difficulty in conducting such experiments lies in the comparatively low neutron fluxes with an energy of 14.1 MeV and, consequently, the small quantities and low concentrations of tritium obtained in these experiments, which makes it extremely difficult to determine the tritium with satisfactory accuracy by known methods. The geometric approximation of neutron generators, giving rise to difficulties when comparing experimental and calculated results, also hinders investigations in this area.

Two main directions are distinguished in the development of compositions of materials for thermonuclear reactor blankets, i.e., with and without fissionable materials [1-4]. It is proposed to reduce radiation damage by softening the spectrum of thermonuclear neutrons and to bring it closer to the spectrum of fission neutrons from fast reactors [3], i.e., in blankets with fissionable materials in the case of softening of the spectrum of the fast neutrons of the plasma, the zone producing the tritium will be subject to the action of neutrons whose spectrum is close to the spectrum of fission neutrons of breeder reactors. This allows K_T to be determined experimentally by using ^{252}Cf whose neutron spectrum is close to the fission—neutron spectrum of fast reactors.

In the present paper we give the results of determination of the build-up of tritium formed in lithium carbonate under irradiation with a californium neutron source. The spatial distribution of tritium accumulated in lithium carbonate was determined by both calculation and experiment. The tritium conversion ratio, calculated according to two-group theory with the first two collisions taken into account, is 0.35.

Irradiation of Salt. Lithium carbonate was irradiated with a californium source with an initial neutron flux $(1.3 \pm 0.2) \cdot 10^8$ neutrons/sec. The lithium-containing material used was lithium carbonate (3% ^6Li). The lithium carbonate was placed in seven hermetically sealed coaxial cylinders (Fig. 1) of stainless steel. In the assembly the cylinders approximates a sphere with a point californium neutron source at its center. The dimensions of the cylinders are given in Table 1.

The radius of the spherical assembly coincided with the thickness of the first lithium zone of the blanket of a hybrid thermonuclear reactor [11]. The entire assembly was placed in a vessel measuring 800 × 800 mm with a height of 1115 mm and was sealed in paraffin.

TABLE 1. Dimensions of Cylinders of Assembly with Lithium Salt

Parameter		Cylinder						
		I	II	III	IV	V	VI	VII
Height, mm		76,8	32,5	32,5	140	20	20	81
Diameter, mm	External	78	78	78	139	78	78	188
	Internal	17	17	17	79	17	17	140

Translated from Atomnaya Énergiya, Vol. 48, No. 1, pp. 44-46, January, 1980. Original article submitted January 30, 1979.

0038-531X/80/4801-0059$07.50

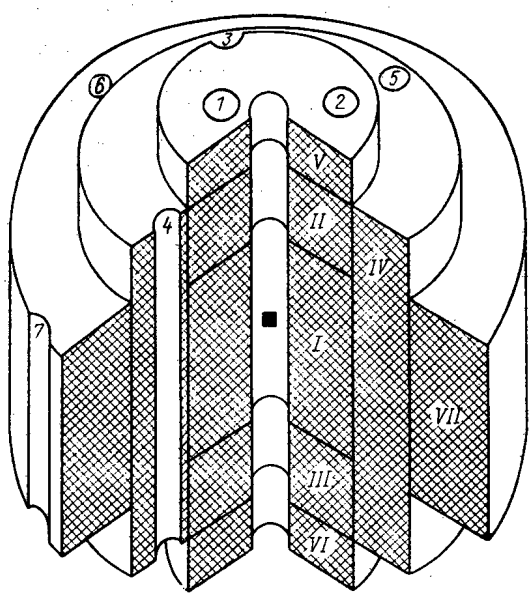

Fig. 1

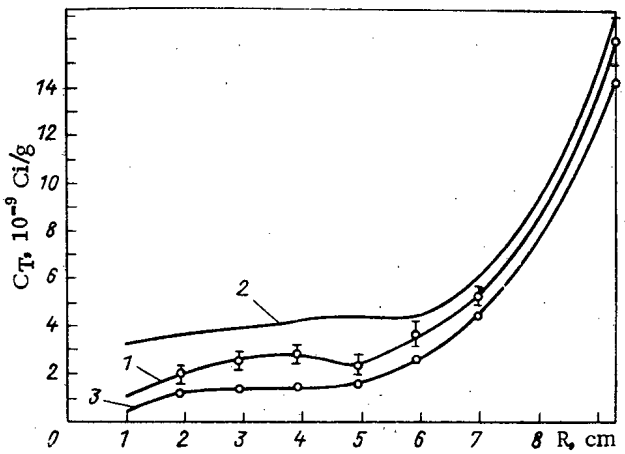

Fig. 2

Fig. 1. Assembly with lithium carbonate for irradiation with ^{252}Cf fission neutrons: I-VII) cylinders; 1-7) experimental channels; ■) californium source; cross-hatched area, Li_2CO_3.

Fig. 2. Tritium concentration vs radius of assembly: 1) measurements by scintillation method; 2) calculation by two-group technique; 3) calculation on basis of detector activation.

The lithium-containing assembly was provided with seven vertical channels, with a diameter of 18 mm, for experimental containers. The wall of the first container, facing the source, was at a distance of 1 cm from the source. The seven containers were located so as to ensure that the entire radius of the assembly was covered and were arranged so that not more than one container was in the path of the direct flight of a neutron. The experimental containers held lithium carbonate and neutron detectors (^{58}Ni, ^{27}Al, ^{197}Au, and ^{63}Cu), the gold and copper nuclides being with and without a cadmium shield.

For a more accurate determination of the K_T for tritium produced in lithium carbonate, we analyzed two stages. The first measurement of tritium was made after 4 months of irradiation; tritium was analyzed only from the experimental channels. In addition to analyzing the tritium, we also measured the characteristics of the neutron activators [10].

The lithium carbonate contained in the coaxial cylinders themselves was irradiated for 16 months. In that time, one the basis of the data of the first stage [10] we refined the spectrum and spatial distribution of neutrons in the assembly and made a correlation of the calculations by the small-group technique.

Calculation of Neutron Fluxes and Tritium Build-Up in Assembly. The neutron fluxes of ^{252}Cf in the lithium-containing assembly were calculated by the few-group technique with allowance for the first two collisions. The neutron fluxes in the assembly were found by the activation method. To measure the fast-neutron fluxes ($E_n \leq 2.6$ MeV) we employed nickel and aluminum targets and to measure fluxes of neutrons with an energy of $0.5 \leq E_n < 2.6$ MeV, targets of gold and copper with a cadmium shield. The activity of the neutron detectors was determined by measuring their β and γ activity [10].

Direct Measurement of Tritium in Lithium Carbonate by Scintillation Method. To determine the tritium content the irradiated lithium carbonate was withdrawn from the assembly and packaged in 0.7-g portions in polyethylene measuring cells. The specimens were prepared by the technique described in [7, 8], including the following chemical reactions:

$$Li_2CO_3\,(T) + 2nH_2O + 2CH_3COOH \rightarrow 2\,(CH_3COOLi)\,nH_2O + CO_2 + H_2O\,(HTO); \quad (1)$$

$$(CH_3COOLi)\,nH_2O + HF \rightarrow LiF\downarrow + CH_3COOH + nH_2O. \quad (2)$$

After the addition of a scintillating solution (up to 20 ml per test) the specimens were identified and measured in an SL-300 liquid scintillation spectrometer. Three specimens were prepared for each test along with background and standard specimens. The specimens were measured with an error not exceeding 7% and a significance level of 0.95.

Unlike the case in [10], here the calculation of curve 2 (Fig. 2) by the two-group technique (few-group technique) was carried out with allowance for the density factor for lithium carbonate. Direct experimental determination of the concentration of the accumulated tritium (1) is in fair agreement with the values calculated on the basis of data concerning the activation of the neutron detectors (3). The fact that curve 1 has a "dip" at $R = 5$ cm can be explained by the deviation of the real experimental assembly from the real sphere assumed in the calculations.

The sharp increase in the tritium concentration in the assembly for $R > 6$ cm is a consequence, most likely, of the fact that paraffin, as a strong moderator, generates thermal neutrons in the experimental lithium assembly and the bulk of these neutrons are absorbed by the boundary layer of the lithium carbonate (the cross section for the $^6Li(n, t)^4He$ nuclear reaction in the thermal region is 945 b).

Data from neutron-activation analysis and measurements of tritium produced in the lithium carbonate at various irradiation and cooling times confirmed the values of the initial neutron flux from the californium source and the absence of any appreciable diffusion of tritium from the salt. On the basis of the experimental data for the distribution of the tritium concentration over the radius of the experimental assembly we calculated the tritium conversion ratio $K_T = 0.33$, which accords with the result calculated by the two-group method (0.35).

LITERATURE CITED

1. E. P. Velikhov et al., in: Proc. All-Union Conf. Engineering Problems of Thermonuclear Reactors [in Russian], Vol. 1, NIIÉFA, Leningrad (1977), p. 5.
2. B. Leonard, Nucl. Tech., 20, 161 (1973).
3. R. Conn et al., Nucl. Tech., 26, 125 (1975).
4. M. Abdou, L. Wittenberg, and C. Maynard, Nucl. Tech., 26, 400 (1975).
5. D. Rose, Usp. Fiz. Nauk, 107, No. 1, 106 (1972).
6. P. Spangler, Report 437, Cambridge (1965).
7. R. Dierckx, Nucl. Inst. Methods, 107, 397 (1973).
8. R. Herzing, L. Kugpers, P. Cloth, et al., Nucl. Sci. Eng., 60, 169 (1976).
9. H. Bachmann et al., Nucl. Sci. Eng., 67, 74 (1978).
10. D. I. Evgrafova et al., in: Proc. All-Union Conf. Engineering Problems of Thermonuclear Reactors [in Russian], Vol. 2, NIIÉFA, Leningrad (1977), p. 309.
11. V. V. Kotov and G. E. Shatalov, in: Proc. US—USSR Symp. Fusion—Fission Reactor, Livermore, July 13-16 (1976).

POSSIBLE USE OF ^{145}Sm SOURCE FOR ISOTOPE-EXCITED X-RAY FLUORESCENCE ASSAYING OF TIN ORES

V. V. Smirnov, A. P. Ochkur,
N. G. Bolotova, A. D. Gedeonov,
E. P. Leman, V. N. Mitov,
and B. N. Shuvalov

UDC 550.835.41

In isotope-excited x-ray fluorescence assaying and analysis of tin ores use is most often made of ^{241}Am and ^{147}Pm radioisotope sources [1-2]. However, ^{241}Am is not optimal for exciting fluorescence in tin since its principal γ line (60 keV) is more than double the energy of the K absorption edge of tin. Moreover, when NaI(Tl) crystals or xenon-filled proportional counters are used as the detectors the secondary γ-ray spectra are made more complicated by iodine or xenon escape peaks whose energy is close to the Kα line of tin. A ^{147}Pm source is also rather ineffective in determining tin because of the high background in the secondary γ-ray spectrum as the result of the bremsstrahlung of the source.

Of existing radioactive nuclides, a promising one for excitation of tin fluorescence is ^{145}Sm which has a comparatively long half-life (340 days) and which, in the process of electron capture, emits a 61.2-keV γ-ray line and the K series of characteristic x-radiation of promethium (38 keV). Nevertheless, thus far no data have been published on the effective use of ^{145}Sm in isotope-excited x-ray fluorescence analysis, this being due apparently to difficulties encountered in obtaining this nuclide with a sufficiently high specific activity and the necessary degree of purity.

The nuclide ^{145}Sm is formed in the reaction ^{144}Sm(n, γ)^{145}Sm during neutron irradiation of samarium oxide Sm_2O_3, enriched with ^{144}Sm [3-4]. In the resulting compound, along with the main nuclide ^{145}Sm there are impurities of long-lived radionuclides with high-energy γ rays. The high content (27.6%) hinders the practical use of the ^{145}Sm as a source of low-level monoenergetic radiation [3, 4]. In view of this, longlived radioactive impurities present in the irradiated samarium oxide were identified and radiochemically pure ^{145}Sm was isolated from the mixture.

To obtain ^{145}Sm enriched to 92.4% ^{144}Sm samarium oxide (14.5 mg) was irradiated in a flux of thermal neutrons with a density of $8.4 \cdot 10^{13}$ neutrons/cm^2·sec for 30 days. Analysis of the γ-ray spectrum of the irradiated compound after cooling for a long time showed that only radioisotopes of europium (^{152}Eu, ^{154}Eu, and ^{155}Eu) are present in considerable quantity. Thus, obtaining radiochemically pure ^{145}Sm boils down to purifying the irradiated compound to remove europium microimpurities. Purification of irradiated samarium oxide from europium by electrolysis on a mercury electrode allowed ^{145}Sm to be isolated with a 98.63% radiochemical purity.*

Tests with ^{145}Sm compound with an activity of 1 mCi, placed in a hermetically sealed aluminum capsule with a diameter of 20 mm and height of 7 mm, were carried out on models of tin ores. The measurements were made in the geometry of wide divergent beams. The detectors used were xenon- and krypton-filled SI11P proportional counters in a BVDP pick-up and a NaI(Tl) crystal measuring 10 × 10 mm in a BVDS pick-up [2].

Figure 1 shows the secondary γ-ray spectra of models of tin ore as well as the γ-ray spectra of the ^{145}Sm source, as measured with a pulse-height analyzer. There are distinct photopeaks corresponding to the 38.7- and 61.2-keV lines of the ^{145}Sm source, photopeaks of singly scattered γ rays and attendant iodine and xenon escape peaks, as well as photopeaks of the Kα line of the characteristic x-rays of tin.

*The authors express their gratitude to A. V. Malyshenkov and A. A. Novikov for γ-ray spectrometric measurements and determination of the absolute activity of the source.

Translated from Atomnaya Énergiya, Vol. 48, No. 1, pp. 46-48, January, 1980. Original article submitted February 22, 1979; revision submitted July 16, 1979.

 0038-531X/80/4801-0062$07.50

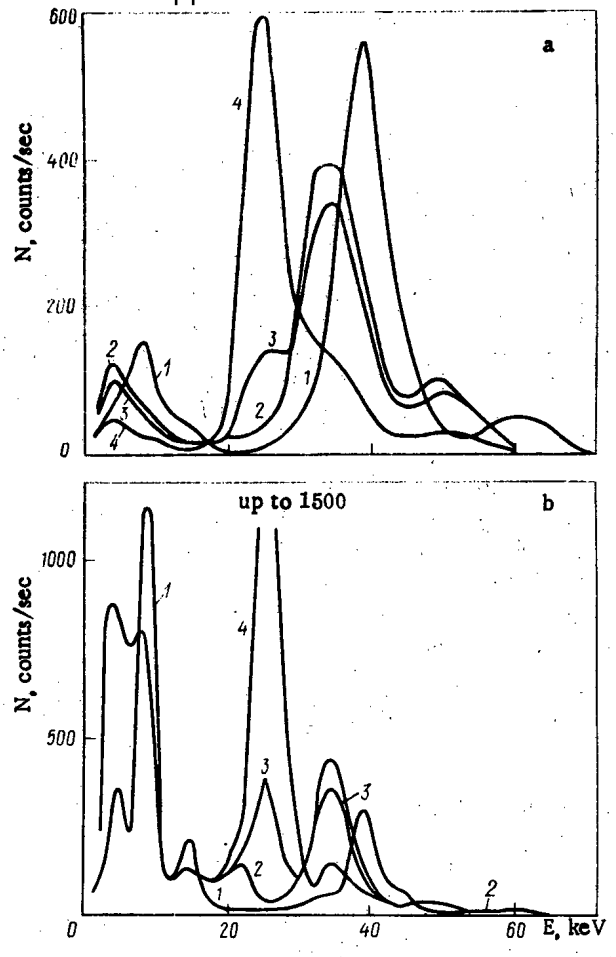

Fig. 1

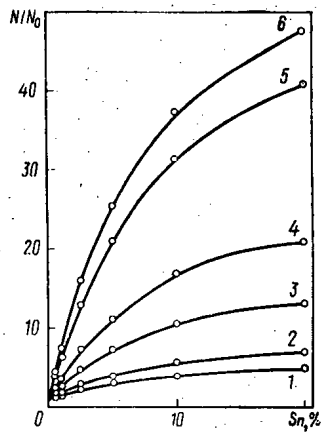

Fig. 2

Fig. 1. Primary and secondary γ-ray spectra of ^{145}Sm source, measured by scintillation (a) and xenon proportional (b) counters: 1) γ-ray spectrum of ^{145}Sm; 2-4) secondary γ-ray spectra obtained with models of ore containing 0.1 and 10% tin, respectively.

Fig. 2. Analytical plots obtained with models of tin ores: 1, 2) ^{147}Pm source; 3) ^{241}Am; 4-6) ^{145}Sm. The measurements were made with an NaI(Tl) crystal (1, 4) and xenon (2, 5) and krypton (3, 6) proportional counters; 0) experimental points.

The analytical line of tin and the peak of singly scattered radiation of the Kα line of promethium are almost completely resolved by both the scintillation and the proportional counter. In both cases the background in the region of the analytical line of tin (∿25 keV) is low. Its value is determined primarily by the contribution of singly scattered γ rays, which is due to the finite energy resolution of the detectors. The spectra do not contain any other lines of other nuclides or of bremsstrahlung which usually occurs if a nuclide emits β particles in addition to photons. This indicates the high degree of purity of the ^{145}Sm source in respect of extraneous impurities.

Figure 2 shows the plots of the intensity of the secondary radiation in the region of the analytical line of tin against the tin content. The intensity values measured on ore models with various tin contents were normalized to the value of the intensity from a model imitating barren rock. The integrated charge of the detectors during the measurements ensured the statistical significance of the counts with a 5-sec exposure and constituted 5000 counts/sec for proportional counters and 10,000 counts/sec for scintillation counters. In fact, the plots shown in Fig. 2 characterize the contrast (i.e., the signal/background ratio) in the region of the analytical line, which can be taken as a criterion in estimation of the threshold of sensitivity of the method and in comparison of the efficiency of radionuclide sources or detectors. As follows from Fig. 2, the use of a ^{145}Sm source with any

detectors ensures the best signal/background ratio and, therefore, the highest sensitivity in tin determinations in comparison with ^{147}Pm and ^{241}Am. The advantage of ^{145}Sm over ^{147}Pm, notwithstanding the equality of the energy of their lines, lies in the existence of a lower background in the region of the analytical line of tin owing to the absence of bremmstrahlung. In comparison with ^{241}Am, the ^{145}Sm source not only produces a lower background in the region of the K line of tin but also excites it more effectively since the energy of its radiation is closer to that of the K absorption edge of tin.

Measurements on models of tin ores with allowance for only the statistical accuracy with an exposure time of 5 sec showed that the sensitivity to the tin content is 0.05% for proportional counters and 0.1% for scintillation detectors. When the exposure time is increased to 20 sec the sensitivity threshold is reduced by half. Let us point out that in order to attain such thresholds of sensitivity to tin with ^{147}Pm and ^{241}Am sources the exposure should be increased by a factor of no less than 10 and the activity of the sources in respect of γ rays should be no less than 10-15 mCi, i.e., must be 10-15 times higher.

The ^{145}Sm-based source can also be used to determine other elements with atomic numbers close to 50 (molybdenum, antimony, silver, cadmium, etc.). Its advantages are obvious also in comparison with two-stage excitation [5]: an isotope activity lower by 1.5-2 orders of magnitude, and smaller mass and size of the probe device. The ^{145}Sm source is particularly promising for use in well-logging instrument in which case, because of their small diameter, it is extremely difficult to use two-stage excitation.

Thus, the creation of the ^{145}Sm source considerably extends the capabilities of the isotope-excited x-ray fluorescence method in the analysis and assaying of ores containing elements with intermediate atomic numbers.

LITERATURE CITED

1. A. P. Ochkur et al., The Gamma Method in Mining Geology [in Russian], Nedra, Leningrad (1976).
2. E. P. Leman, Isotope-Excited X-Ray Fluorescence Method of Assaying Deposits of Nonferrous and Rare Metals [in Russian], Nedra, Leningrad (1978).
3. S. V. Rumyantsev et al., At. Energ., 15, No. 6, 511 (1963).
4. S. V. Rumyantsev, E. E. Kulish, and O. I. Borisov, Sources of Low-Energy Radiation in Nondestructive Testing [in Russian], Atomizdat, Moscow (1976).
5. A. N. Zhukovskii et al., Geofiz. Apparatura, No. 65, 120 (1978).

GAMMA RAYS AND NEUTRONS FROM ^{239}Pu FLUORIDES

V. V. Ovechkin

UDC 539.17.3

Compounds of α-active elements (U, Pu, Am, etc.) with ^{19}F emit γ rays and neutrons as a result of (α, pγ), (α, nγ), and (α, α'γ) reactions. These radiations can be used in technological monitoring in reprocessing and producing nuclear fuel [1]. However, the published data on the α+F reaction, including the use of α-particle accelerators [2], are still incomplete and not always self-consistent. The present work was undertaken to refine the values of the energies and intensities of the emitted γ rays, and to determine the specific yields of neutrons from PuF_4 and PuF_3. Practically no information has previously been published on the emission of γ rays and neutrons from these compounds.

We used aged samples of $^{239}PuF_4$ containing 33.4 and 20.5 g of ^{239}Pu and a known amount of other Pu isotopes which we corrected for in the effect being investigated. In addition, using the method described in [3], we prepared samples of $^{239}PuF_3$ and $^{239}PuO_2$ with fluorine (1.1 and 2.5%) having a total mass of 1g each. The spectra were measured with a Ge (Li) detector having a sensitive volume of ∿50 cm^3; the γ spectrometer had an energy resolution of 4.2 keV for ^{60}Co radiation (E_γ = 1332 keV). The counting efficiency $\varepsilon_\gamma = f(E_\gamma)$ was determined with OSGI standard γ radiators whose intensities were known to within 3%.

Results of Measurements. Our measured values of the energies and relative intensities of γ lines are listed in Table 1 together with ^{241}AmF data from [4]. The measured values of the intensities for these compounds are clearly in good agreement.

We note the relatively small difference between the yields of 197 and 1357 keV γ rays which correspond to the deexitation of ^{19}F levels which differ in energy by almost 1400 keV. This may show the relatively small contribution of the formation of the compound nucleus ^{23*}Na in the (α, α') reaction in comparison with the contribution of the direct interactions of α particles with ^{19}F nuclei.

To determine the neutron yield from PuF_3, lengthy (more than 4.5 years) measurements of the relative areas of the γ peaks $S_t/S_i = S_{1275}/S_{891}$ and S_{511}/S_{583} were performed for the same experimental geometry. The dependence of these values on the parameter $x = 1 - \exp(-\lambda t)$, where t is the time and λ is the ^{22}Na decay constant, is shown in Fig. 1. Since both the initial and final values for $x = 1 (t = \infty)$ have been found, they can be used to determine the neutron yield I_n

$$I_n = \frac{S_\infty - S_0}{k\varepsilon} = \frac{S_t}{k\varepsilon}\left[\left(\frac{S_\infty - S_0}{S_i}\right)\Big/\left(\frac{S_t}{S_i}\right)\right]$$

taking account of the ^{22}Na decay scheme, k = 1 for $S_t/S_i = S_{1275}/S_{891}$ and k = 1.78 for $S_t/S_i = S_{511}/S_{583}$.

The values of $S_t = S_{1275}$ and S_{511} were measured separately under conditions of good geometry using sufficiently accurate values of the counting efficiency ε_γ. Such determinations with respect to annihilation and γ radiation gave $(4.3 \pm 0.3)\cdot 10^3$ neutrons/sec·g for the specific yield of neutrons from ^{239}Pu trifluoride. Check measurements with a neutron counter

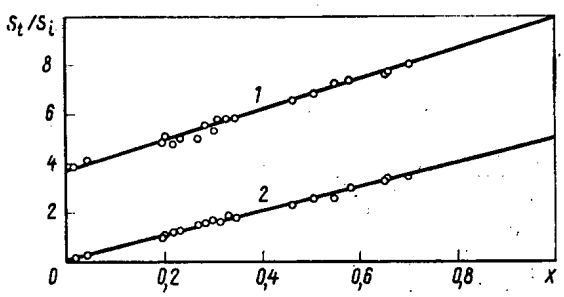

Fig. 1. Ratio of areas S_t/S_i as a function of $x = 1 - \exp(-\lambda t)$: 1) S_{1275}/S_{891}; 2) S_{511}/S_{583}.

Translated from Atomnaya Énergiya, Vol. 48, No. 1, pp. 48-49, January, 1980. Original article submitted March 12, 1979.

0038-531X/80/4801-0065$07.50

TABLE 1. Relative Intensities and Energies of γ Rays from ^{239}Pu Fluorides and ^{241}AmF

γ energy, keV	Reaction	Phase content, % by γ transition [2]	Rel. intensity		
			Our data		Data from [4] on ^{241}AMF
			$^{239}PuF_3$	$^{239}PuF_4$	
197,0±0,5	α, α′	197→0	(0,78)		
583±0,5	α, n	583→0	2,36±0,24	2,56±0,20	2.50
891±0,5	α, n	891→0	1,00	1,00	1,00
1238±0,7	α, α′	1348→110	0,52±0,05	0,55±0,06	0,50
1274,5±0,3	α, p	1274,5→0	(6,0±0,2)†	(6,0±0,2)†	
1349±1	α, α′	1459→110	0,43±0,07		
1357±1	α, α′	1555→197	0,35±0,06	0,66±0,08‡	0,73‡
1369±1	α, n	1952→583	0,20±0,04		
1400±0,5	α, n	1984→583	0,12±0,02	0,14±0,02	0,16
1459±1	α, α′	1459→0		0,10±0,03	
1528±0,3	α, n	1528→0	0,41±0,04	0,45±0,05	0,39
1555±1	α, n	2212→657	0,04±0,01		0,08
2082,0±0,5	α, p	3357→1275,5	0,72±0,07	0,75±0,08	0,67
3180±1	α, p	4456→1274,5		0,19±0,03	0,19
3869	α, p	5144→1274,5			0,004

*Errors of results do not exceed 20%.
†This value is for a freshly prepared sample.
‡Total value for 1349, 1357, and 1369 keV γ rays.

calibrated with a standard ^{240}Pu-based spontaneous fission neutron source gave nearly the same value $(4.65 \pm 0.30) \cdot 10^3$ neutrons/sec·g. For samples of ^{239}Pu tetrafluoride measured by γ radiation (1275 keV) the average yield was $(4.6 \pm 0.4) \cdot 10^3$ neutrons/sec·g, which is in satisfactory agreement with one of the later published results of direct neutron measurements $(5.4 \pm 0.5) \cdot 10^3$ neutrons/sec·g of PuF_4 [1].

Our measured values of the intensity of γ rays from the ^{19}F (α, nγ) ^{22}Na reaction and the total neutron yield were used together with an account of the investigated γ transitions in the ^{22}Na nucleus according to [2] to determine the contributions of the groups of neutrons corresponding to the excited ^{22}Na levels. Table 2 shows the results of our spectrometric measurements and data from [5] for PuF_4 obtained by using photoemulsions.

Our results are in satisfactory agreement with those in [5]. At the same time the γ method indicates the presence in the neutron spectrum of a low-intensity group with minimum energy.

Our check measurements showed that the broad γ peak at ∿690 keV practically completely vanished when a 7.5-cm-thick layer of paraffin was placed between the PuF_4 sample and the Ge(Li) detector. In this case the areas of the closest peaks of ^{239}Pu (E_γ = 640-660 keV) were changed by only about 15%. This corresponds to the case in [6] where it was shown that inelastic interactions of fast neutrons with ^{72}Ge nuclei in the detector can give rise to conversion electrons and a broad energy peak at ∿690 keV. After studying the α + F reaction with $^4He^+$ ions accelerated to 5 MeV, Giles and Peisach [7] concluded that the peak near 690 keV arises in the successive emission of 690, 3180, and 1275 keV γ rays in the de-excitation of the 5144 keV level of ^{22}Ne populated in the ^{19}F (α, p) reaction. Considering the high intensity and broad width of this peak, their conclusion must be considered incorrect. The arrangement of these authors that the peak observed at 2165 keV is a result of the population

TABLE 2. Relative Contributions of Groups of Neutrons from PuF_4 Related to ^{22}Na Levels, %

Energies of ^{22}Na levels, keV	Data from [5]	Our data	Energies of ^{22}Na levels, keV	Data from [5]	Our data
0 ground	47,2	52,7	1952	0,7	1,3
583+657	32,2	26,4	1984		1,5
891	14,8	13,0	2212		0,8
1528	5,1	4,3			

and deexcitation of a still higher level of ^{22}Ne (E = 5520 keV) is not persuasive either. The energy of this peak (2165 keV) practically coincides with the energy of the double escape peak of 3180 keV γ photons.

The broadening of the annihilation peak was about 20% greater for PuF_3 than for the positron emitter ^{22}Na placed between aluminum, iron, and lead plates. This shows that the process of positron annihilation does not proceed the same way in Pu fluorides as it does in metals.

Measurements of γ spectra of Pu and F compounds permit the development of a highly sensitive and nondestructive method of determining a small fluorine content in plutonium, particularly if the compositions of the other α emitters are known. By using this method and a 150 × 150 mm NaI(Tl) scintillation detector with a well in which the Pu sample is placed in a 5-mm-thick lead shield, and recording the area of the 2080-keV γ peak, as little as $6 \cdot 10^{-4}$ wt.% of fluorine can be detected (5-g Pu sample, time of measurement 2 h), which is smaller than the value of $3 \cdot 10^{-3}$ wt.% obtainable by using a Ge (Li) detector [3].

LITERATURE CITED

1. É. M. Tsenter et al., in: Proc. of Third COMECON Symp. on "Research in the field of the reprocessing of irradiated fuel" [in Russian], Vol. 3, Czechoslovak Atomic Energy Comm., Prague (1974), p. 202.
2. É. V. Lan'ko, G. S. Dombrovskaya, and Yu. K. Shubnyi, Probabilities of Electromagnetic Transitions of Atomic Nuclei Z = 1-30 [in Russian], Nauka, Leningrad (1972).
3. V. V. Ovechkin, V. I. Melent'ev, and V. F. Gorbunov, Radiokhimiya, 18, 152 (1976).
4. E. Less and D. Lindley, Ann. Nucl. Energy, 5, No. 3-4, 133 (1978).
5. R. Lehman, Phys. Rev., 171, 1311 (1968).
6. D. Smith, Nucl. Instrum. Methods, 102, 193 (1972).
7. I. Giles and M. Peisach, J. Radioanal. Chem., 32, 105 (1976).

EFFECT OF ADDITIVES SIMULATING FISSION PRODUCTS ON THE ELASTICITY CHARACTERISTICS OF UC

S. A. Balankin, V. S. Belevantsev,
A. S. Bubnov, V. A. Zelyanin,
R. B. Kotel'nikov, and D. M. Skorov

UDC 621.039.54:539.32

The use of uranium monocarbide makes it possible to improve considerably the economic indicators of fast reactors [1]; an estimate of the working capacity of the fuel element requires some knowledge of the changes in the properties of the fuel during the process of operation. In order to determine the effect of solid fission products on the characteristics of the elasticity of UC, fission-product simulators in an amount corresponding to an 8% burn-up of the heavy atoms were added to prepared specimens [2]. The phase composition of the specimens, calculated on the basis of data from micro-x-ray spectrum and chemical analyses, are shown in Table 1.

The moduli of elasticity of pellets with a diameter of 10 mm and a thickness of 2 mm were measured by the ultrasonic resonance method [3]. The error in determining the Young's modulus E and the Poisson coefficient μ with a confidence coefficient of 0.95 does not exceed 2% and 2.5%, respectively. The error in determining the relative variation of E when the temperature varies is 0.1%.

Since the investigated specimens had different porosities, the values of E and μ were recomputed for the theoretical density according to the formulas:

$$\begin{aligned} E_0 &= 9K_0G_0/(3K_0+G_0);\\ \mu_0 &= (3K_0-2G)_0/2(3K_0+G_0);\\ K_0 &= K(1-P)^{-\beta/\alpha}\ [4];\\ G_0 &= G(1-P)^{-2\beta/3\alpha}, \end{aligned} \qquad (2)$$

where Eq. (2) was obtained from the expression (1), taking account of the relation

$$\frac{\partial \ln G}{\partial P} \approx \frac{2}{3}\frac{\partial \ln K}{\partial P}\ [5].$$

Here K and G are the bulk modulus and the shear modulus, respectively; P, porosity; α, volumetric coefficient of thermal expansion; $\beta = -1/K(\partial K/\partial T)_p$, temperature coefficient of variation of the bulk modulus; the subscript 0 refers to the compact material. The values of β for UC and the irradiated-fuel simulator were, respectively, $1.16\cdot10^{-4}$ K^{-1} and $1.09\cdot10^{-4}$ K^{-1}, and the coefficients of thermal expansion had been determined earlier [6].

It follows from Table 2 that the accumulation of solid fission products in UC increases the modulus of elasticity and reduces the Poisson coefficient, An increase in E may, in particular, be caused by the appearance of ZrC, which has a Young's modulus of $(39-55)\cdot10^{10}$ Pa [7, 8].

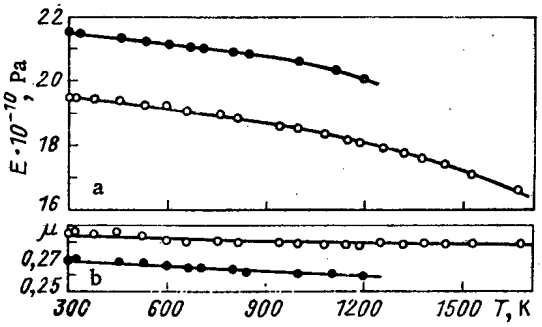

Fig. 1. Variation of the Young's modulus (a) and the Poisson coefficient (b) of UC (○) and the irradiated-fuel simulator (●).

Translated from Atomnaya Énergiya, Vol. 48, No. 1, pp. 49-50, January, 1980. Original article submitted April 23, 1979.

 0038-531X/80/4801-0068$07.50

TABLE 1. Phase Composition of Specimens

Material	Phase composition	Phase content, % by vol.
Uranium carbide	UC	87,5
	$UC_{1,88}$	12,5
Simulator of irradiated carbide fuel	$(U_{0,963}Zr_{0,03}Mo_{0,007})C$	78,38
	$(U, REE)_2C_3$	13,55
	$UMoC_2$	2,09
	$(REE)_2O_3$	3,07
	$Ba_{0,56}Zr_{0,44}O$	0,74
	$U(Ru_{0,63}Pd_{0,37})_3$	2,17

TABLE 2. Physicomechanical Properties of Specimens (T = 298°K)

Material	$\rho \cdot 10^{-3}$, W/m³	P, %	$E \cdot 10^{-10}$, Pa	μ	$E_0 \cdot 10^{-10}$, Pa	μ_0
Uranium carbide	11,69	12,5	13,56	0,252	19,48	0,285
Simulator of irradiated fuel	12,52	3,5	19,51	0,260	21,50	0,269

The variation of E and μ as functions of temperature is shown in Fig. 1. The moduli of elasticity of UC and the simulator at first decrease practically linearly, but they deviate from the linear law at higher temperatures. This deviation (ΔE) increases exponentially with increasing temperature [$\Delta E \sim \exp(-\Delta H/RT)$]. For metals [9] and a number of carbides of transition metals [10] such a deviation is attributable to the formation of thermal vacancies. In the case of UC and the simulator ΔH is equal to 38 and 67 kJ/mole, respectively; the fact that ΔH_{UC} is much lower than the value published in [7] is apparently due to the presence of UC_2, as was established for the activation energy for peak internal friction [11], coinciding in temperature with the beginning of the nonlinear decrease of the modulus of elasticity.

Thus, the accumulation of solid fission products in an amount corresponding to an 8% burn-up of heavy atoms increases the modulus of elasticity of UC by about 10% and reduces the Poisson coefficient by 6% over the entire temperature interval studied.

LITERATURE CITED

1. I. S. Golovnin et al., At. Energ., 30, No. 2, 211 (1971).
2. R. B. Kotel'nikov et al., ibid., 39, No. 4, 255 (1975).
3. V. M. Baranov, Zavod. Lab., No. 9, 1120 (1972).
4. S. A. Balankin, A. S. Bubnov, and D. M. Skorov, At. Energ., 45, No. 3, 220 (1978).
5. V. M. Gropyanov, V. N. Fishchev, and A. I. Avgustinik, in: Proceedings of the All-Union Institute of Refractories [in Russian], No. 40, Leningrad (1968), p. 299.
6. A. A. Ivanov et al., At. Energ., 44, No. 2, 170 (1978).
7. R. A. Andrievskii, A. G. Lanin, and G. A. Rymashevskii, Strength of High-Melting Compounds [in Russian], Metallurgiya, Moscow (1974).
8. I. N. Frantsevich and A. B. Lyashchenko, Poroshk. Metall., No. 7, 73 (1966).
9. V. T. Shmatov and A. V. Grin', Fiz. Met. Metalloved., 12, No. 4, 600 (1961).
10. V. G. Bukatov et al., Izv. Akad. Nauk. SSSR, Neorg. Mater., 11, No. 2, 367 (1975).
11. A. Hall, J. Nucl. Mater., 37, 314 (1970).

NEW RUSSIAN JOURNALS

IN ENGLISH TRANSLATION

BIOLOGY BULLETIN
Izvestiya Akademii Nauk SSSR, Seriya Biologicheskaya

The biological proceedings of the Academy of Sciences of the USSR, this prestigious new bimonthly presents the work of the leading academicians on every aspect of the life sciences—from micro- and molecular biology to zoology, physiology, and space medicine.
Volume 7, 1980 (6 issues) $195.00

SOVIET JOURNAL OF MARINE BIOLOGY
Biologiya Morya

Devoted solely to research on marine organisms and their activity, practical considerations for their preservation, and reproduction of the biological resources of the seas and oceans.
Volume 6, 1980 (6 issues) $115.00

WATER RESOURCES
Vodnye Resursy

Evaluates the water resources of specific geographical areas throughout the world and reviews regularities of water resources formation as well as scientific principles of their optimal use.
Volume 7, 1980 (6 issues) $215.00

HUMAN PHYSIOLOGY
Fiziologiya Cheloveka

A new, innovative journal concerned *exclusively* with theoretical and applied aspects of the expanding field of human physiology.
Volume 6, 1980 (6 issues) $195.00

SOVIET JOURNAL OF BIOORGANIC CHEMISTRY
Bioorganicheskaya Khimiya

Features articles on isolation and purification of naturally occurring, biologically active compounds; the establishment of their structure, methods of synthesis, and determination of the relation between structure and biological function.
Volume 6, 1980 (12 issues) $245.00

SOVIET JOURNAL OF COORDINATION CHEMISTRY
Koordinatsionnaya Khimiya

Describes the achievements of modern theoretical and applied coordination chemistry. Topics include the synthesis and properties of new coordination compounds; reactions involving intraspheral substitution and transformation of ligands; complexes with polyfunctional and macromolecular ligands; complexing in solutions; and kinetics and mechanisms of reactions involving the participation of coordination compounds.
Volume 6, 1980 (12 issues) $255.00

THE SOVIET JOURNAL OF GLASS PHYSICS AND CHEMISTRY
Fizika i Khimiya Stekla

Devoted to current theoretical and applied research on three interlinked problems in glass technology; the nature of the chemical bonds in a vitrifying melt and in glass; the structure-statistical principle; and the macroscopic properties of glass.
Volume 6, 1980 (6 issues) $145.00

LITHUANIAN MATHEMATICAL JOURNAL
Litovskii Matematicheskii Sbornik

An international medium for the rapid publication of the latest developments in mathematics, this quarterly keeps western scientists abreast of both practical and theoretical configurations. Among the many areas reported on in depth are the generalized Green's function, the Monte Carlo method, the "innovation theorem," and the Martingale problem.
Volume 20, 1980 (4 issues) $175.00

PROGRAMMING AND COMPUTER SOFTWARE
Programmirovanie

Reports on current progress in programming and the use of computers. Topics covered include logical problems of programming; applied theory of algorithms; control of computational processes; program organization; programming methods connected with the idiosyncracies of input languages, hardware, and problem classes; parallel programming; operating systems; programming systems; programmer aids; software systems; data-control systems; IO systems; and subroutine libraries.
Volume 6, 1980 (6 issues) $115.00

SOVIET MICROELECTRONICS
Mikroelektronika

Reports on the latest advances in solutions of fundamental problems of microelectronics. Discusses new physical principles, materials, and methods for creating components, especially in large systems.
Volume 9, 1980 (6 issues) $160.00

Send for Your Free Examination Copy

PLENUM PUBLISHING CORPORATION, 227 West 17th Street, New York, N.Y. 10011
In United Kingdom: Black Arrow House, 2 Chandos Road, London NW10 6NR, England
Prices slightly higher outside the U.S. Prices subject to change without notice.